Freie Universität Berlin

# Synthesis of Hyperbranched Polyglycerol Dye Conjugates for *in vitro* and *in vivo* Targeting Studies

Dissertation zur Erlangung des akademischen Grades des
Doktors der Naturwissenschaften
(Dr. rer. nat.)

eingereicht im Fachbereich Biologie, Chemie und Pharmazie
der Freien Universität Berlin

vorgelegt von
**Stephanie Reichert**
aus Berlin

Juli 2011

Die vorliegende Arbeit entstand auf Anregung und unter Anleitung von Prof. Dr. Rainer Haag in der Zeit von November 2006 bis Juli 2011 an der Freien Universität Berlin.

1. Gutachter: Prof. Dr. Rainer Haag, Freie Universität Berlin

2. Gutachter: Jun.-Prof. Dr. Michael Krauß, Freie Universität Berlin

Disputation am: 30.09.2011

*Für meine Familie*

*„ Man muss viel gelernt haben, um über das, was man nicht weiß, fragen zu können.“*

*Jean-Jaques Russeau*

**Acknowledgements**

First I would like to thank Prof. Dr. Rainer Haag for giving me this interesting topic, for the possibility to conduct my thesis in his research group and for the great chance to spend two research visits abroad, in Vancouver and New Delhi.

I am very grateful to Prof. Dr. Donald E. Brooks from the University of British Columbia, who gave me the opportunity to stay at his group. I learned so much by interacting with him and his great group. Special thanks to Sonja Horte for help with problems of any kind and the start of a new friendship. I would also like to thank to Dr. Muhammad Imran ul-haq for taught me about the basic tricks and techniques of HPG synthesis.

I want to thank Prof. Dr. Virinder S. Parmar and Dr. Sunil K. Sharma from the University of Delhi for the amazing experience to join their groups.

I would like to say thank you to all my co-operation partners I have been working with during my Ph.D. I would like to thank Dr. Kai Licha and Dr. Pia Welker for performing the biochemical studies in this project which is an integral part of my thesis and the help in writing my first paper. I am grateful to Irene Schütz of AG Prof. Dr. V. Haucke, Department of Biochemistry, Free University of Berlin, for co-localization studies and for all the fruitful discussions. I would like to thank Dr. habil. Bernd Ebert, Physikalisch-Technische Bundesanstalt in Berlin, for his co-operation and initiative in our *in vivo* project. I sincerely acknowledge the contribution from Dr. Divya Vats of AG Prof. Dr. M. Rudin, Animal Imaging Center of UZH/ETH in Zürich, Switzerland, with additional *in vivo* studies.

Special thanks to Dr. Marcelo Calderón for supervision of the thesis, for a lot of helpful discussions, for his patience and for proof reading. ¡muchas gracias!

Tomake onek dhanyabad to Dr. Mohiuddin A. Quadir! Thanks for the support with the *in vivo* studies and for proof reading!

Also a big thank you to Dr. Chris Popeney for proof reading, corrections and helpful comments!

Aapakaa bahut bahut dhanyavaad, Dr. Jayant Khandare! Thank you very much for help in writing my first paper and for his constructive suggestions.

Special thanks go to Achim Wiedekind for assisting me in surface tension and DLS measurements, and for the nice coffee breaks.

I would also like to thank Dr. Andreas Mohr and all my other office, lab colleges, and all the Haag group members for help, discussions and coffee breaks.

I would like to specially thank Dr. Pamela Winchester and Jutta Hass. Thanks for correcting paper, book chapter, and especially my thesis. And thanks a lot for all the help in bureaucratic things. Without them nothing would work.

I am grateful to the people from the NMR and Mass department and to the all people from Material Store at the Freie Universität Berlin for always being helpful.

A lovely thank you to Burkhard Wettig for his support to submit my thesis!

Last but not least I would like to thank my family and my lovely friends, which always were there for me, ready to give me advice and support. Special thanks to my beloved mom!

# Table of Contents

## Abbreviations

| | |
|---|---|
| A431 | epidermoid carcinoma cells |
| A549 | adenocarcinomic human alveolar basal epithelial cells |
| AP-1 | activator protein 1 |
| asp | asparagine |
| arg | arginine |
| $^t$Boc | *tert*-butyloxycarbonyl |
| C26 | colon carcinoma cell line |
| CaSki | cervical cancer cell line |
| CD63 | cell-surface protein |
| CHC | clathrin heavy chain |
| $CH_2Cl_2$ | dichlormethane (DCM) |
| conc. | concentrated |
| Cyt c | cytochrome c |
| *D* | dendritic |
| DAPI | 4',6-diamidino-2-phenylindole |
| *DB* | degree of branching |
| DCC | dicyclohexylcarbodiimide |
| DIPEA | *N,N'*-diisopropylethylamine |
| DLS | dynamic light scattering |
| DMF | *N,N'*-dimethylformamide |
| DMSO | dimethyl sulfoxide |
| DNA | deoxyribonucleic acid |
| DOX | doxorubicin |
| DOXO-EMCH | (6-maleimidocaproyl)hydrazone derivative of doxorubicin |
| dPGS | dendritic polyglycerol sulfate |
| EDTA | ethylenediaminetetraacetic acid |
| EEA1 | early endosome entigen 1 protein |
| EPR | enhanced permeation and retention |
| eq. | equivalent |
| FA | folic acid |
| FACS | fluorescence-activated cell sorting |
| FDA | food and drug administration |

| | |
|---|---|
| FISH | fluorescence in situ hybridization |
| FITC | fluorescein isothiocyanate |
| FSH | follicle-stimulating hormone |
| G | generation |
| Gd | gadolinium |
| GFP | green fluorescent protein |
| gly | glycine |
| GPC | gel permeation chromatography |
| GTPases | hydrolase enzymes, that can bind and hydrolyze guanosine triphosphate |
| h | hour |
| HBPH | hyperbranched polyhydroxyl |
| HCl | hydrochloric acid |
| Her2 | human epidermal growth factor receptor 2 |
| HIV | human immunodeficiency virus |
| HO$^t$Bu | *tert.*-Butanol |
| HPG | hyperbranched polyglycerol |
| HPLC | high-performance liquid chromatography |
| HPMA | *N*-(2-hydroxylpropyl)methacrylamide |
| HOBt | 1-hydroxybenzotriazol |
| HT29 | human colon adenocarcinoma grade II cell line |
| HUVEC | human umbilical vein endothelial cells |
| Hz | hertz |
| ICC | indocarbocyanine |
| ITCC | indotricarbocyanine |
| ICG | indocyanine green |
| *J* | coupling constant |
| KB | human epidermoid carcinoma |
| kDa | kilo dalton |
| KG6 | a sixth generation lysine dendrimer |
| KO$^t$Bu | potassium tert-butanolate |
| *L* | linear |
| LAMP1 | lysosomal-associated membrane protein 1 |
| LHRH | luteinizing-hormone-releasing hormone |
| mal | maleimide |
| MALDI-ToF | matrix assisted laser desorption ionization time-of-flight |

| | |
|---|---|
| MALL | multi angle light scattering |
| MβCD | methyl-β-cyclodextrin |
| MCF 7 | breast cancer cell line |
| Me | methyl |
| MeOH | methanol |
| min(s) | minute(s) |
| $M_n$ | number average molecular weight |
| M6PR | mannose-6-phosphate receptor |
| MRI | magnetic resonance imaging |
| MTX | methotrexate |
| mV | millivolt |
| $M_w$ | weight average molecular weight |
| MW | molecular weight |
| mPEG | methoxyl polyethylene glycol |
| $NaN_3$ | sodium azide |
| NIRF | near infrared resonance fluorescence |
| nm | nanometer |
| NHS | *N*-hydroxysuccinimide |
| NMP | *N*-methyl pirrolidin-2-on |
| NMR | nuclear magnetic resonance |
| PAMAM | poly(amido amine) |
| PBS | phosphate buffered saline |
| PDI | polydispersity index |
| PDT | photodynamic therapy |
| PEG | polyethylene glycol |
| PEI | poly(ethylene imine) |
| PEO | polyethylene oxide |
| PET | positron emission tomography |
| PG | polyglycerol |
| Ph | phenyl |
| PPCD | PEG–PAMAM-*cis*-aconityl-DOX conjugates |
| PPI | poly(propylene imine) |
| $PPh_3$ | triphenylphosphine |
| ppm | parts per million |
| PPSD | PEG–PAMAM–succinic–DOX conjugates |

| | |
|---|---|
| PtdIns(3)P | phosphatidylinositol-3-phosphate |
| quant. | quantitative |
| RGD | arg-gly-asp peptide |
| RNA | ribonucleic acid |
| RNases | ribonuclease |
| ROMP | ring-opening metathesis polymerization |
| r.t. | room temperature |
| SA | succinic acid |
| sec | second |
| SKOV-3 | ovarian cancer cells |
| SMA | slow monomer addition |
| SPECT | single photon emission computed tomography |
| *T* | terminal |
| $t_{1/2}$ | half-life time |
| TEA | triethylamine |
| TFA | trifluoroacetic acid |
| TGN | trans-Golgi network |
| THF | etrahydrofuran |
| TLC | thin layer chromatography |
| UV | ultraviolet radiation |
| VEGF | vascular endothelial growth factor |
| VEGFR-2 | vascular endothelial growth factor receptor 2 |

# 1. General Introduction

## 1.1. Polymer Therapeutics

"We have to learn how to aim chemically".[1] The therapeutic concept of targeting, the ability to transport an active substance to a certain destination, is based on the idea of Paul Ehrlich to create a "magic bullet". For this concept he received the Nobel Prize for Physiology or Medicine in 1908.

Today, the improvement of the therapeutic index of active substances is a top objective of modern medicine for many applications such as tumor diseases, as well as inflammatory and infectious diseases. In recent years improvements in biochemical, genetic, physicochemical, and biomedical analytic methods have allowed scientists to identify and characterize highly potent drugs. Increased knowledge of the causes of many diseases and the decryption of the human genome have allowed science and research to make a big step forward in the diagnosing and therapy of diverse diseases. There is not a lack of effective active agents but rather a limited usability of such substances. Among the drugs presenting being used in clinic are low-molecular weight drug molecules (typically < 500g/mol). A problem is the short halftime in bloodstream and the fast elimination of low-molecular substances, which can also easily diffuse in healthy tissue to undesired side effects. There is also a risk that only a small amount of the drug and thus lead the target site. Factors such reaches sparingly solubility in biological medium premature enzymatic degradation cause a problem. An additional challenge for certain substances is to overcome anatomic and physiological barriers such has blood-brain barrier, gastrointestinal tracts and alveolus.

Macromolecular transport systems are being investigated to improve their efficiency when applied. Such transport systems can be divided in two distinct classes, namely supramolecular drug-delivery systems and nanoparticulate drug-polymer conjugates. Emulsions, liposomes, and non-covalent polymer carriers can be used as transport systems whereas nanoparticles receive drugs physical. Examples for drug-polymer conjugates are proteins, polysaccharides, and synthetic polymers, which binds the drugs covalently.

In 1975 the development of monoclonal antibodies[2] and the "Ringsdorf-model"[3] for drug delivery based on synthetic polymers was a decisive step forward to the use of macromolecular transport systems.

Polymer therapeutics is the generic term for drug-polymer conjugates and other polymer transport systems.[4,5] For the production of these conjugates, macromolecules should ideally be water soluble, non-toxic, and not immunogenic. It is also important that these compounds can be removed and eliminated by the organism.[6] Furthermore, functional groups for drugs, target molecules such as antibodies or sugar molecules for disease-related antigens or specificy receptors, solubilizing groups, and cleavable linkers should be selectively introduced on polymer surfaces.[3]

Hermann Staudinger is considered to be the "father" of polymer chemistry. In 1920 he published in "Berichten der Deutschen Chemischen Gesellschaft" his article "Über Polymerisation" and that laid the foundation for modern polymeric science.[7] In 1953 he was awarded the Nobel Prize for his pioneering work. Many types of macromolecular architectures namely, linear, crosslinked, star-like, cyclic, and branched architectures, have evolved from Staudinger's work on macromolecular chemistry (Figure 1).

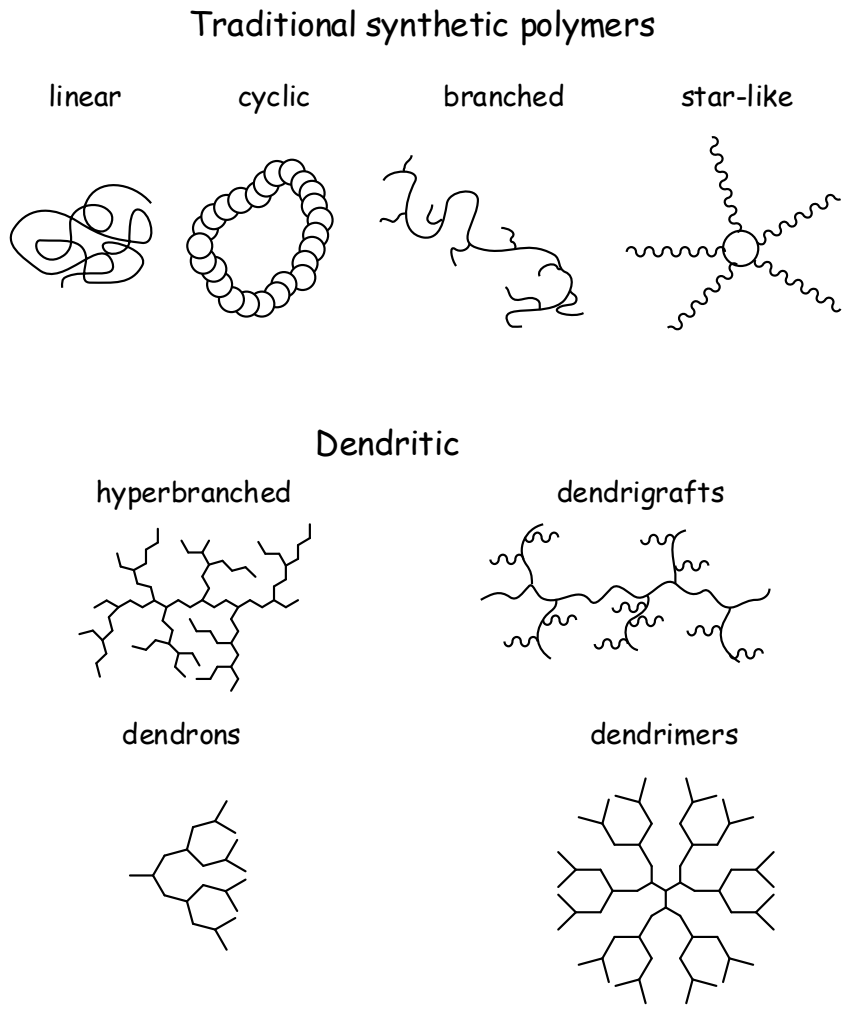


**Figure 1.** Examples of macromolecular architectures.

Although linear polymers and polymer networks have enlarged an important role since the beginning of polymer chemistry, branched polymeric architectures have only been scientifically interesting since the 1950s. Dendritic macromolecules are a relatively new group of synthetic polymers and perfect dendrimers and hyperbranched polymers have become especially interesting because of their chemical and physical advantages.

The market introduction of protein-polymer conjugates (PEG-Adenosin-Desaminase, PEG-L-Asparginase) in the 1990s laid a foundation stone. Additional polymer pharmaceuticals have been able to establish themselves. In particular, this includes the intensive research on *N*-(2-hydroxylpropyl)methacrylamide (HPMA). On the basis of its advantages as a polymer carrier system it has already been used in clinical studies (phase 1 and phase 2).[8]

Another type of polymer therapeutics are the defined multivalent dendritic polymers. This includes: (i) polyanionic polymers, which inhibit virus-receptor-interactions or it can be used as heparin analogues, (ii) polycationic polymers, which can form polymer-DNA/RNA-polyplexes and (iii) polymer micelles with covalently bonded drugs and a dendritic core-shell particles for the encapsulation of active substances.[9]

Several examples of dendritic polymers as effector molecules that take advantage of their multiple functionality are described in literature. One example is the microbiocidic substance 'VivaGel' from Starpharma (Melbourne). It is a dendritic polyanion based on a polylysine core, a topical vaginal gel, which might also be able to inhibit HIV or decrease the risk of infection. 'VivaGel' is the first of this kind of dendrimers to enter into phase II human clinical trials.[10,11]

Kissel et al. investigated in PEGylated polyethylene imine (PEI), an example for polycationic polymers, which are used for transport of siRNA in tumor bearing mice.[12] The *in vivo* results demonstrated that these compounds have a good potential in therapeutically applications. However, the toxicity of these systems has to be reduced.

Recently, first polymer-cytostatic conjugates, such as doxorubicin solubilized in liposomes, have started to be applied medically. One of this drug is known as Doxosom® and is commercially available as chemotherapeutic.[13] Another example is the modification of cytostatica with polyethylene oxide (PEO).[14] This modification improves the solubility as well as the transport to the target site.

## 1.2. Dendritic Architectures in Diagnostics and *Theranostics*

For many authors, September 25, 1998, is considered the birth date of *theranostics*[15] as the FDA (Food and Drug Administration) granted the approval for both Genentech's Herceptin® for the treatment of Stage IV breast cancer and Dako's HercepTest® for diagnosis of Her2 overexpression. But rudimentary examples of these first *theranostics* are still a long way from an early diagnosis of diseases on the molecular level.

The goal of *theranostics* is to achieve a close dovetailing between therapy and diagnostics. *Theranostics* should enhance treatment decisions by providing information to clinicians and their patients. The concept of *theranostic* which means "find, fight, and follow", includes an early diagnosis with specific agents to supply an image of individual cells, the supply of active substances, and then follow up with therapy.[16] The main elements of the diagnosis in *theranostics* include determination of the genetic predisposition, characterization of the stage of disease, and monitoring of the healing progress.[17]

In *theranostics*, dendrimers require an external binding to the drug, fluorescent probes for application in *theranostics* (one-package system), and the ability to interact with the target, usually cell walls and/or proteins (Figure 2).

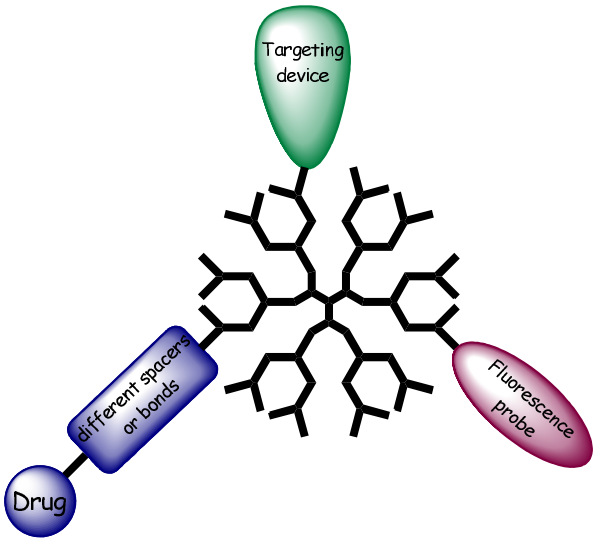


**Figure 2.** Dendrimer properties for theranostic.[18]

Dendritic polymers versatility and compatibility with nanoscale building blocks, such as genetic material, bioactive molecules, and fluorescent probes, make them good candidates for *theranostics*, however.[18] In order to evaluate their true value as multi-functional packages it

is necessary to do comprehensive research *in vivo*. It would be especially attractive to investigate their adsorption and interaction with biological surfaces and to determine the associated uptake mechanisms, long-term effects, and bio-elimination.

Dendrimers and dendritic polymers are emerging as a powerful, multifunctional nanotherapeutic platform for imaging and therapeutic applications. Looking into the future, there are a number of medical needs where multifunctional dendrimers and their derivatives might become important tools, in particular for early detection, diagnosis, and personalized treatment of diseases. It is important to investigate the adsorption and interaction of new multifunctional nanoparticles with malignant materials (such as tissue specimens and circulating tumor cells) to improve their biocompatibility, to test long-term effects, and to standardize the dendrimers and their derivatives for clinical applications which must be done in compliance with US FDA requirements. With regard to the last point, dendrimer based products need further improvement on a high level of productivity with an excellent cost-benefit ratio. VivaGel, Starpharma's dendrimer based microbicide for the prevention of HIV and HSV injection is currently in Phase II clinical trials. These are the first human dendrimer pharmaceutical clinical trials. Baker Jr. and coworkers synthesized a fifth generation polyamidoamine (PAMAM) dendrimer conjugated to fluorescein isothiocyanate for imaging.[19] In these preclinical studies they used recombinant Fibroblast Growth Factor-1 for tumor targeting. These examples show that dendritic polymers will emerge and enter clinical trials in the coming years.

In conclusion, dendrimers may be used as tools for *theranostics* in areas such as the detection and treatment of cardiovascular, cancer, and inflammatory diseases, due to their multifunctional nature. The property of imaging, detection, and treatment of diseases at the same time is interesting for clinical trials. Aside from these advantages issues of safety and complexity must be investigated.

## 1.3. Molecular Imaging

### 1.3.1. Basics of Molecular Imaging

The correct medical diagnosis is an absolute prerequisite for a successful therapy of diseases. The imaging diagnostic is an important tool for depicting the inner structures of the body to ascertain the morphology of organs (morphological diagnostic), functional parameters of body

organs (functional diagnostic), and structures and functions of body tissue on the cellular level (molecular diagnostic).

In the future one of the most promising methods will be molecular imaging which combines conventional imaging with special contrast agents to visualize sickness related changes in metabolism.[20] The hope is to diagnose diseases earlier, if possible, in their preliminary stages. Of special interest is the simultaneous visualization of the effect of a therapy during the therapy.[20] The development of noninvasive, high resolution imaging technologies for *in vivo* diagnostic was a further significant step.[21,22,23]

Specific molecules must satisfy certain criteria for use in *in vivo* studies. Marker molecules must have good pharmacodynamics and be able to overcome biological barriers. There are some known strategies to bypass vascular and interstitial barriers as well as the cell membrane. Weissleder et al. synthesized a PEGylated Gadolinium polymer where the flexible mPEG chains bind to water and create a protective hydrated shell that hinders deposition of complement components.[24] Three years later the same research group could achieve an even distribution by using long circulating markers.[25] Translocation signals were able to induce an active transport of the markers into cells[26] and pharmacological and physical methods improved the targeting.[27] Another essential preliminary for *in vivo* detection of the markers in targeted tissue is a sufficient concentration and a certain length of stay. Fast elimination is necessary to prevent metabolization. In 1999 Weissleder et al. found a strategy to intensify the signal on target.[28] They developed a method to image tumor-associated lysosomal protease activity in a xenograft mouse model *in vivo* using autoquenched near-infrared fluorescence (NIRF) probes. After incubation and binding the probe changed its behavior by enzymatic activation.

Another condition for molecular imaging is a fast and high resolution imaging technique (Figure 3). Two ad dimensional szintigraphy, the single photon emission computed tomography (SPECT), and the positron-emission tomography (PET) are counted among the nuclear medical techniques. Another one is the magnetic resonance imaging (MRI). The third approach is the principle of the optical imaging, which is described in detail below, as it is a major part of this thesis.

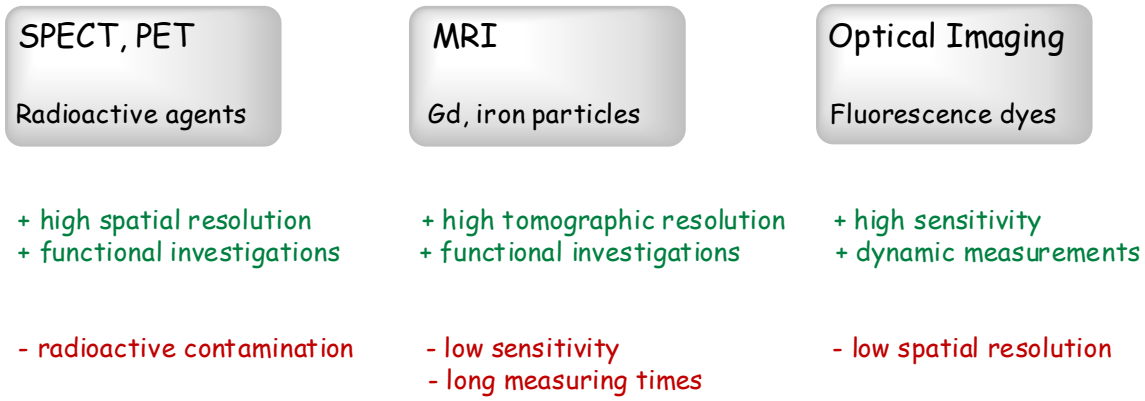


**Figure 3.** Examples for methods of molecular imaging.

### 1.3.2. Optical Imaging

Optical imaging is based on phenomena such as fluorescence, absorption, reflection, and bioluminescence.[20] The *in vitro* studies in the present work are based mainly on fluorescence phenomena. The near infrared (NIR) diagnostic is more advantages than other optical imaging methods. In contrast to visible light, which only penetrates a few millimeters in tissue,[29] light of the NIR region has a larger penetration depth of several centimeters. This can be caused by a low absorption of tissue, hemoglobin, and water in the long-wavelength range which is also called *"diagnostic window"*. For these methods dyes with an absorption- and emission spectrum in the near infrared range between 650-900 nm are used.[30] Additionally, because the autofluorescence of tissue in this region is relatively low, the images has better contrast.[31] Therefore the optical imaging is a promising method to investigate structures non-invasively.[32] Gene expression pattern, metabolic functions, and molecular changes of cells as well as individual molecules can be detected and analyzed high specific.[33] Licha et al. demonstrated that fluorescence dyes as parenterally administered as contrast agents improved the diagnostic significance of optical imaging in investigations of rheumatoid arthritis.[34]

## 1.4. Fluorescence Dyes for *in vitro* and *in vivo* Imaging

The importance of light in the medical diagnostics has increased in recent years (e.g. in endoscopy, mammography, surgery, and gynecology). Light-based procedures have a high instrumental sensitivity. Even small quantities of chromophores and fluorophores afford molecular detection and imaging.[20] Of special interest in the context of *in vivo* studies are dyes, which are supplied as exogenous contrast media, for fluorescence diagnosis and

imaging of the tissue. Fluorescence dyes are particularly demanded which have absorption and fluorescence maxima in the spectral region of 700 - 900 nm.

For a good contrast for *in vivo* and *in vitro*, some conditions have to be obtained: photochemical and chemical stability, high absorption coefficient, high quantum yield, photosensitization, good water solubility, and low toxicity.[35,36,37]

### 1.4.1. Cyanine Dyes

The visualization of tumors can be achieved by the administration of structurally simple fluorescent dyes. The group of polymethines and cyanine dyes, respectively, have come to be regarded as promising contrast agents.[38] In the 1970s Indocyanine Green (ICG) was the first fluorescent dye and diagnostic drug to be used for optical imaging in tumors, both in animal studies and for patients.[34] ICG is a tricarbocyanine dye which has been used in the indicator dilution technique for measuring cardiac output.[39] It is an organic dye with application in several distinct areas. In lasers, it is used as the active medium[40] and as a saturable absorber.[41] In medicine, ICG has been mainly used for diagnosis[42] and photodynamic therapy (PDT) in the treatment of cancer.[43,44]

Carbocyanine dyes, which have visible to near-infrared absorption and fluorescence (approx. 450-900 nm), generally exhibit high molar extinction coefficients (>150,000 $M^{-1}$ $cm^{-1}$) and good fluorescence quantum yields (up to 50%). They were originally used in the photographic industry and have also been designed as probes for a host of applications in analytical chemistry, biophysics, bioanalytics, and biomedicine.[45,46] The CyDyeTM-series (e.g. Cy3, Cy5, Cy5.5, Cy7) is commercially available (Amersham Pharmacia Biotech, Freiburg, Germany). Depending on the length of the polymethine chain (3, 5, or 7 atoms) a fluorescence maximum of 580, 680, and 780 nm can be detected. According to the individual requirements, the suitable dye can be selected (Figure 4).

For this work Indocarbocyanine-maleimide (ICC-mal, mivenion GmbH), Indotricarbocyanine-maleimide (ITCC-mal, Bayer HealthCare, Bayer Schering AG), and a Cy5.5 derivative (mivenion GmbH) (Figure 4) have been used for coupling with different sizes of amino-bearing hyperbranched polyglycerols (HPG).

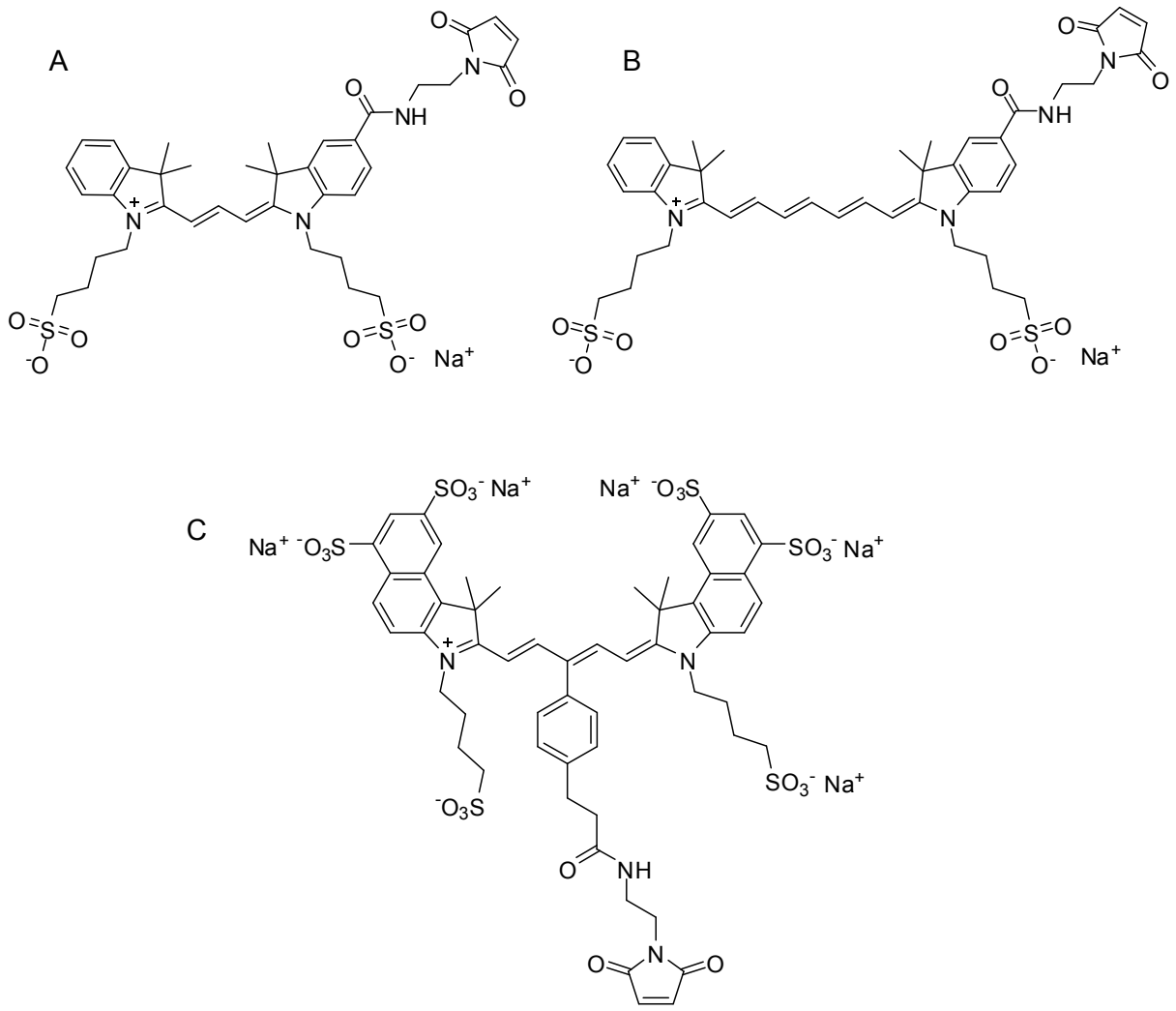


**Figure 4.** Indocarbocyanine-maleimide, ICC-mal (A), Indotricarbocyanine-maleimide, ITCC-mal (B), and the Cy5.5 derivative (C).

With regard to this thesis, HPG-indocarbocyanine was used for size-dependent cellular uptake in different cancer cell lines, for visualizations of intracellular mechanisms, and for receptor-mediated endocytosis studies. The HPG-indotricarbocyanine and the HPG-Cy5.5 derivative were injected into mice with a human colon carcinoma cell line and implanted subcutaneously.

## 1.5. Biological Scenario

The surface decoration of dendritic nanostructures with solubilizing agents and targeting moieties, along with imaging and therapeutic modalities, together with the inherent charge

profile of the dendritic polymer, confers structural benefits such as faster cellular entry, reduced macrophage uptake, targetability, and easier passage across biological barriers by trancytosis.[47] In addition, their branched nature has been shown to improve the *in vivo* application profile in comparison to linear polymeric analogs. For instance, increasing the number of branches or arms for polymers with similar MW and chemistry has increased the blood circulation half-life. A systematic study with a library of PEGylated polyester "bow tie" dendrimers established the relationship between branching and blood circulation time.[48,49] For a series of bow ties with equivalent MW (~ 40 kDa), there was an increase in $t_{1/2}$, from 1.4 ± 0.4 h for the two-arm dendrimer, essentially a linear polymer, to 26 ± 6 h for the four-arm dendrimer, and finally to 31 ± 2 h for the eight-arm dendrimer. Corresponding biodistribution studies in healthy mice showed no significant variation in tissue uptake among the three polymers and decreased polymer excreted in the urine with increased branching. This polymer drug carrier that was studied in C26 colon carcinoma bearing mice showed long blood circulation times and remarkable efficacy in delivering the chemotherapeutic drug doxorubicin to tumors which led to their complete disappearance in sharp contrast to the free drug, which itself was ineffective.

The aforementioned example illustrates one of the many environmental biological challenges that dendritic polymers face. In the following sections a brief description of the biological scenario will be in regard to the passive and active targeting of dendritic polymer systems to malignant cells and tissues is presented.

### 1.5.1. Particular Features of Malignant Tissues

The term tumor is generally used for an uncontrolled growth of the body's own tissue. Malignant tumors grow into surrounding tissue and destroy local structures. By means of the blood stream or lymphatic fluid tumors can spread in every body region, which is called metastasis formation. Tumors often occur after surgeries and cannot be removed completely. Therefore, in most cases chemotherapy and permanent controls are necessary. For this reason several working groups are investigating in the development of multivalent active agents. Structure defined multivalent and dendritic polymers allow the production of customized self-organized systems or polymer therapeutics.[50] The aim is the right therapy for the right patient at the right time or, in other words, diagnostics is accompanied by therapy which is expressed by the term *theranostics* (*thera*py and diag*nostics*).

### 1.5.2. Passive and Active Targeting

The targetability of dendritic polymers systems to malignant cells and tissues can be achieved by adopting either of the following two approaches: passive targeting and active targeting.[51]

In the passive targeting approach, the dendritic system mediates and localizes delivery of bioactives directly to the cell/tissue as a consequence of the environmental conditions in the malignant tissue. It is well-recognized that tumor microvascular endothelium is more leaky than healthy tissue which results in much greater permeability for macromolecules.[52] Furthermore, tumor tissue is characterized by ineffective lymphatic drainage.[53] The combination of the above characteristics, along with the hypervascularization evident in the tumor microenvironment, leads to an accumulation of low molecular weight drugs coupled with high molecular weight nanocarriers in tumors. This so-called enhanced permeation and retention (EPR) effect[53,54,55,56] is depicted schematically in Figure 5. In this type of passive targeting the macromolecules accumulate in tumor tissue to a greater extent than in healthy tissue.[57] The EPR effect is predominantly observed for biocompatible macromolecules, macromolecular drugs, and lipids in solid tumors.[58]

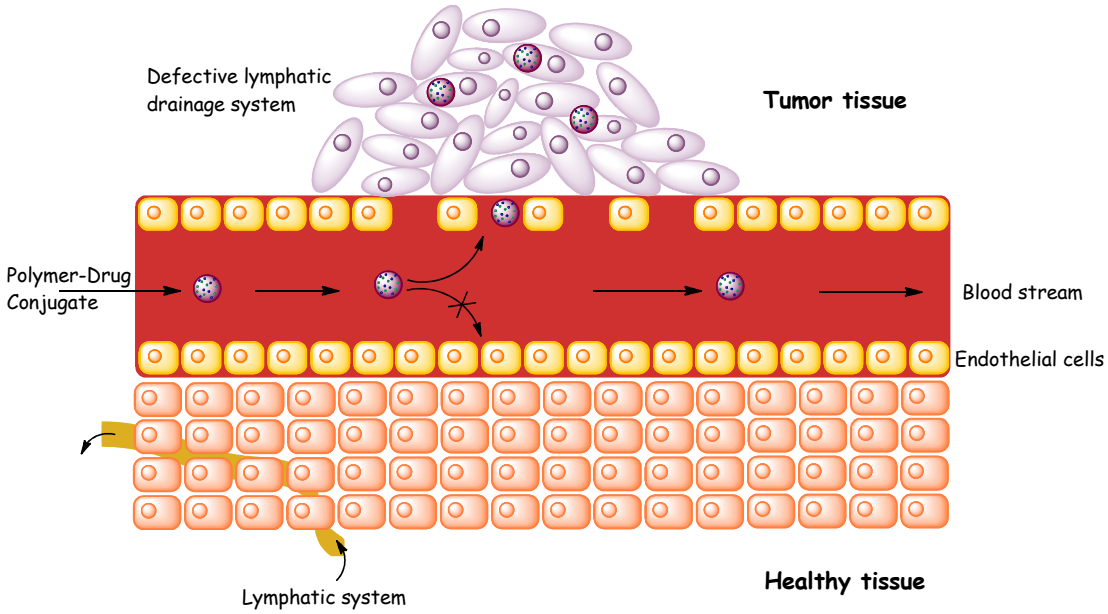


**Figure 5.** Schematic representation of the EPR effect.[57]

The size of the macromolecule is a crucial factor with respect to uptake to the tumor. Following the pioneering work of Maeda, many other groups[59,60,61] were later able to show that polymeric drugs with a molecular weight above the renal threshold (i.e. >40 kDa) accumulate in tumor tissues for prolonged time periods following i.v. injection. Liposomes,

micelles, and polymeric nanocarriers are the most extensively studied drug carriers and possess the most suitable characteristics for encapsulation of many drugs and diagnostic (imaging) agents.

Active targeting of a dendritic system is usually achieved by coupling a targeting component on a dendritic polymer that provides preferential accumulation of the entire drug-delivery system on the bioactive molecule in an organ bearing a malignant tissue in the tissue itself, in malignant cells, or in intracellular organelles of specific malignant cells.[62] The active targeting approach is based on the interactions between a ligand and its cognate receptor or between specific biological pairs (e.g., avidin biotin, antibody-antigen, sialic acid-carbohydrate).[63] In most cases, a targeting moiety in a dendritic polymer is focused on the specific receptor or antigen overexpressed in the plasma membrane or intracellular membrane in the malignant cells.

A good example why dendritic polymers are good candidates has been reported by Hashida et al.[64] They synthesized a sixth generation lysine dendrimer (KG6) and two PEGylated derivatives for tumor selective targeting after intravenous injection in tumor bearing mice. The studies have shown that the PEGylated KG6 conjugates effectively accumulate in tumor tissue by the EPR effect. Many other examples will be explored in the following sections.

### 1.5.3. Cellular Entry (Endocytosis)

In recent years a number of research groups have demonstrated the potential of dendrimers to enhance the cellular delivery of drugs through endocytosis.[65,66]

Endocytic pathways are subdivided into pinocytosis, the uptake of fluid and solutes, and phagocytosis, the uptake of large particles. Phagocytosis is the process of engulfing and destroying extracellularly derived material by a phagocytic cell, such as a macrophage, neutrophil, or amoeba. The pinocytosis includes four basic mechanisms: macropinocytosis, clathrin-mediated endocytosis, caveolae-mediated endocytosis, and clathrin and caveolae independent endocytosis (Figure 6).[67,68]

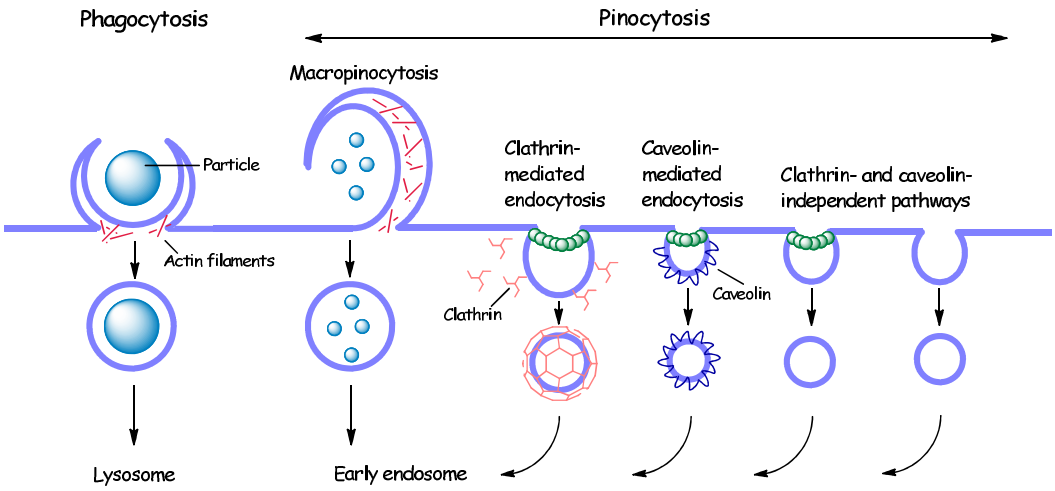


**Figure 6.** Entry of material into cells *via* phagocytosis for engulfing large particles or *via* different ways of pinocytosis for small particles which implies macropinocytosis, clathrin- and caveolin-mediated endocytosis, and clathrin- and caveolin-independent pathways (modified from Kitchens, 2007).

Cells overcome the scarcity or lack of essential nutrients in the environment by expressing high affinity receptors or binding sites on the membrane surface. In case of the receptor mediated process of phagocytosis, the receptors function as adhesive elements that bond the plasma membrane to the particle. As a result, surface membranes contain actin binding proteins that link the phagocytic receptor to the actin cytoskeleton of the cell.

Invagination produces a vesicle called phagosome, which usually fuses with early, then late endosomes, and finally with lysosomes to yield a phagolysosome.[69] In the case of pinocytosis, macropinocytosis is a cell-type specific and a receptor independent endocytic pathway. The function of receptor mediated endocytosis is diverse. It is widely used for the specific uptake of certain substances required by the cell. The best studied endocytosis mechanism is clathrin-mediated endocytosis,[70,71,72] which is the uptake of receptors, membrane, and cargo at the cell surface through a process that specifically involves the coat protein clathrin. Clathrin coated vesicles are found in virtually all cells and from domains of the plasma membrane termed clathrin coated pits. Caveolae mediated endocytosis is a form of uptake at the plasma membrane that involves the protein caveolin.[73] A third pathway, which is both clathrin and caveolae independent, may constitute a specialized high capacity endocytic pathway for lipids and fluid.[74]

Dendrimers have been shown to be a good model for use as potential carrier/delivery systems. Duncan et al. reported that poly(amido amine) (PAMAM) dendrimers generation 2.5 and 3.5 had particularly rapid serosal transfer rates and a low tissue deposition indicating a

very efficient transport pathway.[75] D'Emanuele et al. demonstrated that G3 PAMAM dendrimers and lauroyl-G3 PAMAM dendrimer conjugates could be visualized in individual endocytotic vesicles at the apical domain of the cell and their association with multivesicular bodies in the cell interior.[76]

The size effect on cell uptake of nanoparticles is an important parameter in designing suitable celltracking and drug-carrier nanoparticle systems, because it determines the mechanism and rate of cell uptake of a nanoparticle and its ability to permeate through tissue.[77,78] Independent of many factors, such as surface chemistry, charge, and size, which will affect the uptake, the cell uptake of liposomes,[79] quantum dots,[80] and polymeric,[81,82] gold,[83] and silica nanoparticles[84] has been found to be size-dependent.

### 1.5.4. Blood Compatibility

Good blood compatibility and low cytotoxicity are important biocompatible concerns in potential applications of dendrimers and other polymers as drug carriers. Which means higher molecular weight also leads to a reduced excretion through the kidneys. The polymeric transport system stays in the bloodstream longer. During this time an immune reaction should not initiate or the polymer/cargo might be eliminated out of the body. Good toxicological findings and the success of PEG in drug-transport applications have substantial the use of PEG in medical areas.[58] For example, for better blood compatibility with polyvinyl chloride bags PEG can be used for blood conserves.[85] Recently, Brooks et al. tested hyperbranched polyglycerols in blood compatibility studies on significant effects in complement activation, platelet activation, coagulation, erythrozyte aggregation, and hemolysis and found them to be highly blood compatible.[86,87] In addition, they have investigated the blood compatibility of hyperbranched PG based polymers containing multivalent cationic sites.[86] In comparison to standard cationic polymers such as PEI, PG based polymers showed much lower cytotoxicity and cytotoxicity. Because of their high blood compatibility in regard to hemolysis, erythrocyte aggregation, complement activation, platelet activation, and coagulation, they are potential candidates for polymer therapeutics.

## 1.6. Hyperbranched Polymers

As repeating reactions tends to be costly, hyperbranched polymers have emerged as an alternative. In this context, Figure 7 shows structures which may not be perfectly branched but can be prepared conveniently in one-step procedures *via* polyaddition, polycondensation, and radical polymerization, etc., on kilogram scale.

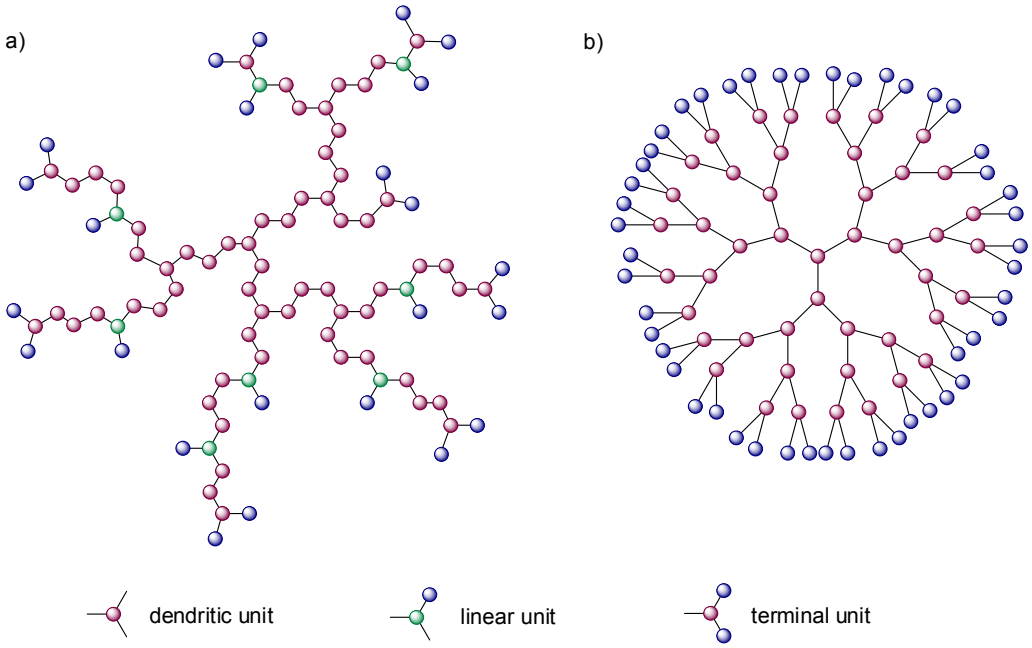


**Figure 7.** Structure of (a) a hyperbranched polymer and (b) a perfect dendrimer with dendritic, linear, and terminal units.

Hyperbranched and perfect dendrimers exhibit similar chemical and physical properties such as high functionality due to their large number of end groups and a high degree of branching that prevents crystallization, low melt, low solution viscosity, etc.

Historically, hyperbranched polymers can be dated back into the end of the 19$^{th}$ century when Berzelius[88] reported on the formation of a resin resulting from the reaction of tartaric acid ($A_2B_2$ monomer) and glycerol ($B_3$ monomer). In 1901 Watson Smith reported from reactions between phthalic anhydride (latent A2 monomer) or phtalic acid (A2 monomer) and glycerol (B3 monomer).[88] The first commercial polymers were phenolic polymers, introduced by Baekeland in 1909.[89] In the 1940s Flory et al.[90,91,92] developed the "degree of branching" and "highly branched species" concepts which resulted from the usage of statistical mechanics to calculate the molecular weight distribution of three-dimensional

polymers with trifunctional and tetrafunctional branching units in the state of gelation. A few years later, in 1952, Flory investigated a one-step process where an $AB_x$-type monomer underwent self-condensation polymerization and resulted in a branched product.[93] The first successful approach of a targeted synthesis of hyperbranched polymers was described by Kricheldorf et al. in 1982 which was based on the copolycondensation of 3-hydroxybenzoic acid and 3,5-dihydroxybenzoic acid.[94] The interest in hyperbranched polymers increased after the catalytical condensation of polyphenylene by Kim and Webster in 1988.[95] These polymers are characterized by their extremely high solubility in organic solvents. However, the molecular weight just ranges in the interval of 3000-6000 g/mol. Some years later Fréchet et al. synthesized hyperbranched polyether with molecular weights between 16000-55000 g/mol.[96] They presented a synthesis of macromolecules without many side reactions, a high yield, and high molecular weights.

Since then, hyperbranched polymers are in the focus of many research teams. Nowadays, hyperbranched polymers are commercial available, for example, Boltorn® (aliphatic polyesters; Perstorp Group, Perstorp, Sweden), Hybrane® (poly(ester amides); DSM Fine Chemicals, Geleen, Netherlands), Polymin® and Lupasol® (poly(ethylene imines); BASF AG, Ludwigshafen, Germany), and Polyglycerol® (aliphatic polyethers; Hyperpolymers GmbH, Freiburg, Germany).

### 1.6.1. Hyperbranched Polyglycerols

The Haag group has focused its attention on the study of dendritic polyglycerols (PGs, Figure 8), which is glycerol based macromolecular architectures with a high degree of branching and end group functionalities. They have compact, well-defined, dendrimer mimicking structures that show appreciable aqueous solubility, facile one-pot synthesis in large scale, and substantially low tissue toxicity. Due to their low degree of molecular weight variation, flexible design, and biocompatibility profile, dendritic polyglycerols have also found a broad range of potential applications in medicine and pharmacology. [97,98,99,100,101]

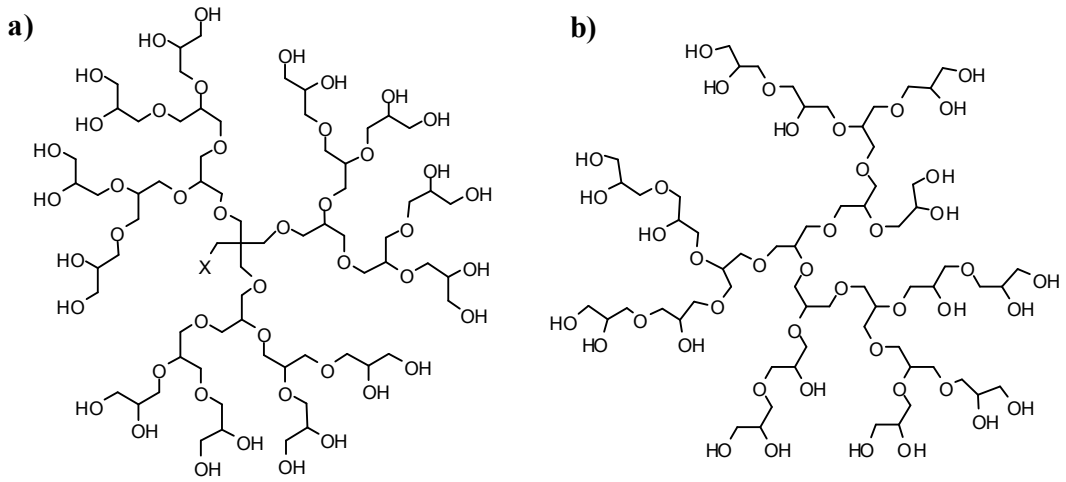


**Figure 8.** (a) Perfect polyglycerols dendrimer. (b) Hyperbranched polyglycerol. The depicted polymer structure represents only one possible isomer and a small part of the polyglycerol scaffold.

Hyperbranched polyglycerols are flexible hydrophilic polyethers which are non-toxic, biocompatible, easy to synthesize, and can be obtained in kilogram scale.[98,99] They represent an architecture of macromolecules with a high degree of branching, high-end group functionality and a compact, well-defined dendrimer-like architecture.[102] They can be obtained with molecular weights between 1,000 and 870,000 g/mol with polydispersities $M_w/M_n$ typically below 1.5, and are therefore suitable as supports for organic synthesis and drugs.[103] The structure of the hyperbranched polyglycerol is characterized by exactly one core unit with multiple hydroxyl groups randomly incorporated as linear (OH groups) and terminal groups (1,2-diols). The total density of similar functional groups in polymers is 13.5 mmol OH per g polymer, of which approximately 60% (8.2 mmol OH per g) are terminal 1,2-diols. These terminal diols (see below) can directly be used as linker functionalities for many applications in organic synthesis.[104] Additionally, the OH groups may further be functionalized with other reactive groups, e.g. amino groups allowing the attachment of a variety of bioactive molecules. Moreover, substances may also be incorporated into the dendritic polymer.

One research area of the Haag group is dendritic PGs as functional dendritic architectures with particular area on their application in drug, dye, and gene delivery. The application of nanotechnology in medicine and pharmaceuticals is a rapidly advancing field that is quickly gaining acceptance and recognition as an independent area of research called ‘‘nanomedicine’’. Urgent needs in this field, however, are biocompatible and bioactive materials for antifouling surfaces and nanoparticles for drug delivery. Therefore, extensive

attention has been given to the design and development of new macromolecular structures. Among the various polymeric architectures, dendritic (‘‘treelike’’) polymers have experienced an exponential development due to their highly branched, multifunctional, and well-defined structures.

Due to their low degree of molecular weight dispersity, their flexible design, and their biocompatible nature, dendritic polyglycerols (PGs) have emerged as scaffolds with a broad range of potential applications in medicine and pharmacology. These polymers exhibit good chemical stability and inertness under biological conditions and are highly biocompatible. Their high chemical functionality allows the coupling of multiple copies of solubilizing groups, bioactive molecules, and chemical entities toward the design of stimuli-responsive nanostructures.

The Haag group recently reviewed different mechanisms of transport, passive/active targeting, and smart delivery and release of the bioactives at the site of action performed by dendritic polymers.[105] Based on other studies about the increasing development of maleimide-bearing prodrugs and diagnostic dyes,[106,107] the Haag research group synthesized thiolated HPG nanocarriers to couple diagnostic or therapeutic agents under physiological conditions.[108,109]

Another project in the Haag group is the preparation of several hyperbranched PGs (10 kDa) with (6-maleimidocaproyl)hydrazone derivative of doxorubicin (DOXO-EMCH).[110] The conjugates showed a lower cytotoxicity than the corresponding free drugs and manifested very good antitumor effects with complete tumor remission up to day 30 without significant changes in body weight.

Another outstanding example is dendritic polyglycerol sulfate (dPGS, Figure 9), primarily reported as an heparin analog by the Haag group,[111] which has emerged as a potential new antiinflamatory agent based in a dendritic polymer.

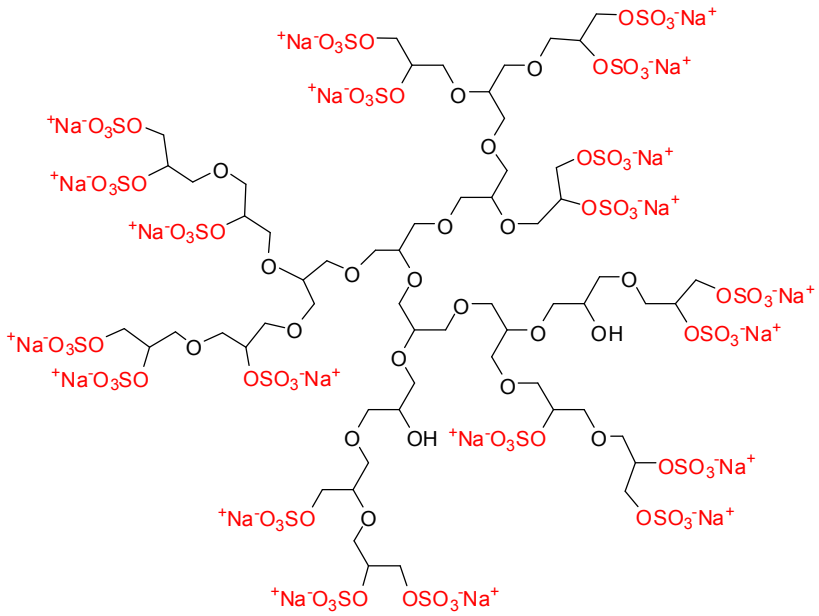

**Figure 9.** Representative and idealized structure of dendritic polyglycerol sulfate (dPGS). Sulfate endgroups are shown in red.

These structures have been found to prolong the time of activated partial thromboplastin as thrombin and to inhibit both the classical and alternative complement activation more effectively than heparin itself. The biocompatible and well tolerated PG sulfate acts as a multivalent selectin ligand mimetic and efficiently blocks leukocyte migration (Figure 10).[112]

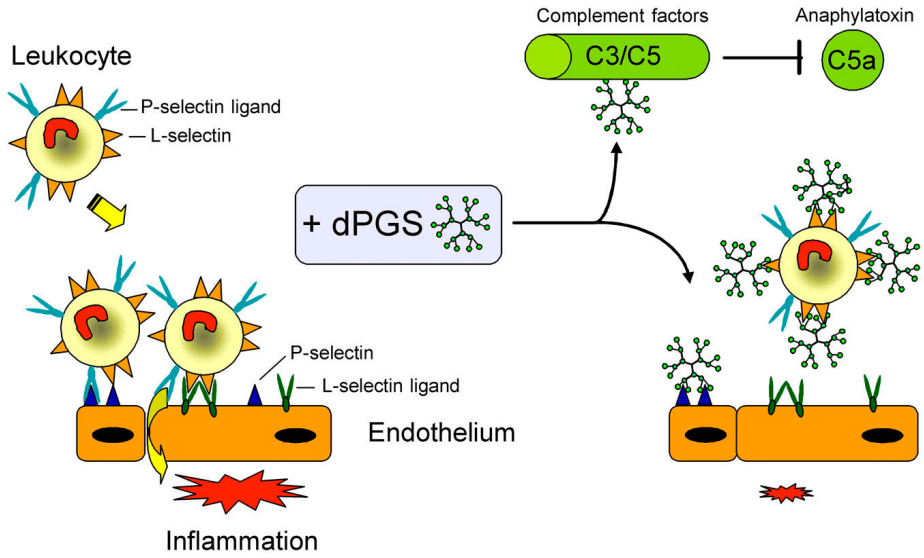


**Figure 10.** The decrease of the inflammatory response is a result of different interactions of polyglycerol sulfate, which binds to L-selectin on leukocytes and P-selectin on inflamed vascular endothelium and reduces leukocyte extravasation by shielding the adhesion molecule. Adapted from ref. [112].

In a preliminary study, HPGs with a different degree of amino functionalization (10, 20, and 30%) were successfully coupled with photosensitizers for the photodynamic therapy (PDT) as another stimuli-responsive system where the light of specific wavelength is used to trigger the therapeutic activity.[113,114]

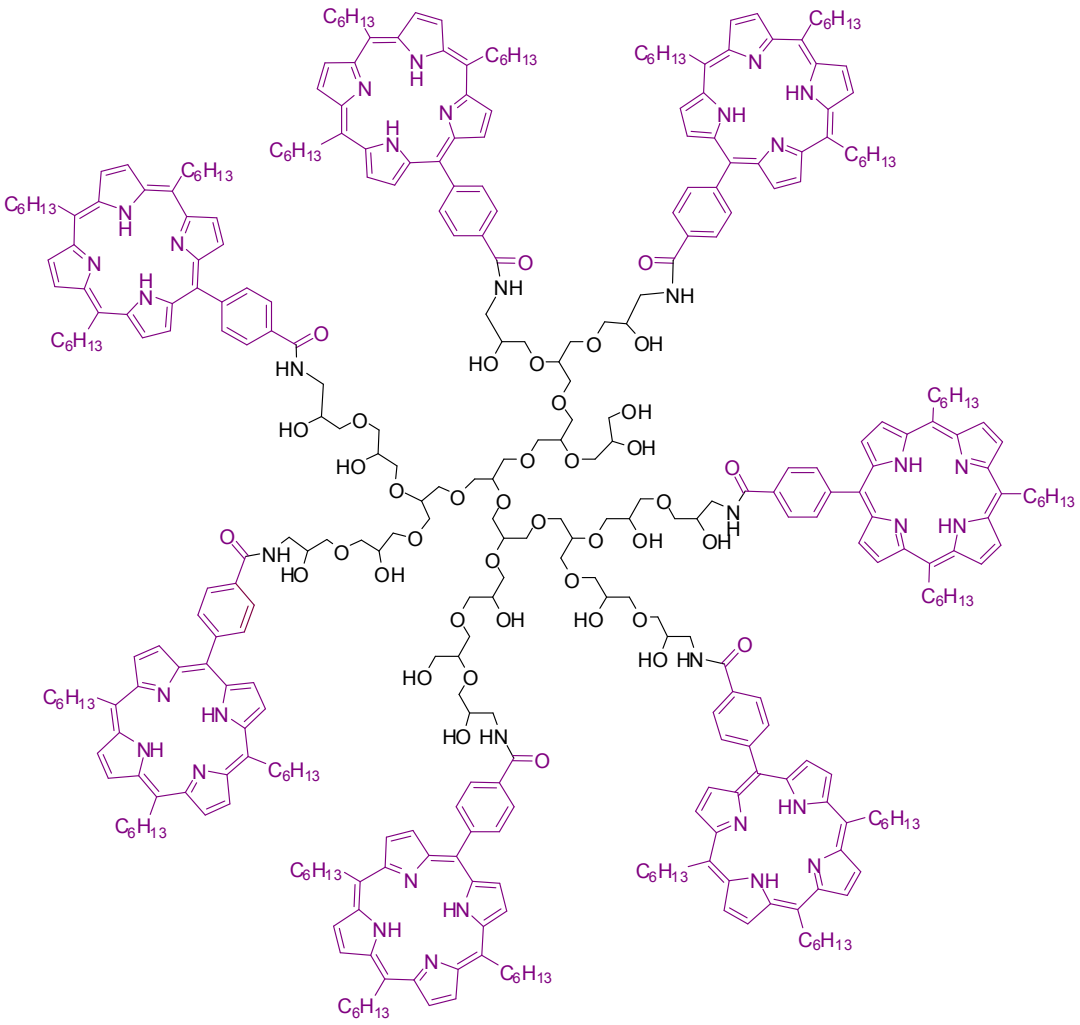

**Figure 11.** Porphyrin-bearing HPG. The depicted polymer structure represents only a small part of the polyglycerol scaffold.

These conjugates were tested for their PDT effect in human colon carcinoma cell line (HT29). The results render these conjugates possible candidates for the development of new photosensitizer carrier systems.

A new class of dendritic architectures are the dendritic core-shell systems. Based on a dendritic polymer core and a biocompatible shell, novel nanotransporter for dyes and active substances have been developed. Genetic active agents, like siRNA are very sensitive in *in vivo* applications (rapid degradation *via* RNases in blood) and because of the charged

structures the target cell uptake is not so easy. In a recent publication,[115] we reported the high siRNA transfection efficiency and low toxicity of dendritic polyglycerols with oligoamine shells in *in vitro* studies (Figure 12).

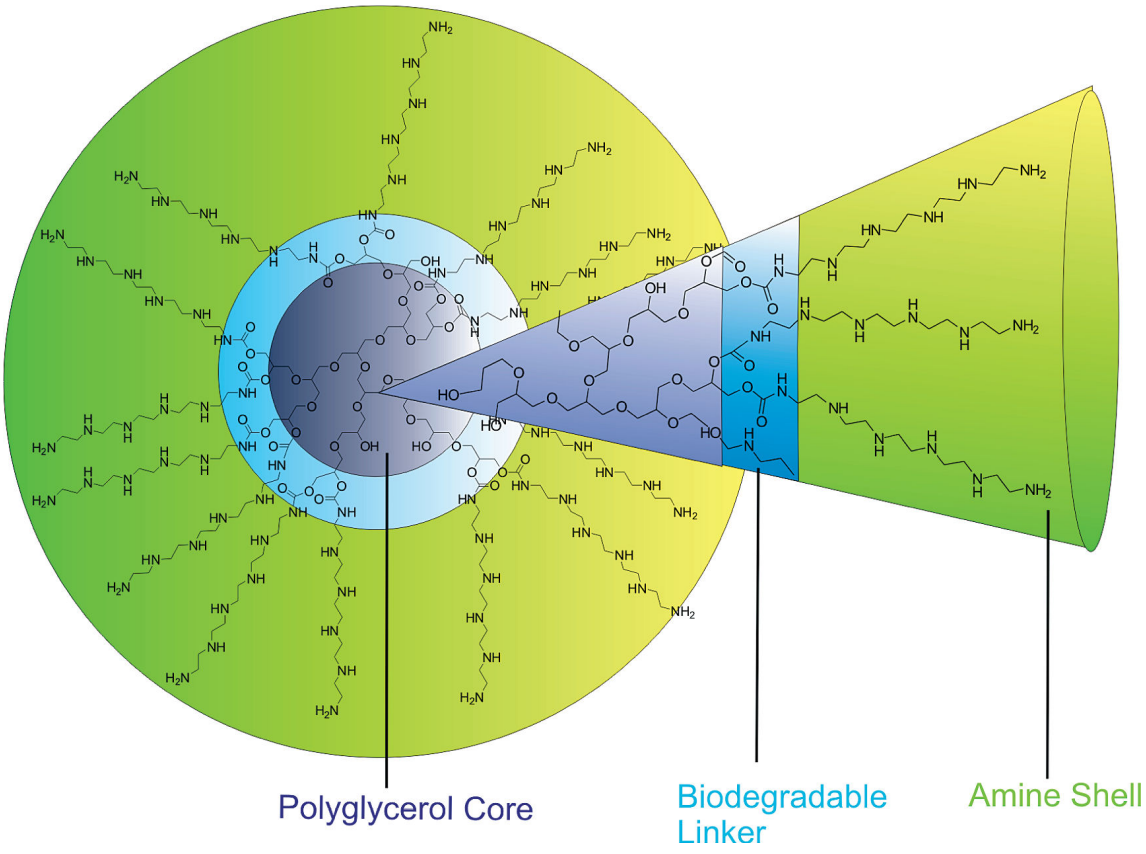


**Figure 12.** The core-shell architecture based on HPG with an acid-labile amine shell. The represented structure shows only a small idealized fragment of the core-shell architecture. Adapted from ref. [115].

It was observed that these new siRNA-nanocarriers show very low levels of toxicity as no significant weight loss was observed after intravenous administration of the polyplexes. Due to their high biocompatibility these nanocarriers are potential candidates for *in vivo* applications and are currently under investigation.

Since the identification of the short peptide sequenze of Arg-Gly-Asp (RGD) as a cell recognition sequence of fibronectine, the investigation of proteins increased.[116] Gyongyossy-Issa and coworkers[117] coupled RGD to hyperbranched PGs *via* a divinyl sulfone linker and were able to show an increase in platelet inhibitory function of RGD.

Kannan and coworkers presented the use of hyperbranched PG as a scaffold in the synthesis of polymer-drug conjugate containing high ibuprofen loading for enhancement of cellular uptake.[118]

The development of polymer therapeutics is an exciting field of research and provides the opportunity to improve the toxicity and efficiency of active substances. Hyperbranched polyglycerols include the particular features of biocompatibility and multiple functionalities. For all these applications the size of the macromolecules is a decisive factor for the uptake in cells or tumor tissue. Therefore this research project examined size-dependant cellular uptake of HPG for *in vitro* and *in vivo* studies, as well as the intracellular mechanism of these conjugates and the receptor-mediated endocytosis with specific peptides.

*A few sections of this part of the thesis are an excerpt of the book chapter published in the following book:*

S. Reichert, M. Calderón, K. Licha, R. Haag: *"Multivalent Dendritic Architectures in Theranostics"* in "Multifunctional Nanoparticles for Medical Applications - Imaging, Targeting, and Drug Delivery", 2010, Springer book chapter, submitted.

# 2. Objective of the Thesis

Dendritic polyglycerols are already being used as carrier systems in many biomedical applications, although with the disadvantages of costly synthesis and purification of the desired products. This makes it more difficult for a widely practical use as pharmaceuticals. Hyperbranched polyglycerols in contrast can be an interesting choice, because of their simpler synthesis and similar properties to perfect dendrimers. In the past few years optical imaging with light in the near infrared range has become increasingly important. Parallel to the technical progress a large number of fluorescent dyes, in particular cyanine dyes, allow a sensitive detection of molecular targets *in vivo* and *in vitro*.

In the present work, the scientific goal was to synthesize different sizes of hyperbranched polyglycerols coupled with various fluorescence dyes and proteins for *in vitro* and *in vivo* studies. The preparation of a library of HPGs starts with emulsion polymerization to obtain well defined polymers with molecular weights up to 1000 kDa and with narrowly polydispersities (PDI = 1.1-1.4). The resulting polymers shall be substituted to low amino-bearing polymers, for a continued good aqueous solubilization, low toxicity and for more suitable end groups.

The thesis can be divided into four parts:

1. Amino bearing hyperbranched polyglycerols should be synthesized with different molecular weights and for investigation of size-dependent cellular uptake with these conjugates (Figure 13, A). Based on these findings, in future research it should be pointed out towards combining HPG-dye conjugates with active targeting molecules for receptor-mediated endocytosis to better understand the cellular uptake mechanism for this type of polymer.

2. For a better understanding of the intracellular mechanism of hyperbranched polyglycerols, HPG-dye conjugates should be labeled with different specific markers for cell organelles (Figure 13, B).

3. Because of the results in the first aspect it is of further interest to synthesize low molecular weight HPG-peptides for active uptake *via* receptor-mediated endocytosis (Figure 13, C).

4. To complete the picture of HPG-dye conjugates the next goal should be to design ITCC- and Cy5.5-labeled hyperbranched polyglycerols for *in vivo* studies (Figure 13, D).

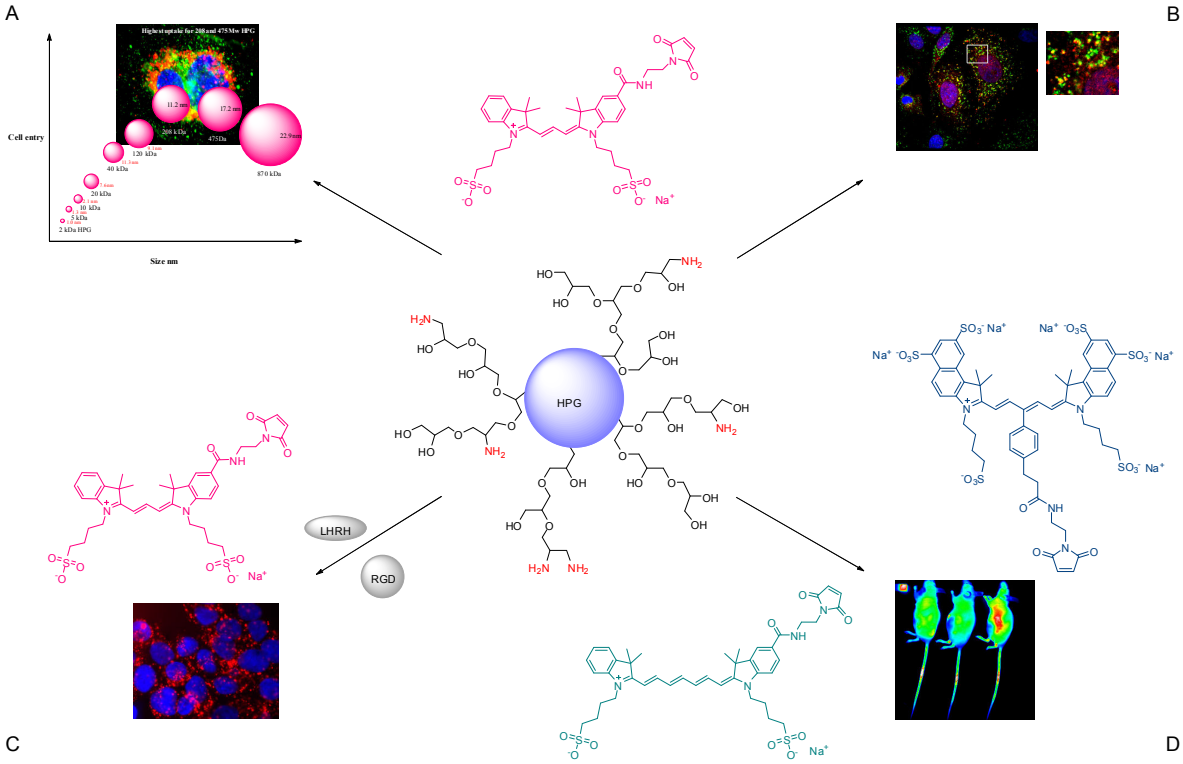


**Figure 13.** (A) Size-dependant cellular uptake of hyperbranched polyglycerol with ICC-mal. (B) HPG-ICC conjugate for investigation of cellular mechanism. (C) Receptor-mediated endocytosis with peptides. (D) *In vivo* studies with HPG-ITCC/Cy5.5 conjugates.

The conjugates are characterized by UV/Vis, fluorescence-profile, zeta potential, and dynamic light scattering. The uptake mechanism was critically studied by FACS (fluorescence-activated cell sorting) analysis, fluorescence, and confocal microscopy with human lung cancer cells A549, human epidermoid carcinoma cells A431, and HUVEC cells. For *in vivo* studies laboratory mice with genetic mutation inhibited immune systems (absent thymus) with a human colon carcinoma cell line, that was implanted subcutaneously, were used.

# 3. Size-dependent Cellular Uptake of Hyperbranched Polyglycerol-Dye Conjugates

In recent years, there has been an increasing interest in dendrimers. The exceptional structural precision of dendrimers has led to a variety of applications in biomedical science. Disadvantages, however, are their tedious multistep syntheses which make them expensive. Therefore, it is a major barrier to any bulk commercial applications.

Approximately twelve years ago, Sunder et al.[99] described the synthesis of the first hyperbranched polyglycerol that can be prepared in a controlled synthesis *via* anionic ring-opening multibranching polymerization (ROMP) of glycidol, carried out under slow monomer addition (SMA) conditions and partial deprotonation of the initiator. The molecular weight of these polymers has been obtained up to $M_n$ = 24000 g/mol under fully controlled conditions and the polydispersities were in the range of 1.3 to 1.8.[119] Recently, Brooks and coworkers presented a new strategy for the synthesis of hyperbranched polyglycerols (HPGs) with higher molecular weights (up to 700 kDa) and a polydispersity index typically within 1.1-1.4 when using dioxane as an emulsifying agent in the ring-opening polymerization of glycidol.[120] The authors explained the narrow polydispersities with the comparably low polarity of dioxane and the accordingly accelerated cation exchange. The results demonstrated that these polymers have spherical conformations in water with no indications of aggregate formation, show low intrinsic viscosities, and small hydrodynamic radii.

Hyperbranched polyglycerols (HPGs) exhibit all the attributes for therapeutic applications[9] and tissue engineering.[121] These polymers are simple and inexpensive to synthesize, noncytotoxic, easy to functionalize, and show excellent biocompatibility.[122] Using these hyperbranched polymers as multifunctional nanocarriers for imaging, drug delivery, and other applications in polymer therapeutics is a current topic of considerable interest.

To investigate the dependency of polymer size on cellular uptake of HPG conjugates, both low molecular weight HPGs were prepared by the Sunder strategy and high molecular weight HPGs were synthesized by the procedure based on emulsion polymerization.

## 3.1. Synthesis of different molecular weight hyperbranched polyglycerols

The controlled synthesis of hyperbranched polyglycerol by anionic ring-opening polymerization of glycidol was developed by Sunder et al.[99,123] and has been improved and enabling the synthesis of polyglycerols **1** with higher molecular weight ($M_n$ = 2, 5, 10, 20 kDa, Scheme 1a). This was prepared according to the previously published procedures of Haag and coworkers.[124,125] Generally, a starter molecule with multiple OH groups is partially deprotonated with potassium *tert* butylate (KO$^t$Bu). Glycidol in tetrahydrofuran (THF) was added drop-wise over a period of 18 h at 120 °C to the homogeneous solution of dipolar aprotic and base-stable *N*-methylpyrrolidone (NMP), THF, and initiator. Through the use of a polymerization reactor it is possible to reduce the consumption of THF. One of the major disadvantages of the synthesis of hyperbranched polymers is their large polydispersity.[126] Under these conditions it is also not possible to synthesize hyperbranched polymers with very high molecular weights above 20 kDa with low polydispersities.

Brooks et al. improved this polymerization and described the synthesis by emulsion polymerization (Scheme 1b) to obtain well-defined HPGs with molecular weights up to 1000 kDa and narrow polydispersities (PDI = 1.1-1.4).[120] In this synthesis diethylene glycol dimethyl ether (diglyme) or 1,4-dioxane were used as emulsifying agents to reduce the viscosity of the polymerization mixture. Glycidol was added drop wise over a period of 12 to 15 h using a syringe pump (Figure 14). The polydispersity could be reduced by removing the low molecular weight fraction by dialysis against water. Compared to polymerization in solution the lower intrinsic viscosity explained the high degree of emulsion polymerization. The polymers were characterized by a GPC/MALLS system and a triple detector system containing a refractive index detector, right angle light scattering detector, and a viscosity detector.

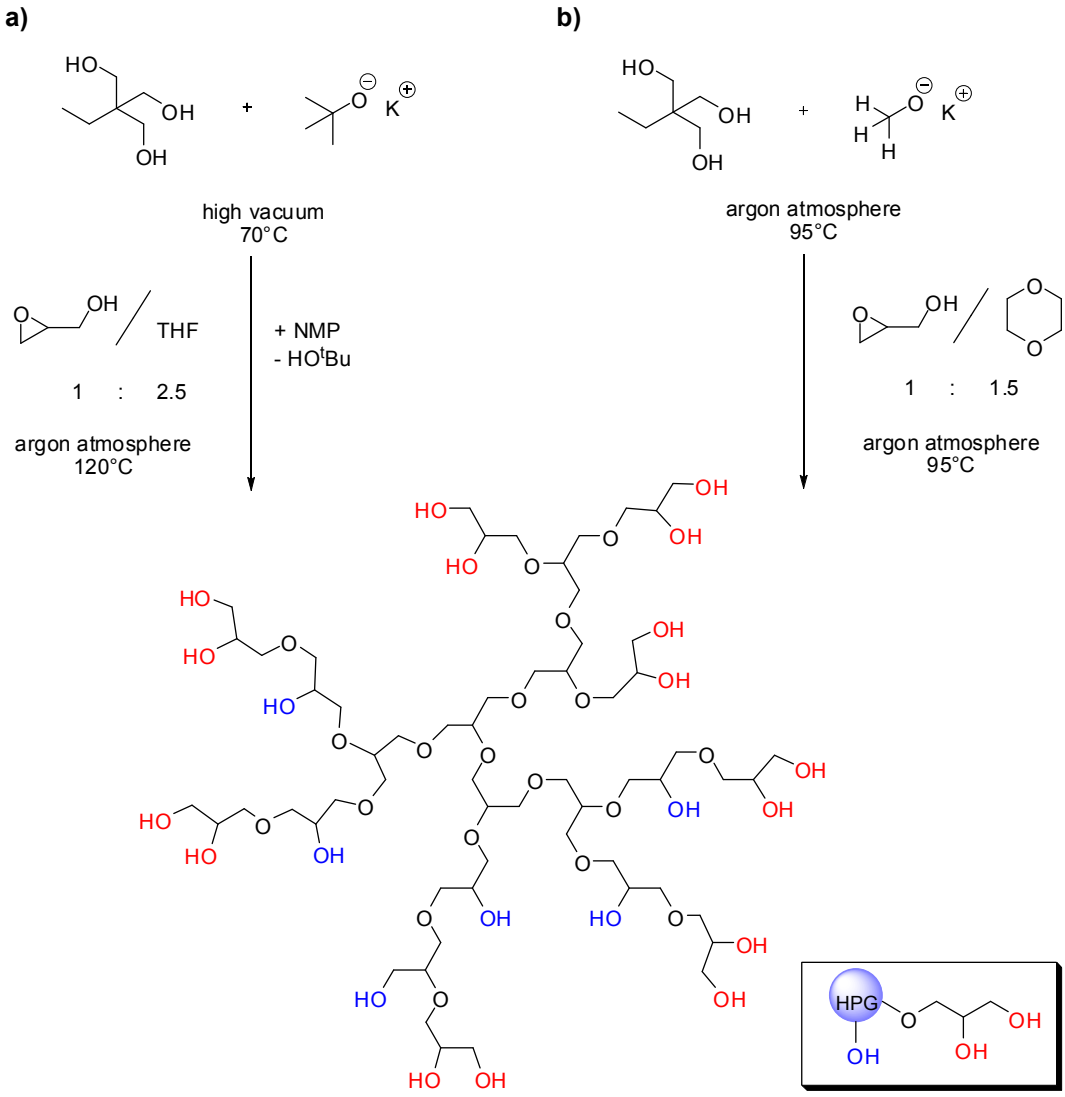


**1**

**Scheme 1**. Two strategies of HPG-synthesis: (a) synthesis of HPG on a batch reactor and (b) procedure based on emulsion polymerization.

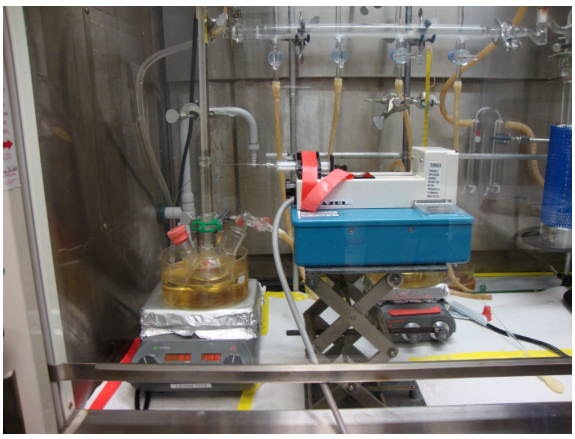

**Figure 14.** Polymerization setup. 1,4-dioxane was added and glycidol added dropwise over a period of 12 to 15 h using a syringe pump.

Polyglycerols with molecular weights from 90 to 624 kDa and with predominantly narrow polydispersities were synthesized. The HPGs were obtained in moderate to good yields (27-72 %). The results of the polymerization of high molecular weight hyperbranched polyglycerols are summarized in Table 1.

**Table 1.** Synthesis of high molecular weight hyperbranched polyglycerols (before purification *via* dialyses).

| Compound | $M_n$ (kDa) | PDI | Yield (%) |
|---|---|---|---|
| HPG-1 | 90 | 1.8 | 67 |
| HPG-2 | 130 | 1.5 | 72 |
| HPG-3 | 250 | 1.46 | 69 |
| HPG-4 | 483 | 1.0 | 51 |
| HPG-5 | 503 | 1.1 | 66 |
| HPG-6 | 535 | 1.0 | 61 |
| HPG-7 | 557 | 1.0 | 50 |
| HPG-8 | 585 | 1.1 | 27 |
| HPG-9 | 624 | 1.0 | 52 |

In these procedures 1,4-dioxane was used as the emulsifying agent. It was observed that higher molecular weight HPGs (<483 kDa) were obtained with a very narrow polydispersity. However, in the case of HPG-1, HPG-2, and HPG-3, it made sense to purify the polymers with dialysis to narrow their polydispersity.

## 3.2. Synthesis of HPG-$NH_2$ with different loadings

To probe cellular uptake of such HPGs, it was necessary to functionalize the OH groups to provide a facile route to amino functionalized HPGs and made it suitable for processing.

As a first approach, hyperbranched polyglycerols with different molecular weights were functionalized with different loadings of amino groups (Figure 15) to obtain amino-bearing polymers for coupling to dyes or targeting molecules. The core molecules were synthesized *via* a three-step synthesis. In the first step the HPGs were mesylated, followed by the azidation of the HPG-mesylate. Finally the resulting azide groups were reduced to

the corresponding amines.[127] The loadings of amino groups could be controlled by varying the stoichiometric amount of mesyl chloride in the first step.

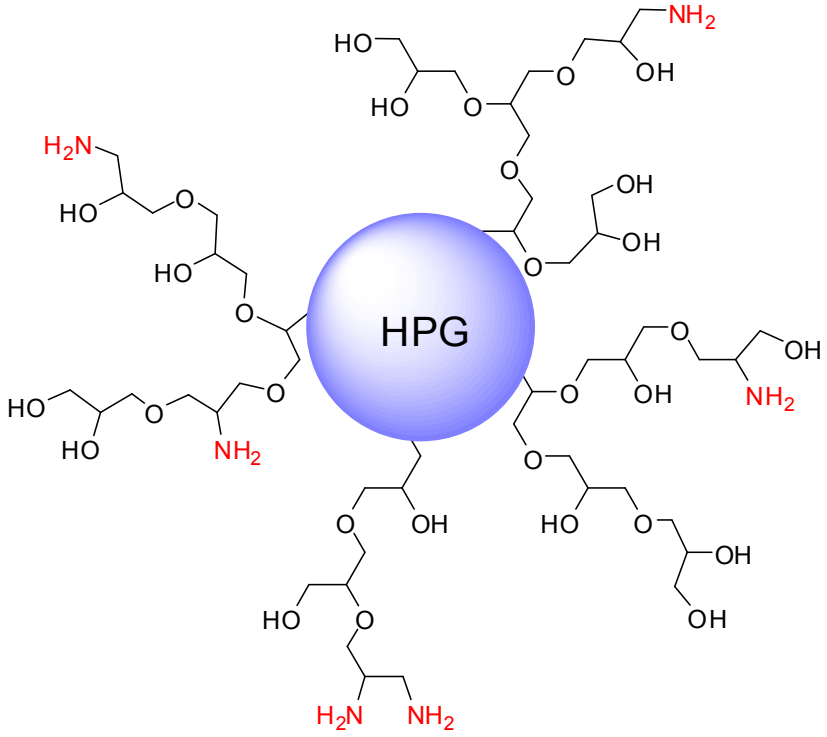


**Figure 15.** Schematic representation of amino-bearing hyperbranched polyglycerol.

**Mesylation of polyglycerol**[128,129]

Methanesulfonyl groups are well known as good leaving groups for nucleophile substitutions. The mesylation was performed with methanesulfonyl chloride in dry pyridine (Scheme 2). Pyridine is often used as a solvent for these synthesis in order to react with the HCl that is produced as a side product. The main disadvantage of this method is the sticky consistency of the solution of methanesulfonyl chloride in pyridine. Additionally, the solution turned brown, which indicated a continuing decomposition process. Due to these problems, the methanesulfonyl chloride was added directly and very slowly to get a better control of the reaction mixture. The temperature was always kept below 5 °C to avoid too fast conversions.

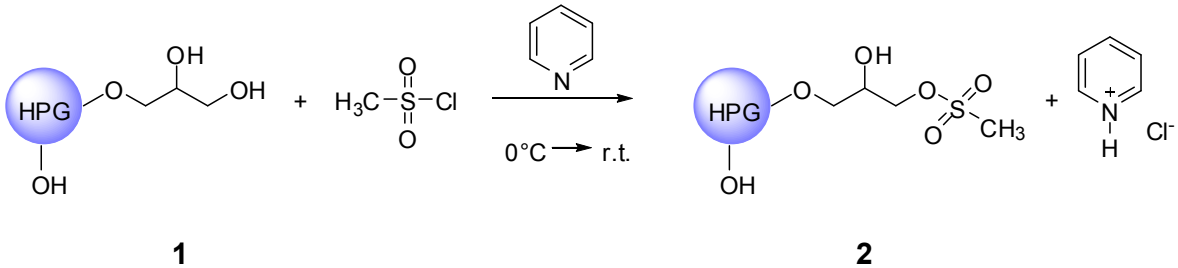


**Scheme 2.** Synthesis of mesylated HPGs with methanesulfonyl chloride in dry pyridine.

The purification of *O*-mesylpolyglycerol **2** was performed by dialyses. The dialyzing solvent depended mainly on the degree of functionalization of the HPG core. Lower-loaded *O*-mesylpolyglycerol was not soluble in acetone (under 20 % mesyl groups) but, in contrast to full mesylated HPGs, they are soluble in water and methanol.

**Azidation of *O*-mesylpolyglycerol**

Mesylate is a leaving group good enough to perform the nucleophilic substitution with sodium azide under gentle heating, but it was also possible to heat up the mixture to 110 °C to reduce the reaction time (Scheme 3). The excess of sodium azide was removed by filtration and dialysis in chloroform (depending on solubility).

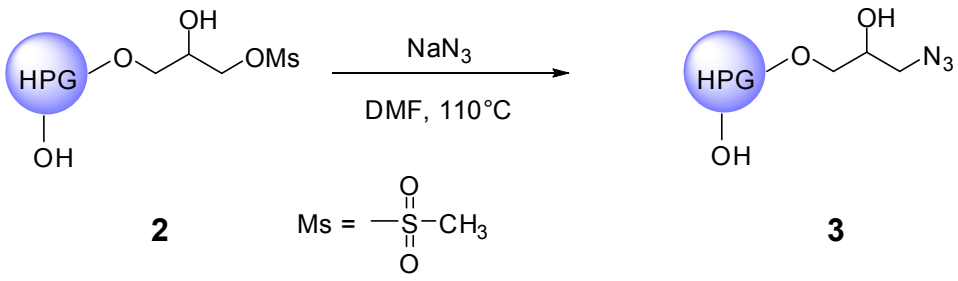


**Scheme 3.** Azidation of O-mesylpolyglycerol with sodium azide in DMF.

**Reduction of the azide to amino-bearing polyglycerols**

The reduction of the azide groups into the corresponding amines was done by the Staudinger reaction with triphenylphosphine as reducing agent (Scheme 4). During the reaction triphenylphosphine was oxidized to triphenylphosphine oxide which precipitated while the azide groups were reduced to amino functions. Because of the different solubilities of the HPG-azide and HPG-amine it was necessary to add small portions of water during the reaction to avoid precipitation of the product. Furthermore, an evolution of nitrogen gas was observable. The functionalization sequence was performed with different-sized HPGs under varying conditions to achieve controlled loadings (Table 2).

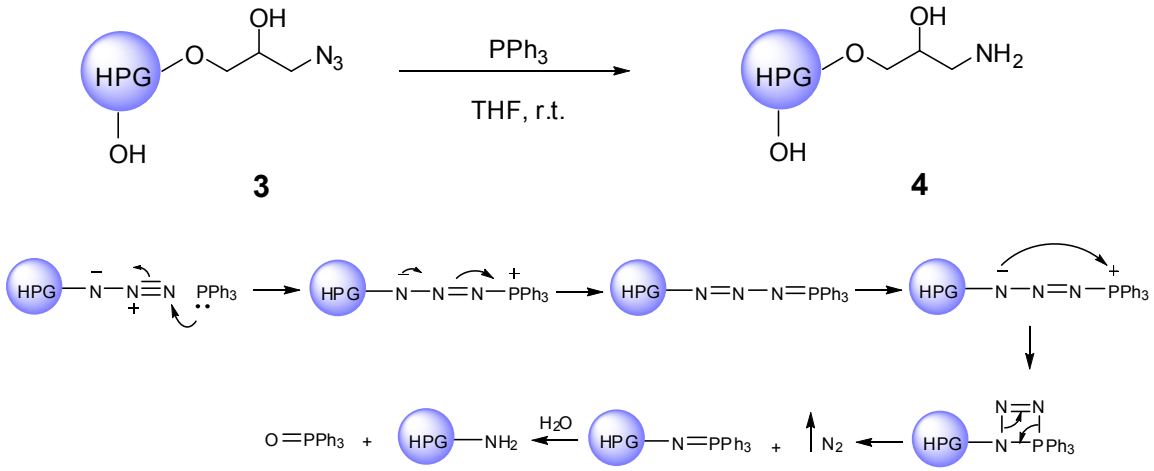


**Scheme 4.** Staudinger reduction of the azide to amino-bearing polyglycerols.

**Table 2.** Synthesis of amino-bearing polyglycerols with controlled loadings.

| Molecular Weight (kDa) | Loading (%) | Number of $NH_2$ groups |
|---|---|---|
| 2 | 23 | 6 |
| 5 | 31 | 21 |
| | 47 | 31 |
| 10 | 3 | 4 |
| | 21 | 28 |
| | 27 | 36 |
| 20 | 2.3 | 6 |
| | 5.5 | 15 |
| | 23 | 61 |
| 120 | 2 | 32 |
| | 2.5 | 40 |
| | 14 | 224 |
| | 49 | 800 |
| 208 | 1.6 | 45 |
| | 9 | 252 |
| | 50 | 1600 |
| 475 | 3 | 190 |
| | 50 | 3350 |
| 870 | 3 | 325 |
| | 50 | 5800 |

The conversions were determined by $^1$H-NMR analysis.

Several problems in the reactions appeared during the synthesis. The degree of functionalization had a strong influence on the solubility behaviour, requiring the reaction conditions to be varied. Secondly the choice of the right solvent for the heavier derivatives was a difficult task. In order to increase the stability of the products it was decided to store them as the aqueous or methanolic solution and to avoid cross-linking between the amine groups and unreacted traces of HPG-mesylate.

## 3.3. Synthesis of 40 to 60 kDa Polymers with HPG and PEG

The *in vivo* and *in vitro* studies by Brooks et al.,[130,131] showed that high molecular weight polyglycerols (HPG) are not excreted by the kidney (molecular weight cut off for renal excretion around 40 kDa), the blood circulation time was increased, and the "enhanced permeability and retention effect" (EPR) was improved. Tissue accumulation was found to decrease with time in the case of kidney, lungs and heart. Disadvantageous, however, is a very limited urinary excretion and slow polymer degradation, whereby accumulation in the liver and spleen could be observed for at least 30 days after application. Brooks et al. studied the biocompatibility of polymers depending on molecular weight and found out that there is no toxicity up to 540 kDa for HPGs.

In order to reach polymers with molecular weights with sizes between 20 and 120 kDa, new strategies have been developed. Based on hyperbranched polyglycerols with low molecular weights (5, 10, 20 kDa) as a core, different synthetic routes were investigated to conjugate poly(ethylene glycol) of different length formed on the periphery as a shell to enlarge the whole molecule (Chapter 3.3.1 and 3.4.).

### 3.3.1. Succinate functionalization of HPG and PEGylation of HPG-SA

Succinylation was done according to the published procedure of Paleos et al.,[132] who prepared functional HPGs based on polyether polyol conjugated to protective poly(ethylene glycol) PEG chains or PEG chains with folate targeting ligands at their end. The varying length of available PEG chains allowed a simple synthesis of different polymers with varying molecular weights. The synthetic route that was used to create these macromolecular architectures started with a hyperbranched polyglycerol core that was connected with a poly(ethylene glycol) shell *via* a succinic diester. This strategy was

adapted to synthesize copolymers with molecular weights between 20 and 120 kDa (Scheme 5).

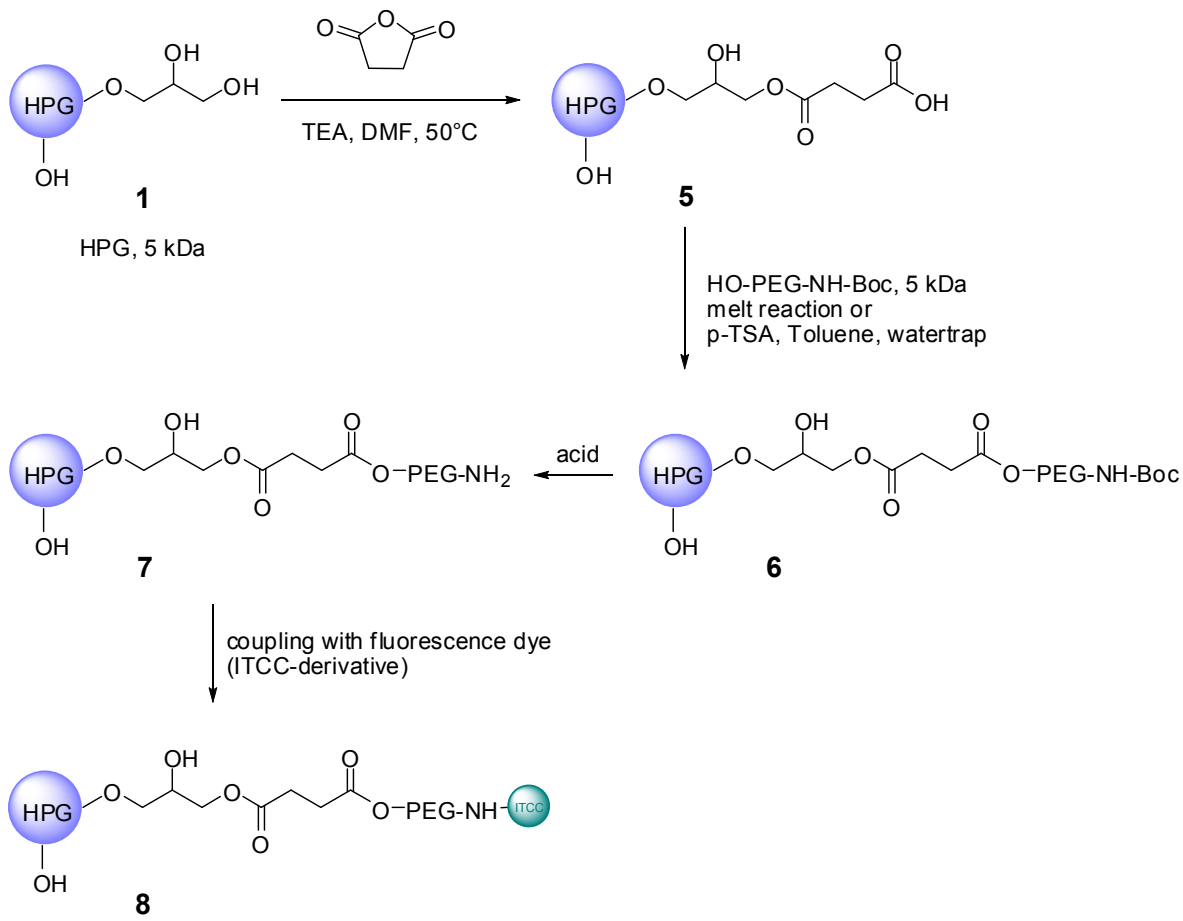


**Scheme 5.** Synthesis of conjugatable HPG-PEG core-shell structures.

The first approach started with the functionalization of the hydroxyl groups of a 5 kDa hyperbranched polyglycerol **1** with succinic anhydride (Scheme 5) and triethylamine in DMF at 50°C. After purification of HPG-SA **5** *via* dialysis in water the conversion was determined by $^{1}$H-NMR analysis. The functionalization was calculated to be 25 % (~ 17 OH groups).

In the following reaction HPG-SA **5** was PEGylated with 1-hydroxybenzotriazol (HOBt) and dicyclohexylcarbodiimide (DCC) (Scheme 5). For the PEGylation HO-$PEG_{5000}$-NH-Boc was tested. The motivation to take this PEG compound was the high molecular weight and the Boc saved amino group that can be cleaved easy with TFA to get the free amine. By $^{1}$H-NMR analysis an incomplete PEGylation of only 2 % (~ 2 PEG groups) was shown. Further deprotection steps have not been accomplished yet. In order to simplify and improve the synthesis the strategy was changed (see Chapter 3.4).

## 3.4. Synthesis of HPG-ICC

With the aim of determining the cellular uptake dependency of dendritic polyglycerols on molecular weight, a series of hyperbranched amino-bearing polyglycerols with MWs ranging from 2 to 870 kDa was prepared in a one-pot synthesis as previously reported.[133,131] Fluorescently-labelled derivatives were successfully obtained by a maleimide-mediated coupling between a maleimido indocarbocyanine dye (ICC-mal) and the thiol groups from the pre-activated polyglycerol scaffolds. Special care was taken to prepare dye-polyglycerol conjugates bearing the same dye loading in percent which ended up in labelled macromolecules with an equivalent surface charge as determined by zeta potential measurements. Briefly, the labelling of the dendritic amino-bearing polyglycerols was performed by a one-pot process, including a pre-activation of the polyglycerols through the reaction with 2-iminothiolane followed by a selective Michael addition between the maleimide groups of the ICC-mal dye and the sulfhydryl groups from the thiolated polyglycerol in PBS solution at pH 7 (Scheme 6).

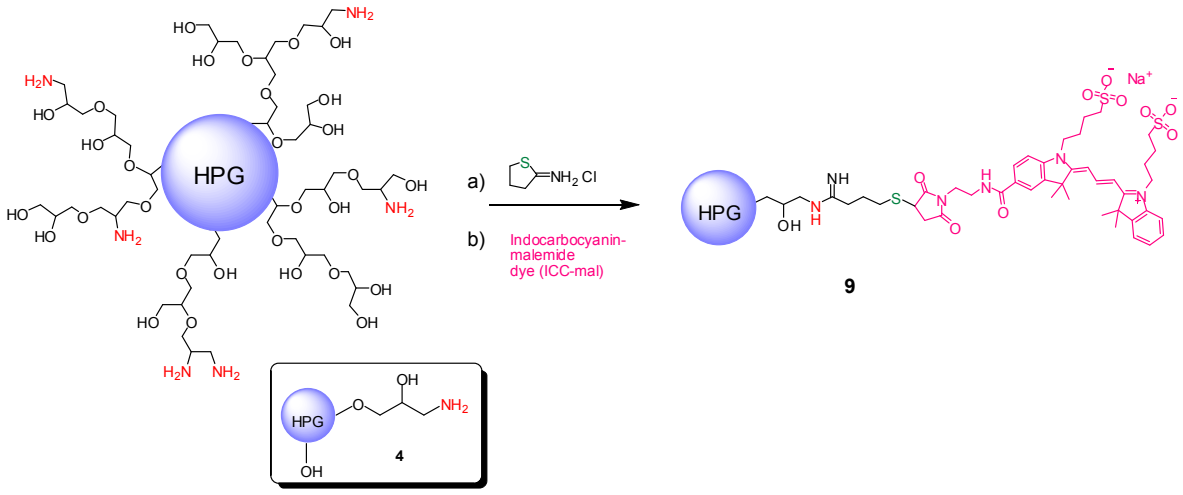


**Scheme 6.** Pathway for the synthesis of labelled-polyglycerol conjugates. (a) phosphate/EDTA buffer, pH 7.0, r.t., 20 min and (b) phosphate/EDTA buffer, pH 7.0, r.t. 60 min. The depicted polymer structure represents only one possible isomer and a small part of the amino-bearing polyglycerol scaffold.

The thiol group added to the double bond of the maleimide group in a fast and selective reaction at room temperature formed a stable thioether bond.[134] Conjugate formation was confirmed by the appearance of a faster band on a Sephadex G25 column and by size-

exclusion HPLC. Fluorescence measurements demonstrated that the ICC dye kept its fluorescence activity after conjugation.

To achieve molecular weights between 20 and 120 kDa, 20 kDa HPG was coupled with a 2 kDa polyethylene glycol (PEG) maleimide along with the dye. Polyethylene glycol chains were used as shell components to amplify the size of the HPG and to render it water soluble.

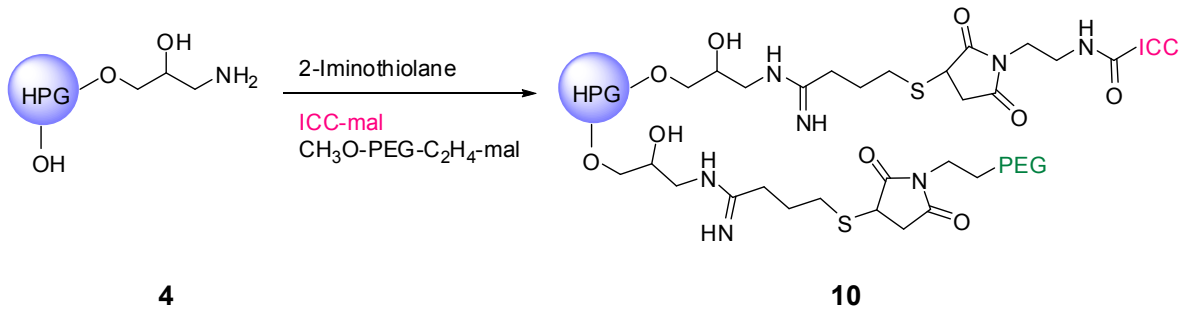


**4** **10**

**Scheme 7.** Synthesis of $HPG_{20}$-PEG-ICC.

## 3.5. Results

Analysis by dynamic light scattering (DLS) showed that average diameters of these labelled polyglycerols increased with the MW of the hyperbranched polyglycerol as expected, and were in the range of 1 to 23 nm. Zeta potential measurement demonstrated that the products have negative surface in the range of -6 to -13 mV as aimed for in the synthetic strategy. Table 3 summarizes the properties of the series of dendritically labelled polyglycerol prepared.

**Table 3.** Differently sized HPGs under varying conditions, and physical properties of the fluorescent polymers (their zeta potential and identification of the size by DLS).

| Nomenclature | Average MW of the core (kDa) | Surface charge | Mean diameter (nm)[a)] |
|---|---|---|---|
| $HPG_2$-ICC | 2 | b) | 1.0 ± 0.2 |
| $HPG_5$-ICC | 5 | b) | 1.3 ± 0.1 |
| $HPG_{10}$-ICC | 10 | b) | 2.1 ± 0.3 |
| $HPG_{20}$-ICC | 20 | -13.00 | 7.6 ± 0.1 |
| $HPG_{20}$-PEG-ICC[c)] | 36 | -9.72 | 11.3 ± 2.6 |
| $HPG_{120}$-ICC | 120 | -5.42 | 9.1 ± 1.7 |
| $HPG_{208}$-ICC | 208 | -12.30 | 11.2 ± 0.8 |
| $HPG_{475}$-ICC | 475 | -8.33 | 17.2 ± 3.1 |
| $HPG_{870}$-ICC | 870 | -10.40 | 22.9 ± 1.5 |

(a) Determined by dynamic light scattering. (b) The high fluorescence of these samples prevented their measurement. (c) HPG-20 with about 8 PEG molecules (2 kDa).

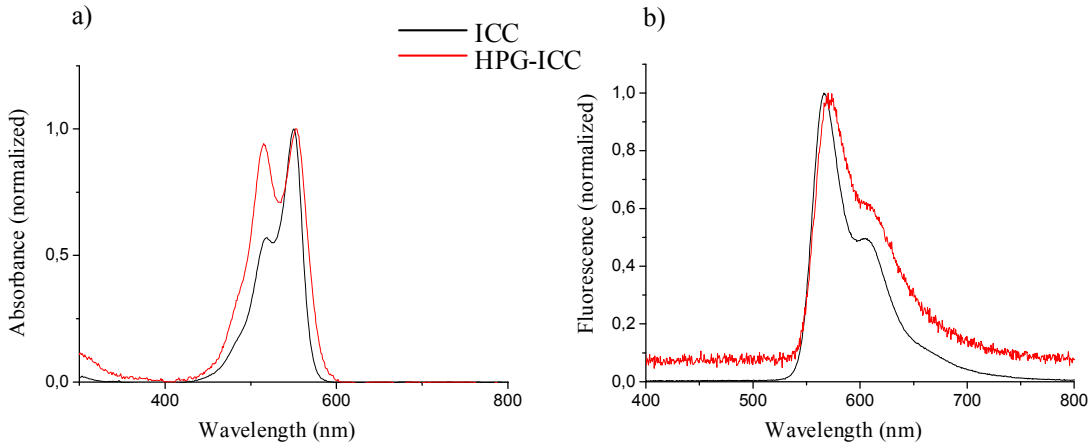


**Figure 16.** Absorbance (a) and fluorescence (b) spectra of free indocarbocyanine and HPG covalently coupled to indocarbocyanine (about 4 %).

As absorbance maxima of the coupled compound were more widely spaced, the main maximum was bathochromically shifted about 3 nm. The shoulder of the dye was clearly pronounced and became also shifted about 3 nm, but hypsochromic. The absorption band was enlarged. There was an enlargement of the band in the fluorescence spectrum and a relative increase of the shoulder. The fluorescence maximum was shifted bathochromically

about 4 nm, whereas the fluorescence quantum yield remained unchanged. Table 4 gives a summary about the absorbance and fluorescence results.

**Table 4.** Absorbance and fluorescence data of free ICC and HPG-ICC

| | ICC | HPG-ICC |
|---|---|---|
| Absorption maximum | 550 nm | 553 nm |
| Absorption (shoulder) | 518 nm | 515 nm |
| Fluorescence maximum | 566 nm | 570 nm |
| Fluorescence (shoulder) | ~ 604 nm | ~ 604 nm |
| Fluorescence quantum yield | $\phi$ = 4.6 % | $\phi$ = 4.3 % |

### 3.5.1. Cellular uptake in three different cell lines

In order to establish the retention between the size of HPG and its intracellular delivery potential, a systematic study was performed to compare the cell entry pathway and extent of the cellular uptake in three different cell lines: epithelial human lung cancer cell line A549, human epidermoid carcinoma cells A431, and human umbilical vein endothelial cells (HUVEC). Particularly, cancer cell lines were used in a view towards anticancer and other therapeutic drugs. Cancer cells are subject to apoptosis and have other phenotypic properties such as elevated proliferation rates, migration capacity, and ability to induce angiogenesis more significantly than normal cells. Thus, it would be preferable to study cancer cells *in vitro* and *in vivo* rather than normal cells. Through fluorescence microscopy, the dendritic polyglycerols could be seen inside the cells with the help of the ICC dye which gives a red fluorescence. Cytoskeleton and nuclear staining, performed with Alexa Fluor 488 Phalloidin (green) and DAPI (blue) respectively, allowed determination of the intracellular distribution.

Cellular uptake experiments were performed by Dr. Pia Welker (mivenion GmbH, Berlin, Germany). Fluorescence images of A549 lung epithelial cancer cells are shown in Figure 17. Glycerol-ICC as negative control was not localized in the cell. Similarly, lower molecular weight HPG-ICC-conjugates (2-10 kDa) were only detected in minimal amounts inside the A549 cells. On the other hand, the derivates with higher molecular weights (20-870 kDa) were found to be predominantly localized in the cytoplasm after 1 hour of incubation, with an increased uptake for higher molecular weight polyglycerols. The cells

with HPG-870kDa showed very strong fluorescence signals in regions inside the cells, which could be assigned as endocytotic vesicles.

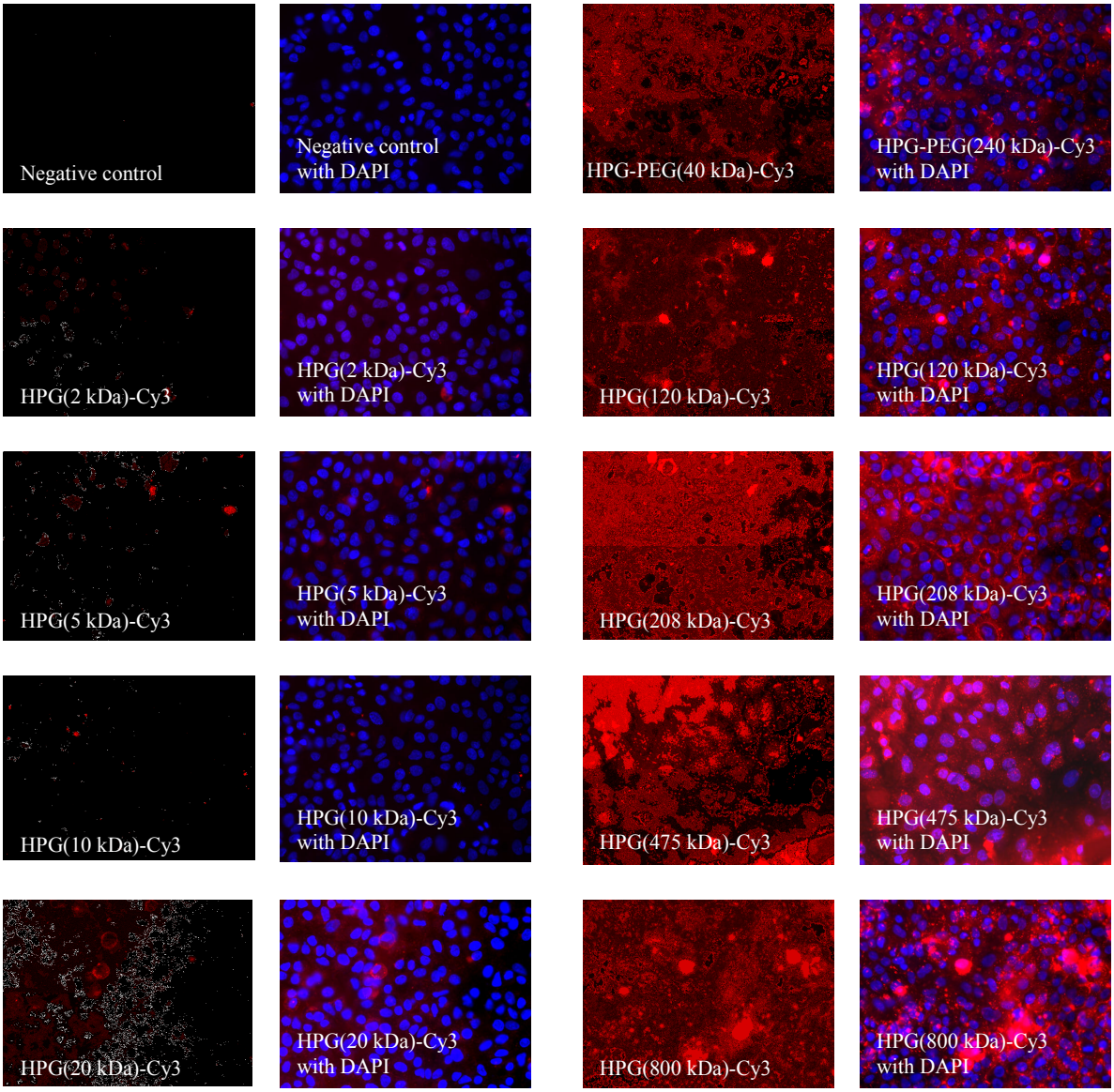


**Figure 17.** Fluorescence images of A549 lung epithelial cells incubated with 1 µM of test material for 4 h at 37 °C with glycerol-ICC as a negative control. HPG-dye conjugates with higher molecular weight showed higher cellular internalization mainly inside the cytosol. Merge pictures show labelled polyglycerols in red and stained nuclei in blue (DAPI). Low-molecular-weight compounds from 2 to 20 kDa did not show cell entry, in contrast to high-molecular-weight HPGs. One representative experiment of $n = 3$, where $n$ is the number of samples. Scale bar: 50 µm. (Experiments performed by Dr. Pia Welker at mivenion GmbH).

In addition, a similar pattern was observed with an increasing cellular uptake for higher molecular weights, with a maximum at 208 kDa, for human epidermoid carcinoma cell line A431. In the studies with the human umbilical vein endothelial cells (HUVEC) the same pattern was observed, which demonstrates a maximum cellular uptake for the polyglycerol with MW 475 kDa.

These results indicated a size-dependent endocytotic mechanism of cell entry, which generally points out appropriate polyglycerol diameters for cellular penetration in the range of 10-20 nm and molecular weights above 100 kDa. This finding was further confirmed by FACS analysis, which was performed to quantify the uptake of HPG-ICC-dyes by A549 human lung cancer cells. Figure 18 presents an analysis of the fluorescence (570 nm) in cells gated for normal size and granularity (viable cells). Cells incubated with lower-molecular-weight HPG-ICC conjugated for 1 h only exhibited an insignificant fluorescence increase compared with cells incubated with the control substance glycerol-ICC, whereas the uptake of HPG with a molecular weight of 120, 208, 475, and 870 kDa was clearly demonstrated. The highest value of the difference between the mean fluorescence of cells after incubating with HPG-dye conjugate and the control substance glycerol-ICC was detected after incubation of HPG-208-ICC.

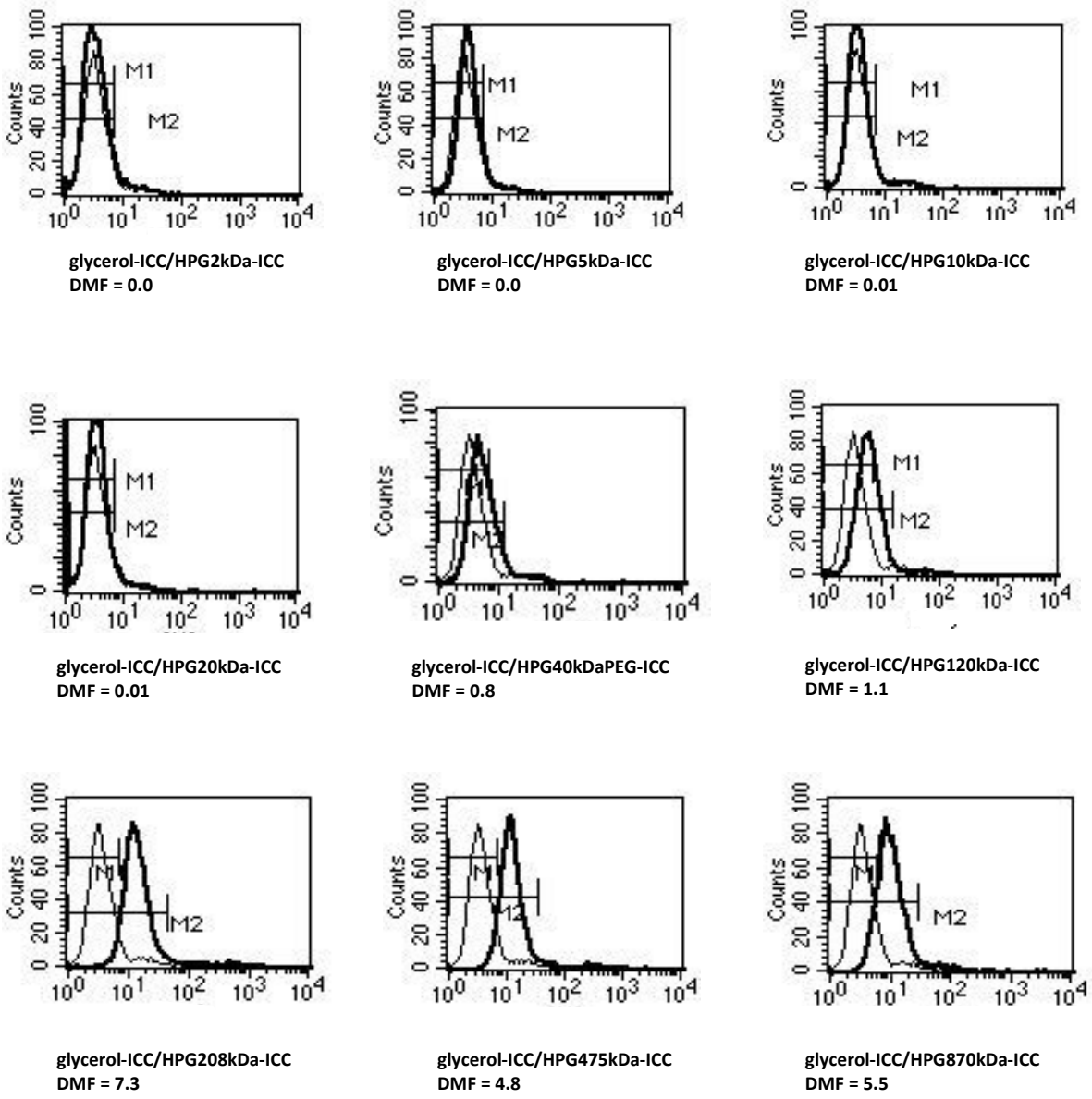


**Figure 18.** Histogram of human lung cancer cells A549 incubated for 1 h with ICC-conjugated glycerol as control (gray) or ICC-conjugated polyglycerols with different molecular weights (2, 5, 10, 20, PEG-40, 120, 208, 475, 870 kDa; black). x-axis: fluorescence intensity (570 nm). Difference of mean fluorescence (DMF), polyglycerols (M2), glycerol (M1; control). One representative experiment of $n$ = 3. (Experiments performed by Dr. Pia Welker at mivenion GmbH).

Similarly, intracellular localization and cellular uptake showed HPG-dye conjugates to be localized in the perinuclear region in different human cells (Figure 19a). Staining of the cytoskeleton component actin (green) demonstrated in conventional fluorescence microscopy that HPG-dye (red) was localized inside of the cell after incubation for 4 h both

in the epidermal (A431) and lung (A549) tumor cell lines, as well as in the nonmalignant normal endothelia cells (HUVEC).

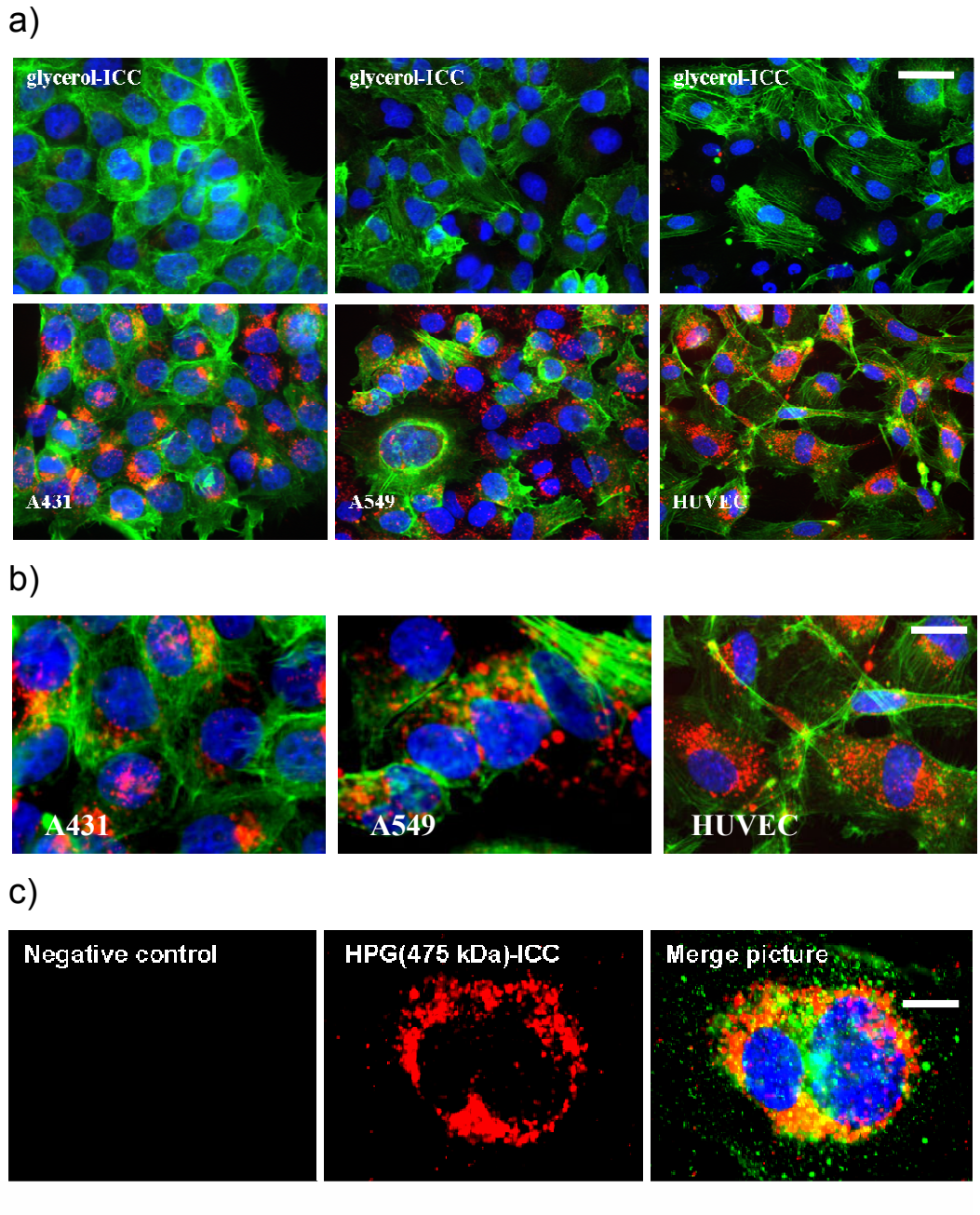


**Figure 19.** Different human cancer cell lines were incubated with ICC-conjugated glycerol or HPG-475-ICC for 4 h (red). Actin was stained with Phalloidin conjugated with Alexa488 (green). Nuclear staining with DAPI (blue). (a) Overview and (b) detailed view of cells incubated with HPG-475-ICC. (c) Confocal microscopy of HUVEC cells cultured with HPG-475-ICC (red) for 4 h. Double staining with a late endosome marker (green). Co-localization (yellow) in the merge picture. Optical sectioning in the *Z* axis. Section of the nucleus level. One representative experiment of $n = 3$. Scale bars: 25 (a), 5 (b), and 3 µM (c). (Experiments performed by Dr. Pia Welker at mivenion GmbH).

A representative example for the HUVEC cells (Figure 19b) was evidenced for this observation by "Z" section imaging using a confocal microscope at the level of the nucleus. The HPG–dye is clearly enriched in the perinuclear region. The cells were incubated with a fluorescently-labelled mannose-6-phosphate-receptor antibody (green), a marker protein for late endosomes. The majority of HPG-dye molecules co-localized with the late endosome marker after incubation of 4 h, which indicated the uptake and metabolism of HPG-475-dye by endocytosis.

The viability of the cells was studied with the FACS analyses. Cells with normal size (x-axis) and granularity (y-axis) were gated (viable cells) and compared with cells outside the gate (Figure 20a). These analyses showed that the viability of the cells after 1 hour is only minimally influenced, whereas after 4 hours the viability with HPG-PEG-40 and the HPG-ICC conjugates (475 and 870 kDa) was reduced substantially. Figure 20b demonstrates a representative figure of gated cells in the framed area. Cells outside this area are apoptotic (smaller cells) or necrotic (enlarged cells).

a)

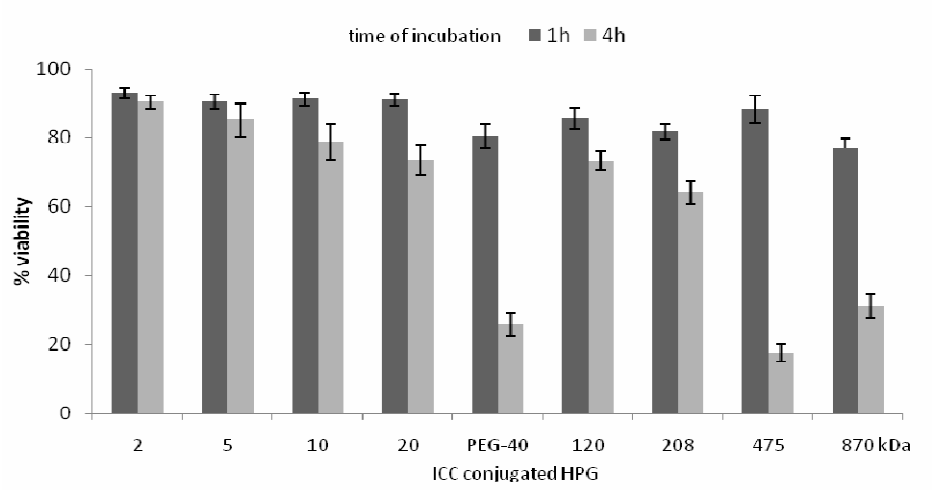


b)

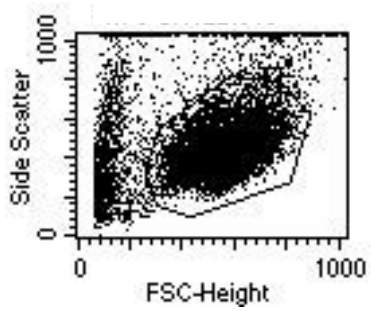


**Figure 20.** FACS analysis of size and granularity of human lung cancer cells A549 incubated for 1 or 4 h with HPG with different molecular weights, all conjugated with ICC.

(a) % gated cells. (b) Density Dot Plot of HPG-870-ICC; X-axis: size of the cells; Y-axis: granularity of the cells. (Experiments performed by Dr. Pia Welker at mivenion GmbH).

Furthermore, the uptake mechanism was studied by FACS analysis, wherein the invagination of clathrin-coated pits during endocytosis was strongly inhibited by removal of cholesterol from the membrane of cultured cells. The water-soluble methyl-β-cyclodextrin (MβCD) is known to form a soluble inclusion complex with cholesterol, thereby enhancing its solubility in aqueous solution. Therefore, A549 cells were pretreated for 30 min with MßCD and lovastatin to prevent the cholesterol synthesis by the cells.[135] Figure 21 demonstrates the decrease of HPG-870-ICC uptake in cells treated with MβCD alone or in combination with lovastatin verifying the role of endocytosis in this process.

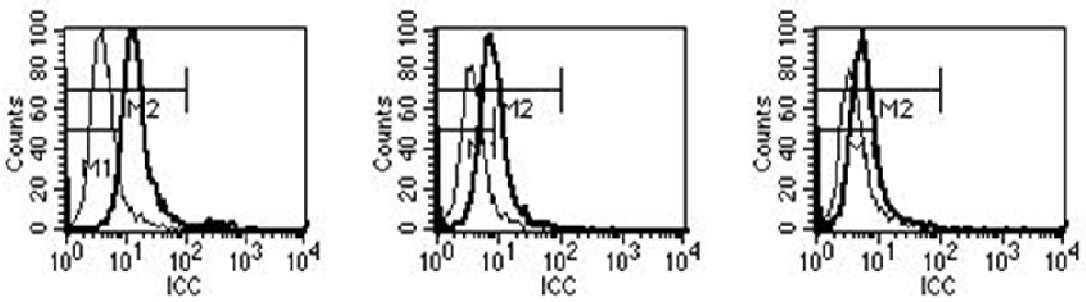


**Figure 21.** FACS analysis of human lung cancer cells A549 incubated for 0.5 h with glycerol-ICC as control (gray) and polyglycerols 870 kDa (black). Cells were treated only with medium (left), with the endocytosis inhibitor MβCD (cholesterol depletion) or MβCD and lovastatin (cholesterin synthesis inhibitor). Cells with normal size and granularity were gated and analyzed for their fluorescence intensity. x-axis: fluorescence intensity (570 nm). DMF: Difference of mean fluorescence: test substance (M2) - glycerol (M1; control). One representative experiment of $n = 3$. (Experiments performed by Dr. Pia Welker at mivenion GmbH).

In another experiment, the cells were incubated for up to 24 hours with HPG-120-ICC and subsequently cultured with normal medium to study the release from the cell (Figure 22). The uptake was comparatively very rapid and remained static in the first hours and

continuously increased after 3 hours. The kinetics of release after the incubation time with HPG-120-ICC was similar, providing further indication of vesicular transport.

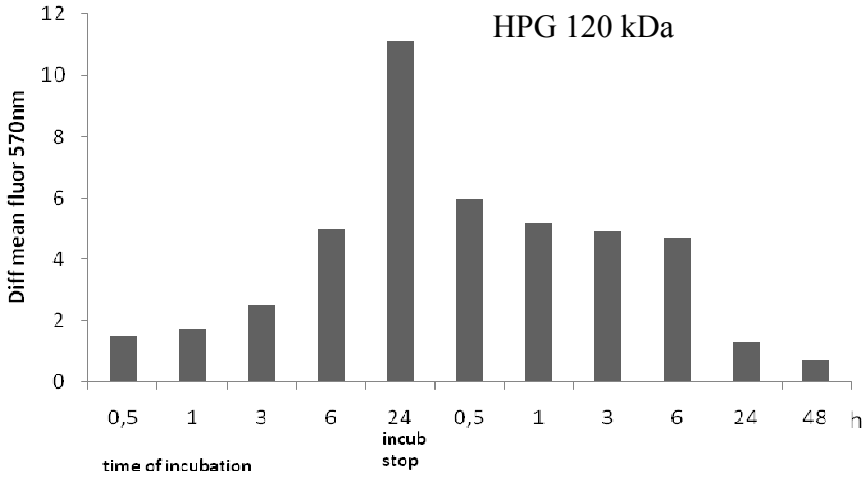


**Figure 22**. FACS analysis of human lung cancer cells A549 incubated for different times with glycerol-ICC as control and HPG-120-ICC. Cells with normal size and granularity were gated and analyzed for their fluorescence intensity (570 nm). Difference of mean fluorescence: HPG-120-glycerol (control). After 24h of incubation, medium with test substances was removed and the kinetics of release from the cells was studied. Mean of $n = 3$. (Experiments performed by Dr. Pia Welker at mivenion GmbH).

## 3.6. Discussion and Conclusion

**Synthesis and substitution of different molecular weight hyperbranched polyglycerols**

Hyperbranched polyglycerol is typically synthesized from the commercially available glycidol by slow monomer addition and partial deprotonation of the initiator.[99] The disadvantage in this strategy is the problem of high polydispersity and their limitation to relatively low molecular weights (6000 g/mol).[126] Molecular weights up to 20000 g/mol have been reported by the use of diethylene glycol dimethyl ether (diglyme) as an inert emulsifying solvent to reduce the viscosity of the polymerization mixture.[136] Brooks et al. reported the synthesis of very high molecular weight HPGs (up to 700 kDa) with narrow polydispersities ring-opening multibranching polymerization of glycidol using dioxane as the reaction medium.[120]

In this study different sizes of hyperbranched polyglycerols were synthesized to investigate in several studies, such as the size-dependant endocytosis, different intracellular mechanisms, the specific receptor-mediated endocytosis, and for the application in *in vivo* studies. For this purpose, low molecular weight HPGs (2, 5, 10, and 20 kDa) were used, which were synthesized by the Haag group based on the strategy of Roller et al. and Türk et al.[124,125] High molecular weight HPGs (from 120 to 870 kDa) has been partly provided by the group of Prof. Dr. D. Brooks or synthesized based on their strategy. To fill the lack between the size of 20 and 120 kDa HPG, HPG core was connected with a PEG shell *via* a succinic diester according to the published procedure of Paleos et al.[132] However, this route proved difficult, because of too many synthesis steps and difficult purification. Due to a simplification of the synthesis the strategy was changed to a one-pot process (Chapter 3.4).

For the next step, hyperbranched polyglycerols with different molecular weights were functionalized with amino groups to obtain amino-bearing polymers for simple coupling synthesis with dyes or targeting molecules. In the first step the HPGs were mesylated, followed by the azidation of the HPG-mesylate. Finally the resulting azide groups were reduced to the corresponding amines.[124] The loadings of amino groups could be controlled by varying the stoichiometric amount of mesylchloride in the first step.

In conclusion, in the focus of the thesis presented herein, a library of different molecular weight and amino-bearing hyperbranched polyglycerols was established. Due to their highly biocompatible nature, high loading capacity, good solubility, non toxicity, and low viscosity, these polymers are potential candidates of applications in medicine and pharmacology.

**Size-dependant cellular uptake of HPG-Dye conjugates**

Endocytosis is an essential function of the cell since it regulates many processes, including nutrient uptake, cell adhesion and migration, receptor signaling,[137] pathogen entry,[138] neurotransmission, receptor downregulation, antigen presentation, cell polarity, mitosis, growth and differentiation, and drug delivery.[139,140,141] Receptor mediated endocytosis is an endocytotic mechanism in which only specific molecules are ingested into the cell. This specificity results from various factors such as receptor-ligand interaction, but is still not fully understood for its permeation role with respect to charge, size, and molecular mass of the carriers. Since the receptors on the plasma membrane of the target tissue specifically bind to the ligands outside of the cell, it is presumed that the process will have an impact

for polymeric architecture and other physico-chemical properties. In the past, cellular uptake has been well established for small molecules and macro or nano carriers being used in a variety of delivery systems.[142,143] At the same time, other parameters of nanocarriers, including composition, architecture, etc., can be selected based on other considerations such as type of imaging or therapeutic agents, their aqueous solubility, electric charge, chemical structure, etc. Therefore, the main objective of this work was to evaluate and study the cellular uptake mechanism of HPGs of various molecular masses and size. The outcome of these studies could be explored to optimize the polymeric architecture and size to target the nanocarrier developed using HPG polymers.

Towards this direction, HPGs were labelled with ICC to image endothelial and cancer cells for its endocytosis process. The studies were carried out for *in vitro* uptake and the intracellular behavior of high-molecular polyglycerols in comparison to low molecular glycerol in human lung cancer cells A549 (Figure 17). In addition, the effects were also evaluated by flow cytometry for ICC-labelled polyglycerols. It was interesting to note that the mean fluorescence signal inside the cells was most significant after incubation of cells with 208 kDa with 11.2 nm in size (Figure 17 and Figure 18). Treatment with methylcyclodextrin in Figure 21 (depletion of cholesterol, inhibition of the synthesis of new cholesterol by the cell with lovastatin) inhibited the HPG uptake. This inhibition was observed, as expected, for higher molecular weights HPG, i.e. 870 kDa, which evidences that this cell entry may be attributed due to the caveolin-mediated endocytosis pathway. It can be concluded that this process is size dependent for the HPG molecule: i.e. higher the size, more the endocytosis (Figure 17 and Figure 18). While the size is below 20 kDa, no endocytosis is expected. However, the fluorescence signals in the A549 cells were lower after incubation with ICC labelled 120, 475, or 870 kDa polyglycerol. The choice of ICC as fluorescent probe has already proven to be valuable in connection with HPG[144] due to its high labeling efficiency and good fluorescence quantum yield in the conjugated state. For subsequent *in vivo* imaging, the respective near-infrared homolog ICC can be applied.

In conclusion, it was shown for the polymeric class of polyglycerols that cellular uptake is size-dependent. Based on these findings, in future research should be conducted towards combining HPG-dye conjugates with active targeting molecules for receptor-mediated endocytosis to better understand the cellular uptake mechanism for this type of polymer.

This observation could have a broad impact on cancer drug delivery and imaging. A proper selection of size and thus the ability to achieve intracellular delivery is crucial for drug targeting. The data for polyglycerols suggest that endocytotic uptake of macromolecules can be achieved above a certain molecular weight level, on the one hand, or it can be suppressed at lower sizes. In particular, for an extention to molecular targeting of nanocarriers, for higher antitumor therapeutic activity and imaging efficacy, it might be a reasonable approach to combine receptor-mediated molecular targeting with the uptake behavior driven by the particle properties. However, one might as well consider using smaller polymers in combination with receptor targeting entities, when uptake is only wanted on the targeting unit and not on the macromolecular or particle properties.

*This part of the thesis is an excerpt of the review published in the following article:*
S. Reichert, M. Calderón, J. Khandare, P. Welker, D. Mangoldt, K. Licha, R. K. Kainthan, D. E. Brooks, R. Haag, *Small*, **2011**, *7*, 820-829.

# 4. Intracellular Localization of Hyperbranched Polyglycerols

Growth and division of cells in an organism are tightly controlled. If these controls are disturbed cancer can develop. Therefore the underlying intracellular mechanism is a central topic for cancer research.

One pathway for cellular uptake for macromolecules and nanoparticles of size up to 100 nm is endocytosis, where the cell membrane flows around the material and joins together to a vesicle. These split-off vesicles called early endosomes. They can recycle them back to the surface or sort them to degradation in late endosomes or lysosomes (pH 4-5). Under standard physiological conditions a pH of 7.4 is present. Because of the acidic area and around 40 different types of hydrolytic enzymes in the lysosomes, they are thought to mediate a final set of sorting events prior to delivery of material to other cell organelles like mitochondria, Golgi apparatus or endoplasmic reticulum.[145] These pH-value shift was used to investigate of selective drug delivery in cells. Although the mechanism of endocytosis has been studied a lot[146] all details have not been clarified up to now.

In chapter 3 it could be shown that cellular uptake is size-dependent. A specific size of the polymers is necessary to break the barrier of the cell wall. Therefore it could be demonstrated that HPGs with a higher molecular weight go inside the cells. But now the next question is where within the cytoplasmic compartment are the HPGs localized? To determine which organelles are involved in the cytoplasmic distribution of the polymers, triple-labeling experiments were performed with DAPI, a nucleus-selective dye, the fluorescent HPGs and dyes selective for early endosomes, clathrins, Golgi apparatus, late endosomes and lysosomes (Figure 23).

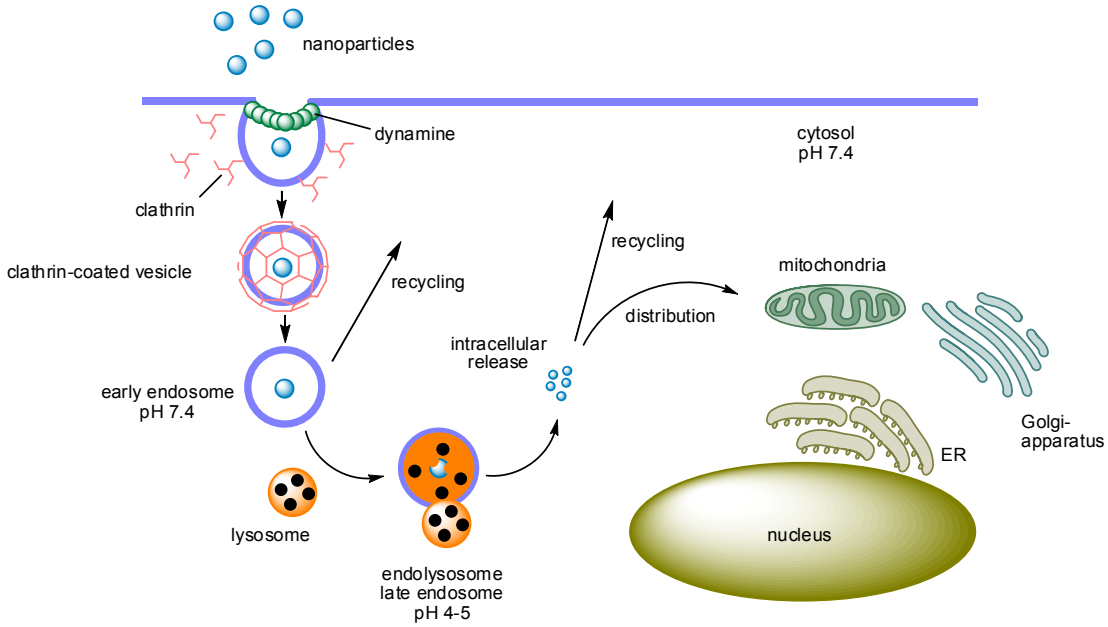


**Figure 23.** Clathrin-mediated endocytosis.

## 4.1. Results of the co-localization studies

For the several endocytotic pathways inhibitors and other substances are already well known, which would make it possible to obtain the uptake mechanism information required. By means of fluorescence labelling of these substances and by marking of the internalizing material it is possible to investigate in co-localization studies.

Cell compartments have different specific receptors, proteins, antigens, or surface modifications. Based on specific antibodies it is possible to visualize cell organelles such as early and late endosomes, lysosomes, actin cytoskeleton, cell nucleus, mitochondria, or the trans Golgi network.

In order to identify the subcellular localization of uptaken hyperbranched polyglycerol, co-localization studies were performed with markers for various intracellular compartments using fluorescence labelling and confocal microscopy. HPG (208 kDa, ~11.2 ± 0.8 nm) was labelled with ICC dye (see chapter 3), which shows a red fluorescence, in order to image cancer cells for endocytosis process. To ensure that there is complete clarity on the size-dependent cellular uptake, HPG with a molecular weight of 10 and 120 kDa were also prepared for a better comparison. The studies were carried out for *in vitro* uptake and the intracellular behavior of high-molecular polyglycerols in human lung cancer cells A549. For the following particle uptakes, the staining of several organelles and the nuclei

was performed with two inhibitors, six different specific antibodies (green), and DAPI (blue) respectively, allowed determination of the intracellular distribution.

The intracellular transport route of the polymer took place by antibody labelling of several cell compartments and co-localization studies (Table 5). Cellular uptake experiments were performed by Irene Schütz (Laboratory of Prof. Dr. Volker Haucke, Department of Biochemistry, Free University of Berlin).

**Table 5.** Overview of the used antibodies, their destination and the experimental conditions.

| Antibody | Cell compartment | Incubation time [min] | Conc. |
|---|---|---|---|
| CHC (clone X22, mouse) | clathrin | 10, 30, 60 | 1:50 |
| EEA1 (mouse BD Transduction) | early endosome | 10, 30, 60 | 1:100 |
| AP-1 (mouse Sigma) | trans Golgi network | 10, 30, 60 | 1:100 |
| M6PR (mouse Affinity Bioreagents) | late endosome | 10, 30, 60 | 1:100 |
| LAMP1 (mouse BD pharmingen) | lysosome | 10, 30, 60 | 1:200 |
| CD63 (mouse Millipore) | lysosomes | 10, 30, 60 | 1:100 |

Clathrin coated vesicles mediate the receptor-coupled endocytosis and the transport of lysosomal acid hydrolyses from the trans Golgi network (TGN).[147] Clathrin is a protein with a three-legged structure (*Triskelion*) which is involved in the invagination of the cell membrane and the formation of vesicles.[148] The driving force for clathrin mediated endocytosis is the ability of the clathrin to form polyhedral cages of pentagons and hexagons. As shown in Figure 24, HPG-ICC became co-localized slightly after 30 min of incubation with CHC (clathrin heavy chain) as indicated by the yellow punctured structure in the merged picture.

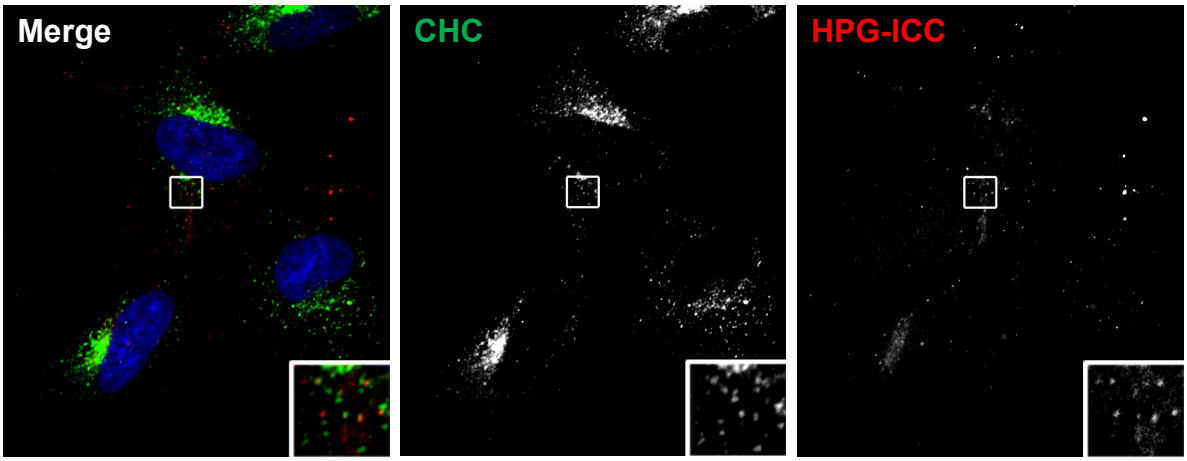


**Figure 24.** Weak co-localization of HPG-ICC with CHC (clathrin heavy chain). The nucleus is stained with DAPI (blue). Incubation for 30 min, at 37°C. Merge (left), CHC antibody (middle), HPG-ICC (right). (Experiments performed by Irene Schütz, Laboratory of Prof. Dr. Volker Haucke, Department of Biochemistry, Free University of Berlin).

Haucke et al. have developed Pitstops as a novel group of small molecule inhibitors that acutely interfere with clathrin function *in vitro* and in living cells.[149] Pitstops prevents the formation of the clathrin network at the plasma membrane, and thereby inhibits the clathrin-mediated endocytosis.

These molecules made it possible to investigate whether the polymer-dye conjugate used the clathrin-mediated endocytosis pathway or not. Figure 25 shows that there was no uptake of HPG-ICC by the use of a clathrin inhibitor. The particles were located on the cell surface, which suggested a clathrin-mediated endocytosis.

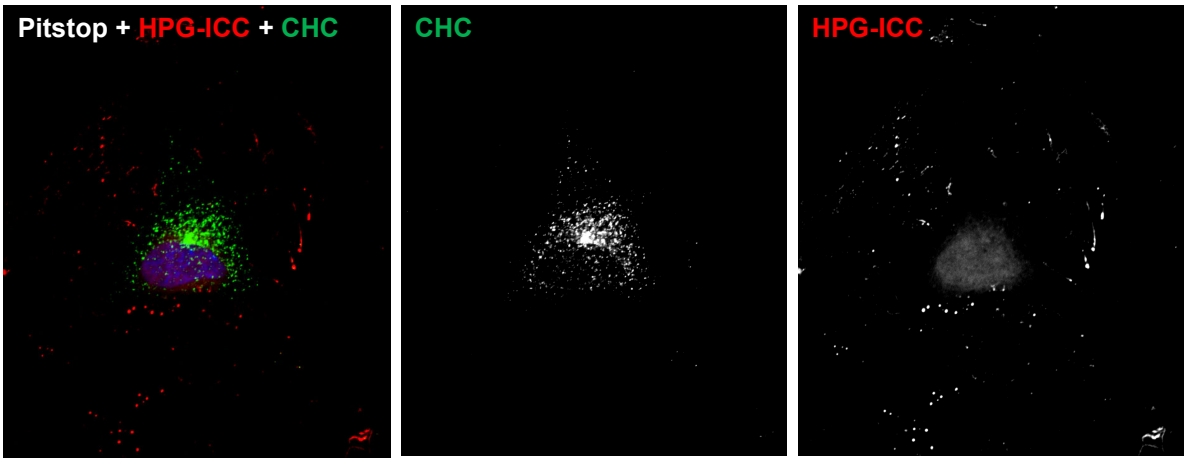


**Figure 25.** Pitstop blocks uptake of HPG-ICC human lung cancer cells A549. The nucleus is stained with DAPI (blue). Incubation for 30 min, at 37 °C. Merge (left), CHC antibody

(middle), HPG-ICC (right). (Experiments performed by Irene Schütz, Laboratory of Prof. Dr. Volker Haucke, Department of Biochemistry, Free University of Berlin).

It is also possible to block endocytotic pathways with Dynasore, a potent inhibitor known to interfere dynamin by rapidly inhibiting coated vesicle formation within seconds of Dynasore addition.[150] Dynamin is an enzyme, or rather a GTPase, which is essential for clathrin-dependent coated vesicle formation, in transport from the trans Golgi network, as well as for ligand uptake through caveolae.[151] Dynasore was used to block vesicular endocytosis by selectively inhibiting dynamin 1 and dynamin 2 GTPases, which are responsible for vesicle scission during both clathrin- and caveolin-mediated endocytosis.[152] To establish whether Dynasore can act in intact cells, we examined its effect on the uptake of HPG-ICC (Figure 26).

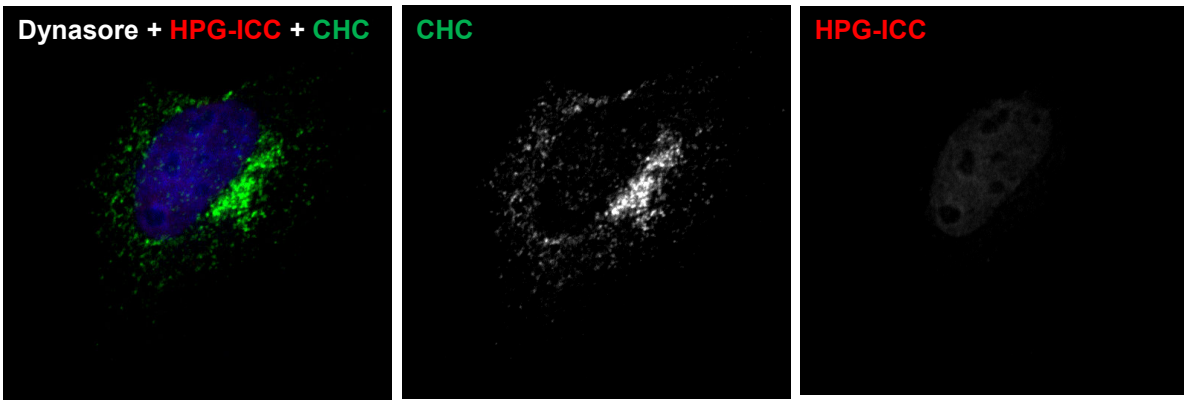


**Figure 26.** Dynasore blocks uptake of HPG-ICC human lung cancer cells A549. The nucleus is stained with DAPI (blue). Incubation for 30 min, at 37 °C. Merge (left), CHC antibody (middle), HPG-ICC (right). (Experiments performed by Irene Schütz, Laboratory of Prof. Dr. Volker Haucke, Department of Biochemistry, Free University of Berlin).

The uptake, trafficking, and intracellular accumulation of HPG-ICC were all strongly blocked in cells preincubated for 30 min with 80 μM Dynasore, which was also present during the uptake assay. Conspicuoously, there was no uptake at all.

A possibility for specific detection of early endosomes is found within the endosomal marker Early Endosome Antibody 1 (EEA1), which is a hydrophilic peripheral membrane protein present in cytosol and membrane fractions that binds to phosphatidylinositol-3-phosphate (PtdIns(3)P) a phospholipid found in cell membranes.[153] With the help of a specific antibody it is possible to demonstrate endosomes with confocal fluorescence microscopy.

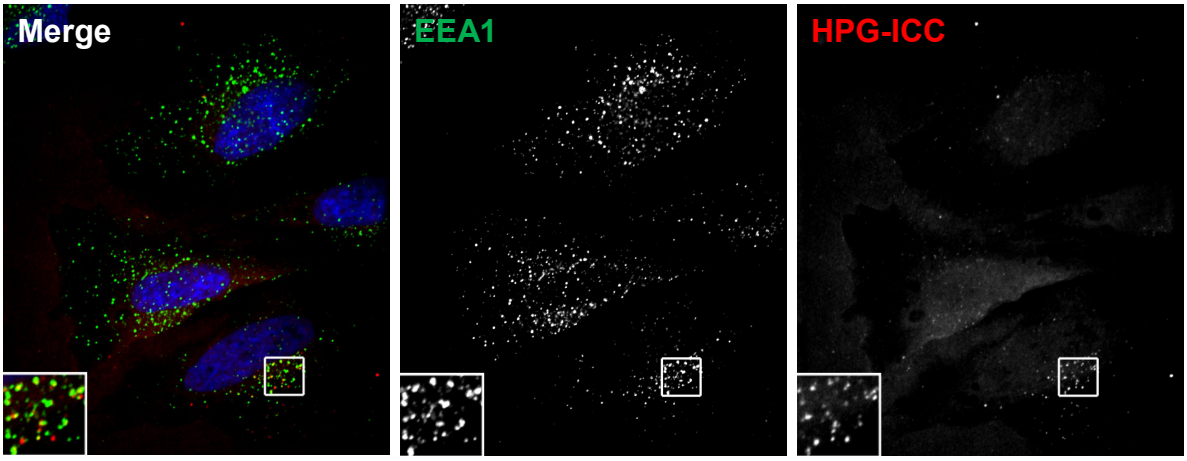


**Figure 27.** Weak co-localization of HPG-ICC with EEA1. The nucleus is stained with DAPI (blue). Incubation for 30 min, at 37 °C. Merge (left), EEA1 antibody (middle), HPG-ICC (right). (Experiments performed by Irene Schütz, Laboratory of Prof. Dr. Volker Haucke, Department of Biochemistry, Free University of Berlin).

After 30 min a weak co-localization in early endosomes was visualized. The fact that the uptake was so low lead to the consideration of a transient process.

In contrast, the Golgi-marker AP-1 did not show any overlap with HPG-ICC staining (Figure 28). AP-1 is one of four Adaptor Protein complexes, comprising different polypeptides and can be found on the external vesicle membrane. It is necessary that clathrin can not bind to membranes by itself. AP-1 mediates clathrin coated vesicle formation at the trans-Golgi network (TGN).[154]

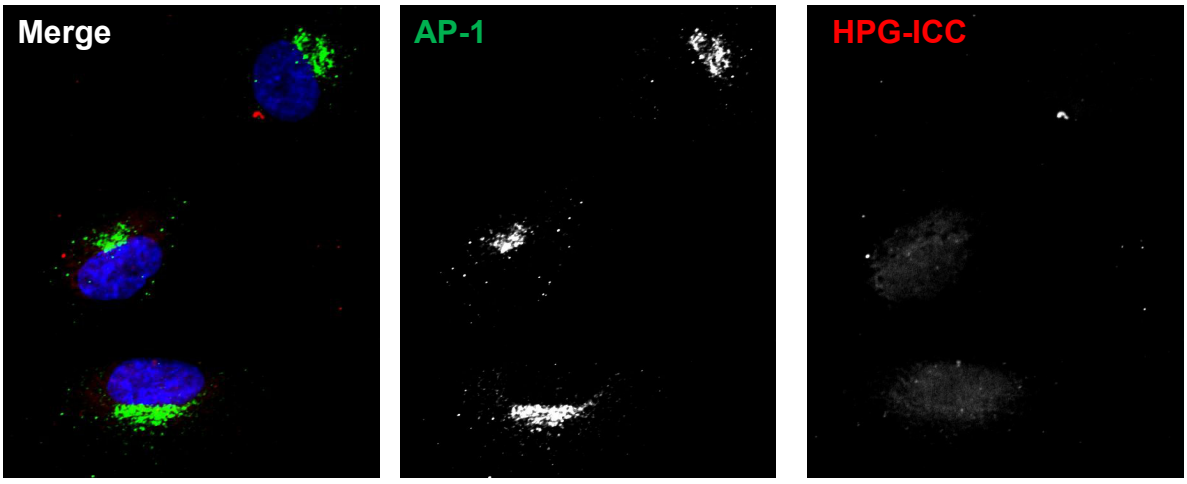


**Figure 28.** No co-localization of HPG-ICC with AP-1. The nucleus is stained with DAPI (blue). Incubation for 60 min, at 37°C. Merge (left), AP-1 (middle), HPG-ICC (right).

(Experiments performed by Irene Schütz, Laboratory of Prof. Dr. Volker Haucke, Department of Biochemistry, Free University of Berlin).

However, the transport process from late endosomes to lysosomes is not entirely understood. At present, three alternative hypothesis are under discussion.[155] The first model is based on a exchange between both compartments through transport vesicles. In this case, it was not decided if and how a fusion of late endosomes and lysosomes take place. The second model described, the so-called "kiss and run" hypothesis, is where late endosomes and lysosomes continuously merge with each other and separate again.[156] The third hypothesis is an elaboration of the "kiss and run" hypothesis and depicts the complete fusion of late endosomes and lysosomes. New lysosomes result from these hybrid organelles and the process repeats itself.[157]

Mannose-6-phosphate receptor (M6PR) are proteins that bind newly synthesized lysosomal hydrolases in the trans-Golgi network and deliver them to pre-lysosomal compartments.[158] In Figure 29 the cultured cells showed weak colocalization of HPG-ICC with M6PR within 60 min after co-incubation in our studies.

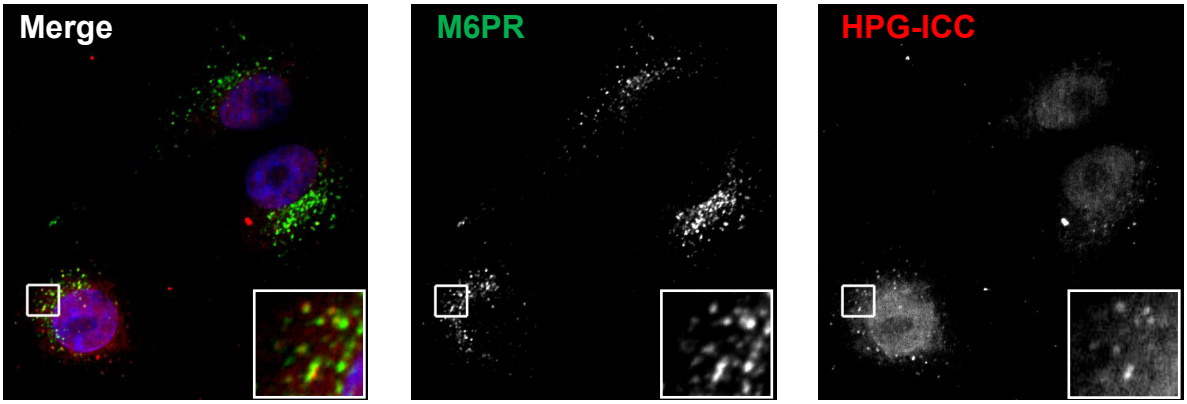


**Figure 29.** Weak co-localization of HPG-ICC with M6PR. The nucleus is stained with DAPI (blue). Incubation for 60 min, at 37 °C. Merge (left), M6PR antibody (middle), HPG-ICC (right). (Experiments performed by Irene Schütz, Laboratory of Prof. Dr. Volker Haucke, Department of Biochemistry, Free University of Berlin).

The lysosomes mark the final stage of the endocytotic process. These organelles posses a size of 0.5 µm and can make up 5-10 % of cell volume.[159] Lysosomes are characterized by a low internal pH value (pH of 5-5.5), integral membrane glycol proteins such as those Lysosomal-associated membrane protein 1 (LAMP1) and the lack of M6PR.[155] In addition

to its function as a terminal compartment of the endocytotic process, degradation of phagocytotic and auto phagocytotic materials as well as proteolyses of cytosolic proteins take place in lysosomes.[160,161]

LAMP1 is a glycoprotein. After leaving the TGN it enter directly in the endosomes without passing the plasma membrane. Being not prone to accumulate in a recycling process, LAMP1 is directly transported from the endosomes to the lysosomes. It is a good marker for late endosomes. To study the application of HPG-ICC in lysosomes, the lysosomes were stained with LAMP1 and monitored the confocal fluorescence micrographs (Figure 30). The red fluorescent spots in Figure 30 represent the HPG-ICC that were able to escape the lysosomes, whereas those that were trapped inside the vesicles are yellow in color, which is the result of overlapping green (lysosomes) and red (HPG-ICC) spots.

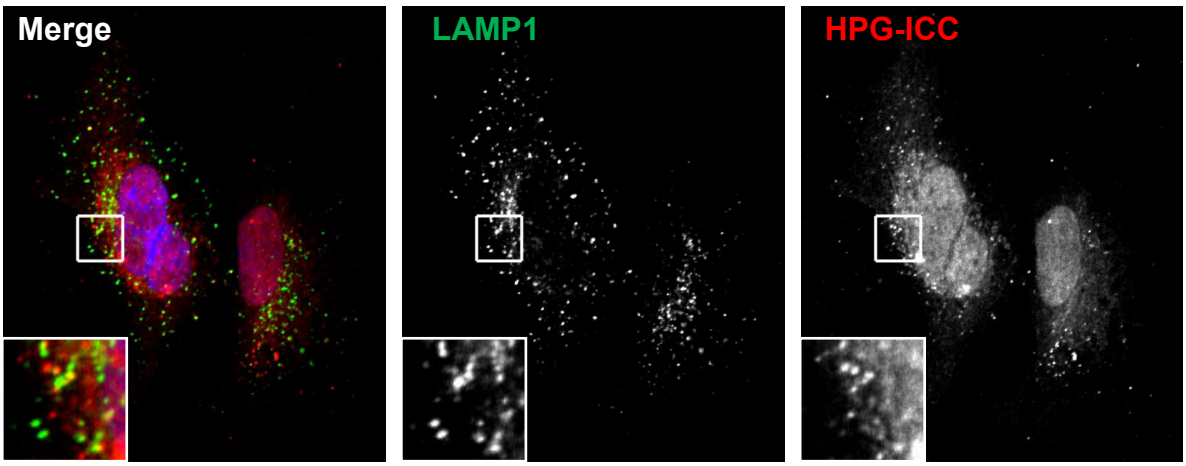


**Figure 30.** Co-localization of HPG-ICC with LAMP1. The nucleus is stained with DAPI (blue). Incubation for 60 min, at 37 °C. Merge (left), LAMP1 antibody (middle), HPG-ICC (right). (Experiments performed by Irene Schütz, Laboratory of Prof. Dr. Volker Haucke, Department of Biochemistry, Free University of Berlin).

Another specific cell organelle marker is Cluster of Differentiation 63 (CD63), localized in the membrane of platelet lysosomes and is known to complex with integrins.[162] Originally observed in melanoma tissue,[163] it can be detected in several types of tissue, including both healthy cells as well as inflammatory or tumor cells, and thus can be used as a biomarker for the recognition of tumor states.[164]

The yellow color in the merge picture in Figure 31 indicates the presence of HPG-ICC in lysosomes. Consequently, it has been shown that HPG-ICC is specific for lysosomes, in which it co-localized with LAMP1 and CD63.

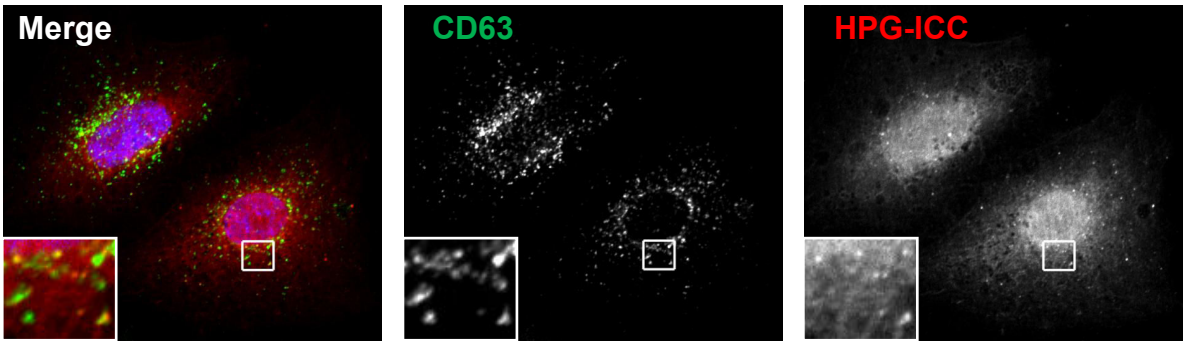


**Figure 31.** Co-localization of HPG-ICC with CD63. The nucleus is stained with DAPI (blue). Incubation for 60 min, at 37 °C. Merge (left), CD63 antibody (middle), HPG-ICC (right). (Experiments performed by Irene Schütz, Laboratory of Prof. Dr. Volker Haucke, Department of Biochemistry, Free University of Berlin).

## 4.2. Discussion and Conclusion

Several studies have investigated the cellular uptake and localization of labelled polyglycerols and derivatives.[112,144] The results demonstrated that these polymers rapidly internalize inside the cells and localize mainly in vesicles.

For the effective fighting of diseases it is particularly important that the endocytosis mechanism and the regulation process be adequately understood. The pathway of particles to enter the cells depends on the mechanism of the vesicle formation, type of charge and the size of the endocytotic vesicles. As previously mentioned (Chapter 1.5.3.), there are different possibilities to enter cells, but the function and regulation confronts the research with many open questions. It is also unclear whether there will be more other entry pathways into cells. According to first assessments, 10 % of the human genome are involved in the regulation of membrane transport.[165] It is not so strange, therefore, that a number of diseases is due to defective expression of membrane transport proteins. Interference in the endocytosis mechanism has been found in several neurodegenerative diseases, tumours, and infections. Today, in particular, a few lysosomal diseases are well known, such as Krabbe-disease, Tay-Sachs-disease, or metachromatic leucodystrophy.[166]

Other studies have shown that the transport of particles is energy dependent and is reduced in the presence of endocytosis inhibitors, signifying the importance of endocytosis in dendrimer transport.[167] Dendrimers have also been reported to co-localize with clathrin

and early endosomes markers, suggesting the involvement of clathrin-mediated endocytosis in dendrimer internalization.[168] Currently, a wide range of questions remain regarding the mechanism by which dendrimers or other polymers enter cells and are transported across the epithelial barrier. In particular, which of the different endocytosis pathways are used for cellular uptake and the specific mechanisms by which dendrimers/polymers open tight junctions have yet to be elucidated.

The results from the size-dependent cellular uptake of hyperbranched polymers led to the decision to investigate the mechanism of cellular uptake HPG-ICC by examining the impact of endocytosis inhibitors on polymer interaction with human lung cancer cells A549. In order to be safe, with the best results of cellular uptake, three different sizes of HPG-ICC (10, 120, and 208 kDa) were tested. As expected, no or weak co-localization was found with lower molecular weight HPG-ICC conjugates (images are omitted because of weak significance). In addition, the intracellular trafficking of the conjugate was monitored from early/late endosomes to lysosomes over time. Knowledge of the specific pathways of endocytosis and intracellular trafficking will aid in rational design of multivalent polymers for oral delivery.

Two endocytosis inhibitors were chosen to examine the pathways of cellular uptake. Inhibitors included chemicals known to prevent clathrin-mediated endocytosis (Pitstop) and dynamin-dependent endocytosis (Dynasore). A549 cellular uptake of HPG-ICC was found to occur primarily through clathrin-mediated endocytosis (Figure 25) and probably dynamin-dependent endocytosis pathways, but the co-localization was quite weak. In an earlier study, Kitchens and coworkers[168] suggested the involvement of clathrin in PAMAM dendrimer endocytosis. In a recent publication, another pathway was reported by caveolin-mediated endocytosis.[169] Many indications suggest that dendrimers and related polymers are not relegated to a single means of cellular entry, but instead take advantage of several specific endocytosis pathways.

Previous reports examined dendrimer colocalization with endosomal and lysosomal markers in Caco-2 cells and reported that dendrimers show constant presence in the early endosomes at 20 and 60 min, with time-trafficking to the lysosomes.[168] In this study hyperbranched polyglycerols were found to localize in the early endosomes after 30 min, displayed fast trafficking to the lysosomes after 30 min and increased endosomal and lysosomal accumulation at 60 min, likely due to pathway saturation. In contrast, the Golgi-marker AP-1 did not show any overlap with HPG-ICC staining.

Due to the mean shift of the pH value between endosomes, lysosomes, and the cytosol, it is possible to conjugate drugs to polymers *via* pH-sensitive linkers that are cleaved in the acidic environment of mature endosomes or peptide linkers that are cleaved by lysosomal enzymes such as cathepsin B.[170] These are promising approaches for cleavage of pH-sensitive linkers in the lysosomes, as polymers are shown to accumulate in these cell organelles over time. Thus it is even more important to understand the cellular uptake and intracellular trafficking pathways of polymers to improve their design for use as drug delivery vehicles.

In conclusion, in this work, the cellular uptake and the intracellular transport of hyperbranched polyglycerol were reported. The presented findings and previous results concerning the size-dependent cellular uptake of the study suggest that there is no endocytosis in case of the 10 kDa HPG-ICC conjugate and redundant fluorescence signals in the cells were redundant after incubation with ICC labelled 120 kDa polyglycerol. From existing results of other research groups[171] as expected it was observed that HPG-ICC (208 kDa) were most likely endocytosed *via* clathrin-mediated pathway, but not exclusively. HPGs are quickly trafficked to the lysosomes, but show increased endosomal accumulation once the lysosomal compartments become saturated. It is demonstrated that HPG was not localized with the Golgi apparatus.

In conclusion, hyperbranched polyglycerols provides a great potential for an efficient more purposefully transport of active substances.

# 5. Active Uptake of Hyperbranched Polyglycerols

The understanding of intermolecular interactions is of key importance for understanding many chemical and biological processes. Already in 1894 E. H. Fischer set a milestone for the comprehension of these processes. He described significant aspects about the configuration of enzymes for interactions with its targeted substrate. In this context, he formulated the well known "key-lock principle".[172]

The specific characterizations of the target molecules can be used for an enrichment of the active agents in "active targeting". For example, tumour-specific surfaces or receptors serve as basis as target structures for conjugate drugs. In particular, peptides play a special role in this mechanism. Their molecular detection is very important for a few biological processes. Figure 32 gives an overview about tumor-homing peptides which can function as therapeutic agents.

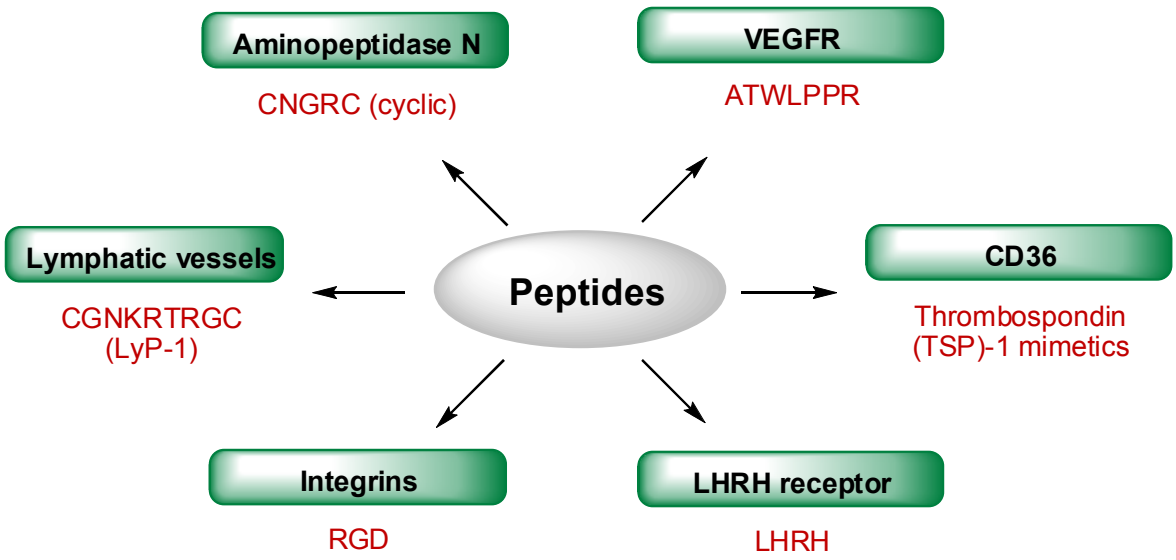


**Figure 32.** Examples of peptides which play a specific role in molecular detection (tumor targets in green, peptides in red).

Synthetic receptors are molecules, which show a structure that is complementary to their target substrate. If the target molecule is known it is possible to design specific receptor molecules. This case is also known as "customized receptors". Such conjugates might be able to involve in biological processes.

The objective of this study was the use of such peptides in combination with low molecular weight hyperbranched polyglycerols to serve as conjugates for transport systems because of their chemical, physical and biological advantages.

**The Tripeptide RGD (Arg-Gly-Asp)**

The recognition and specific interactions between cells or between cells and a physiological matrix are indispensable for a multicellular organism. It is necessary that the cell or the matrix of the cell is clearly identified to guarantee the selective interaction. Thus, it must be different to other substrates, which are not the target of the interactions. Oftentimes such targeting functionalities are saccharides, which can be detected by other cells. Saccharides can be directly anchored within membranes by binding covalently to lipids in the membrane, but localization at a transmembrane protein is also possible. Another option is the direct detection of membrane proteins, such as well defined peptide sequences.[173,174]

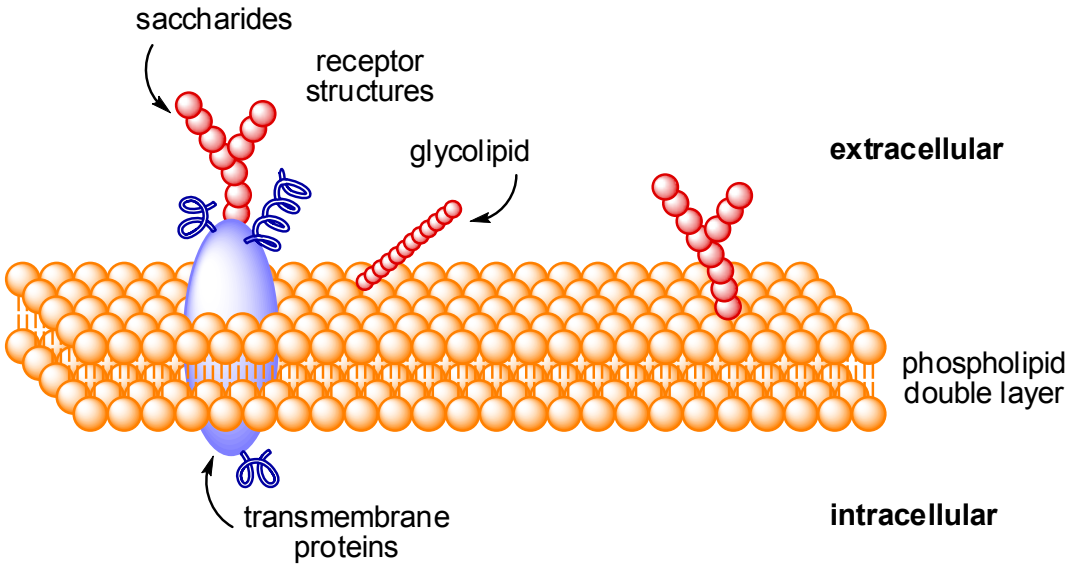


**Figure 33.** Scheme of a cell membrane with transmembrane proteins. Identification with receptor structures (red) or directly with transmembrane proteins (blue).

Four classes of membrane proteins exist, which are involved in recognition interactions: (i) cadherins, (ii) selectins, (iii) receptors of the immunogluboline class, and (iv) integrins.[175] Integrins are transmembrane proteins composed of two heterodimer subunits, named as α and β. There are 9 well-known β- and 17 α-subunits. The combination consisting of each one α- and one β-unit provides a large number of well known integrins. This proteins play an important role in different biological processes, such as the cell-cell and cell-matrix

adhesion involved in the bone growth and angiogenesis (formation of new blood vessels).[176] Accordingly, there are lots of diseases which arise from malfunctions in this control systems. Several extracellular proteins can interact with the integrins, many of which contain the tripeptide sequence Arg-Gly-Asp (RGD), which is termed as the universal cell recognition sequence (Figure 34).[177]

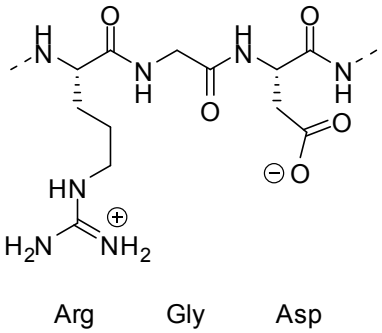


**Figure 34.** RGD sequence (arginine-glycine-aspartate).

Collagen, fibronectin, thrombospondin, fibrinogen, or osteospontin are examples for such RGD-bearing proteins.[178] All of these proteins include the RGD sequence, but interact selectively with their own specific targeted integrin. The reasons for this are still not clear, but possible causes can be the conformal rigidity of the sequence and/or the sequences of the individual amino acids. There are two strategies to handle with this knowledge. On the one hand it is possible to imitate the RGD sequence. Another approach is the development of molecules, which are able to complex the RGD sequence to inhibit integrins competitively.

Janssen and coworkers[179] reported an efficient approach with E-[c(RGDfK)2], the bis-cyclic form of c(RGDfK), in diagnostic studies. It is an $\alpha_v\beta_3$ integrin specific binding moiety and exhibited improved tumor targeting properties over the monomeric form. In a recent study, Satchi-Fainaro et al. presented the design, synthesis and characterization of novel water-soluble PEG-DOX-RGD PM conjugates that target $\alpha_v\beta_3$ integrin overexpressed at the tumor site.[180]

In this study, a low molecular weight hyperbranched polyglycerol (10 kDa) was linked to E-[c(RGDfK)2]. The requirements for the passive targeting to the tumor site by the EPR effect in combination with active targeting to proliferating epithelial human lung cancer cell line A549, human epidermoid carcinoma cells A431, and cervical cancer cell line CaSki. To test specific bioactivity of the conjugates in $\alpha_v\beta_3$ integrin overexpressing cells

(A549) compared to cells that do not show overexpression (A431) of this receptor. The conjugate was labelled with ICC dye which shows a red fluorescence to image cancer cells for its cellular uptake. As a control, an ICC dye-labelled HPG (10 kDa) without an RGD moiety was synthesized. A549 cells were therefore considered receptor-positive, whereas A431 cells were considered receptor-negative.

**The Decapeptide LHRH (luteinizing hormone-releasing hormone)**

In 1971 A. Schally und R. Guillemin discovered the decapeptide LHRH (luteinizing hormone-releasing hormone, Figure 35).[181,182]

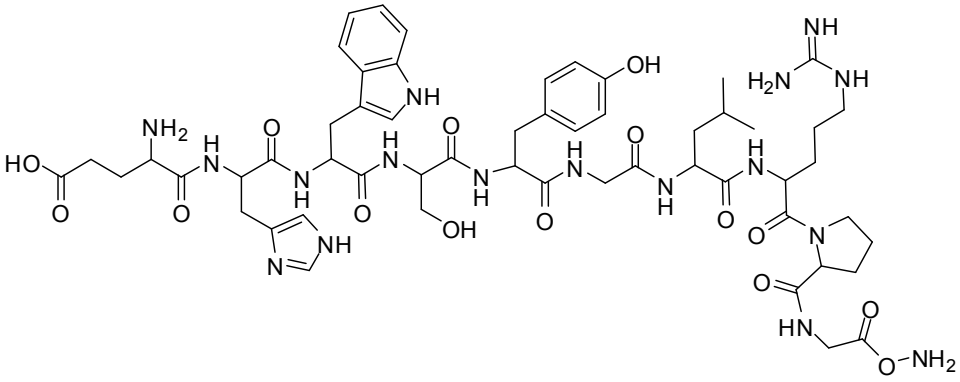

pGlu-His-Trp-Ser-Tyr-Gly-Leu-Arg-Pro-Gly-$NH_2$

**Figure 35.** Native luteinizing-hormone-releasing hormone (LHRH).

LHRH is formed in the hypothalamic neurons and is secreted into the blood stream. It stimulates the release of gender specific sexual hormones (the pituitary gland to release luteinizing hormone (LH) and follicle stimulating hormone (FSH)) in testes and ovaries. Extensive research led to the discovery that specific receptors for LHRH and synthetic analogues can be found in the pituitary gland and other tissues (for example tumor cells), as well as in other organs.[183] Since the structural clarification in the 1970s of LHRH, many agonistic and antagonistic effective analogues of the LHRH were developed, which were far superior in clinical application to the natural LHRH peptide.[184] LHRH analogues are used in treatment of hormone-dependent tumors, such as the prostate carcinoma and the estrogen receptor-positive mamma carcinoma for the pharmacological suppression of the sexual hormones.[185]

Ovarian and endometrium carcinoma cells express the LHRH receptors. In contrast, very few healthy tissues have such receptors. In addition, in hematopoietic and lymphatic system LHRH receptors could not be observed. Thereby, the therapy is highly specific and

has no side effects and is generally well-tolerated. Furthermore, the expression of LHRH receptors is preserved following metathesis. Therefore, the LHRH receptor is an ideal receptor for specific carcinoma. An advantage of the LHRH peptide is that LHRH does not accumulate in healthy tissues and the interacting with specific receptors in the plasma membrane of cancer cells *via* receptor-mediated endocytosis.[186]

In recent years the development of cytostatic drug conjugates with low molecular weight ligands for chemotherapy increased.[187] A good example is the conjugation with doxorubicin, a well known potent tumour therapeutic. A few LHRH conjugates were investigated intensively in preclinical studies and clinical trials with the new therapeutic approach are planned for the coming years.[187]

In this study it was examined, to what extent low molecular weight polyglycerol is operational as a transport system for specific receptor-mediated endocytosis. A LHRH peptide analogue was coupled as a cancer targeting ligand to the HPG (10 kDa). For LHRH receptor overexpressing epithelial human lung cancer cell line A549, human epidermoid carcinoma cells A431, and cervical cancer cell line CaSki, the polymers with LHRH exhibited enhanced cellular uptake compared to those without LHRH, resulting in increased enrichment in cells *via* receptor-mediated endocytosis.

## 5.1. Synthesis of HPG-Peptide-Conjugates

Inspired by the well-functioning synthesis of the fluorescence dye-labelled hyperbranched polyglycerols with maleimido indocarbocyanine dye (ICC-mal), the first aim was to synthesize maleimide-bearing peptides. The most widely-used heterobifunctional crosslinkers are those having an amine-reactive succinimidyl ester (i.e., NHS ester) at one end and a sulfhydryl-reactive group (e.g., maleimide) on the other end. As starting materials for this conjugate, a maleimide-dPEG$_4$-NHS ester and E-[c(RGDfK)2] were coupled in a one step reaction in DMF (Scheme 8).[188] After extraction and lyophilisation, a white powder was obtained and analyzed by mass spectrometry.

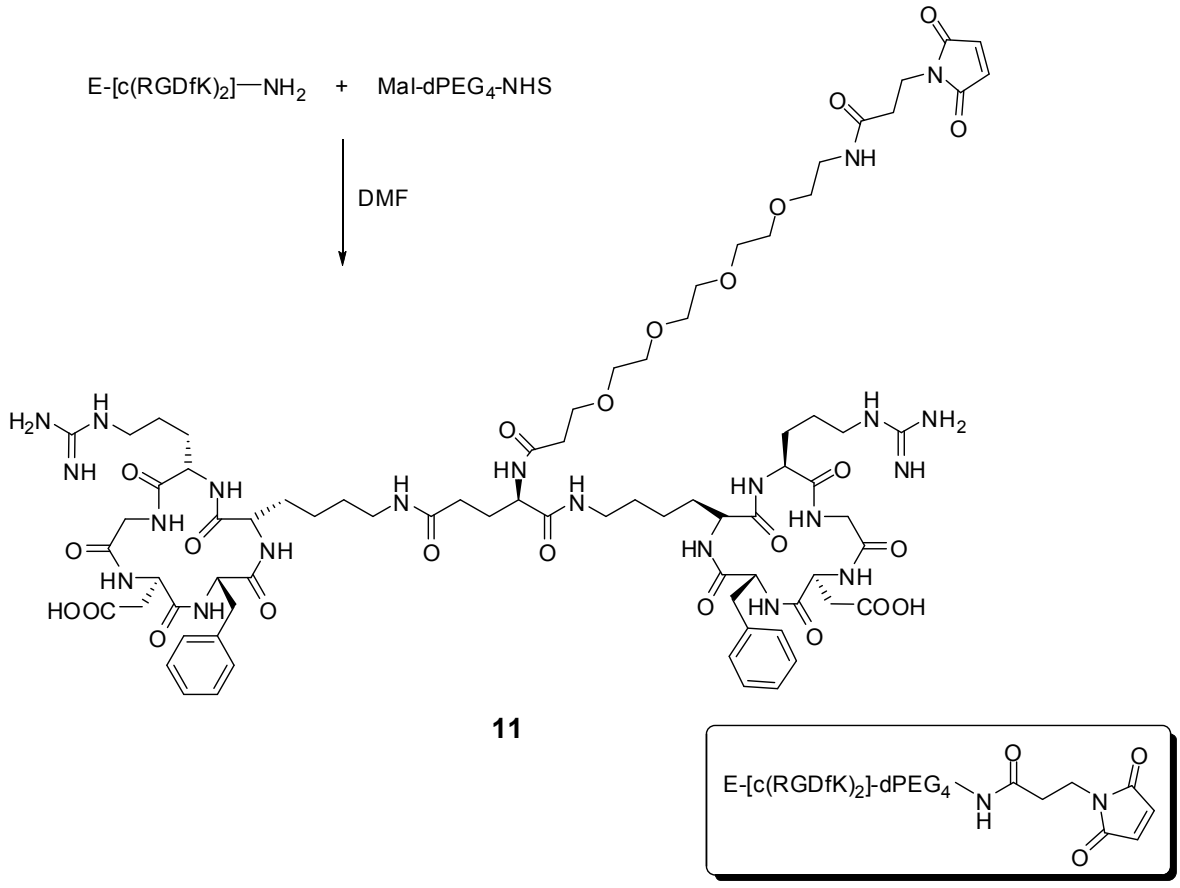


**Scheme 8.** Preparation of E-[c(RGDfK)2]-dPEG$_4$-mal.

In addition, compound **12**, the maleimide-bearing LHRH derivative peptide, was prepared in the same way as above (Scheme 9).

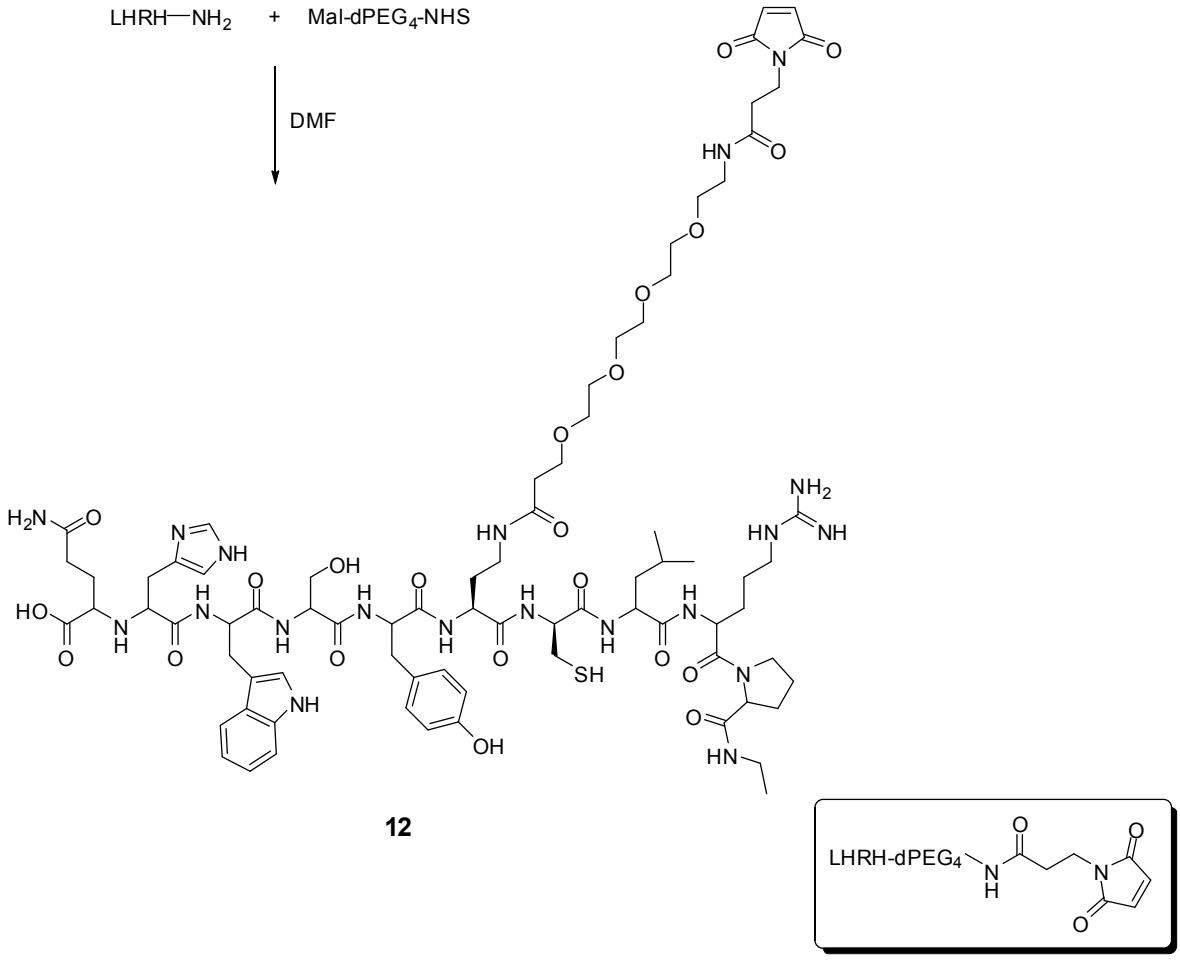


**Scheme 9.** Preparation of LHRH-dPEG$_4$-mal.

With the aim of active cellular uptake of dendritic polyglycerols, hyperbranched amino-bearing polyglycerol with molecular weight of 10 kDa was prepared in a one-pot synthesis as previously reported.[131,133] Peptide and fluorescently labelled derivatives were successfully obtained by a maleimid-mediated coupling between the maleimide-bearing peptides **11** and **12**, a ICC-mal respectively, and the thiol groups from the pre-activated polyglycerol scaffolds (Scheme 10). Briefly, the labelling of the dendritic amino-bearing polyglycerols was performed by a one-pot process, including a pre-activation of the polyglycerols through the reaction with 2-iminothiolane followed by a selective Michael addition between the maleimide groups of E-[c(RGDfK)2]-mal, the ICC-mal dye and the sulfhydryl groups from the thiolated polyglycerol in PBS solution at pH 7.

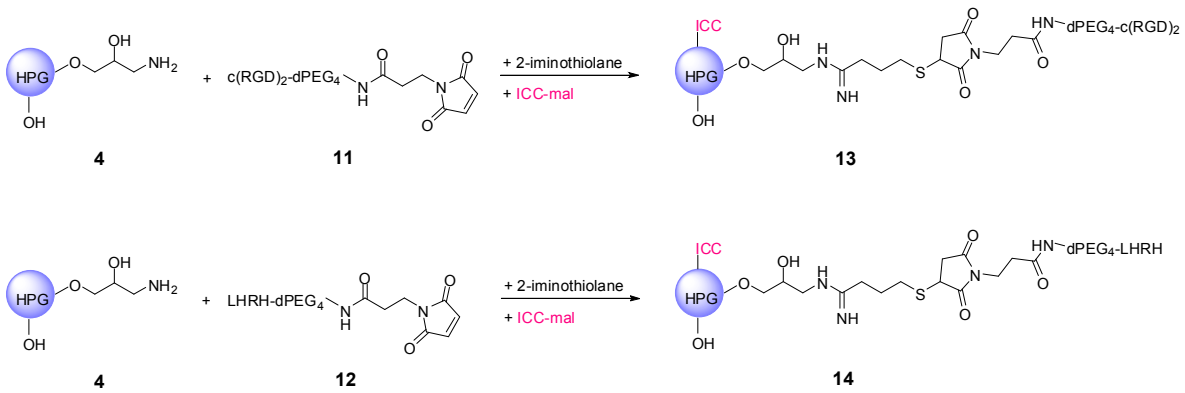


**Scheme 10.** Preparation of HPG-peptide-conjugates.

The thiol group added to the double bond of the maleimide group in a fast and selective reaction at room temperature to form a stable thioether bond.[133] Conjugate formation was confirmed by the appearance of a faster band on a Sephadex G25 column and by size-exclusion dialyses. Fluorescence measurements demonstrated that the ICC dye kept its fluorescence activity intact after conjugation.

## 5.2. Results of cellular uptake

In order to establish the potential for active cellular uptake of hyperbranched polyglycerol with specific cell membrane receptors, a systematic study was performed to compare the cell entry pathway and extent of the cellular uptake in three different cell lines; i.e. epithelial human lung cancer cell line A549, human epidermoid carcinoma cells A431 and cervical cancer cell line CaSki. To visualize the RGD and the LHRH receptor-mediated cellular uptake of HPG-RGD and HPG-LHRH, confocal microscopy was used with the help of the ICC dye which shows a red fluorescence. Cytoskeleton and nuclear staining, performed with Alexa Fluor 488 Phalloidin (green) and DAPI (blue) respectively, allowed determination of the intracellular distribution.

Cellular uptake experiments were performed by Dr. Pia Welker (mivenion GmbH, Berlin, Germany). Fluorescence images of A431 human epidermoid carcinoma cells and A549 lung epithelial cells are shown in Figure 36. HPG-ICC (10 kDa) as negative control was not localized in the cell. RGD-PEG-HPG-ICC-conjugates were not detected inside the A431 cells. A431 cells do not express αvβ3, as expected.[189] On the other hand, the same derivative was found predominantly localized in the cytoplasma of A549 cells after 1 hour

of incubation. In case of HPG-LHRH-ICC cellular uptake was observed in both cancer cell lines, which might indicate that the uptake is a receptor-mediated endocytosis pathway.

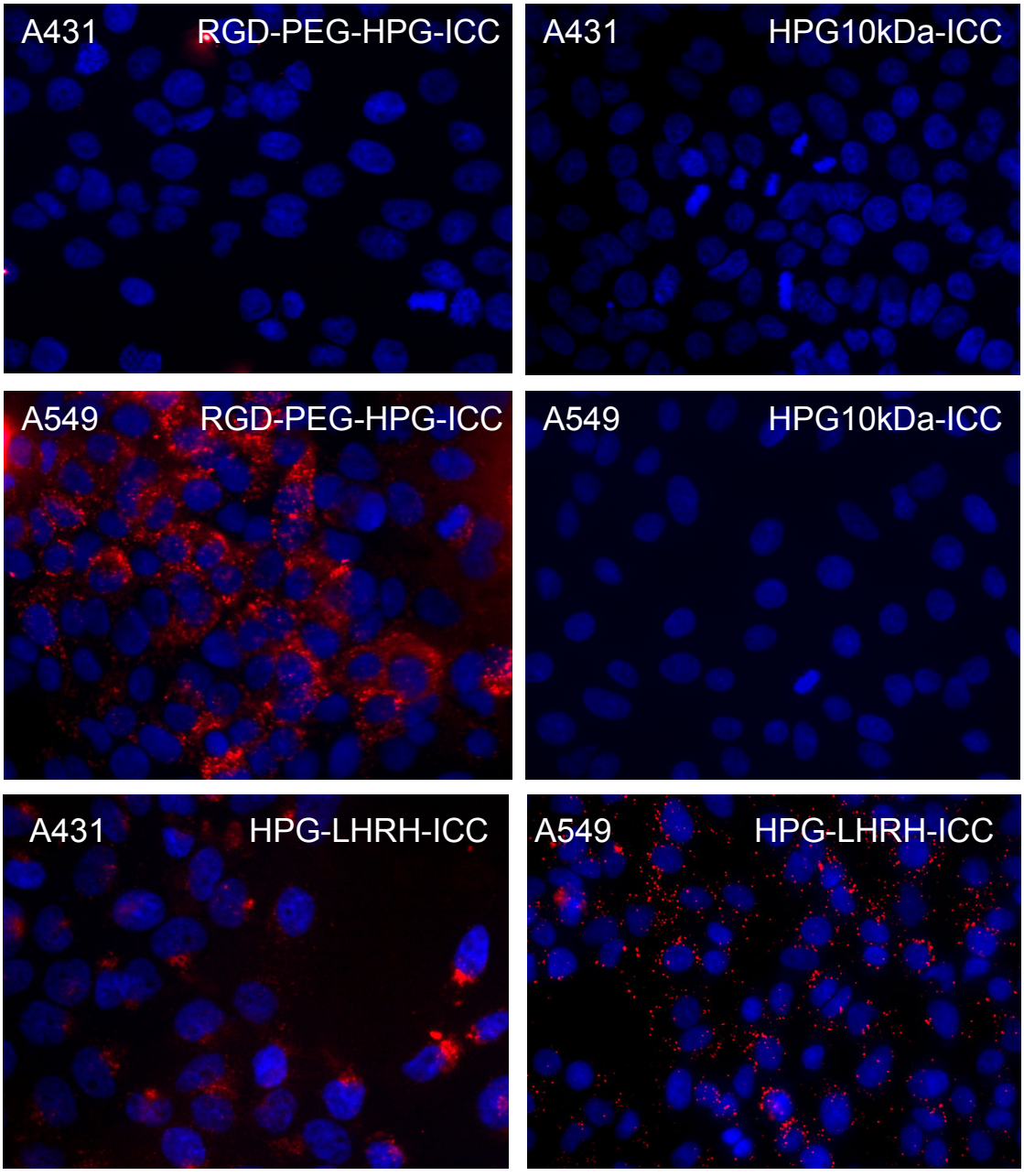


**Figure 36.** Fluorescence images of A431 human epidermoid carcinoma cells and A549 lung epithelial cells incubated with 1 µM of test material for 4 h at 37°C with HPG-ICC (10 kDa) as a negative control. RGD-PEG-HPG-ICC showed no positive cellular internalization inside the cytosol of A431 cells, but a high signal in A549 cells which is positive for the integrin receptor $\alpha_v\beta_3$. HPG-LHRH-ICC showed a cellular uptake in both cell lines. Merge pictures show labeled HPGs in red and stained nuclei in blue (DAPI). (Experiments performed by Dr. Pia Welker at mivenion GmbH).

In addition, intracellular localization and cellular uptake showed HPG-peptide conjugates to be localized in the perinuclear region in different human cells (Figure 37). Staining of the cytoskeleton component actin (green) demonstrated in conventional fluorescence microscopy that HPG-LHRH-conjugate (red) was localized inside of the cell after incubation for 4 h both in the epidermal (A431) and lung (A549) tumor cell lines, as well as in the cervical cancer cell line CaSki. In contrast, CaSki cell lines bind no RGD-PEG-HPG-ICC.

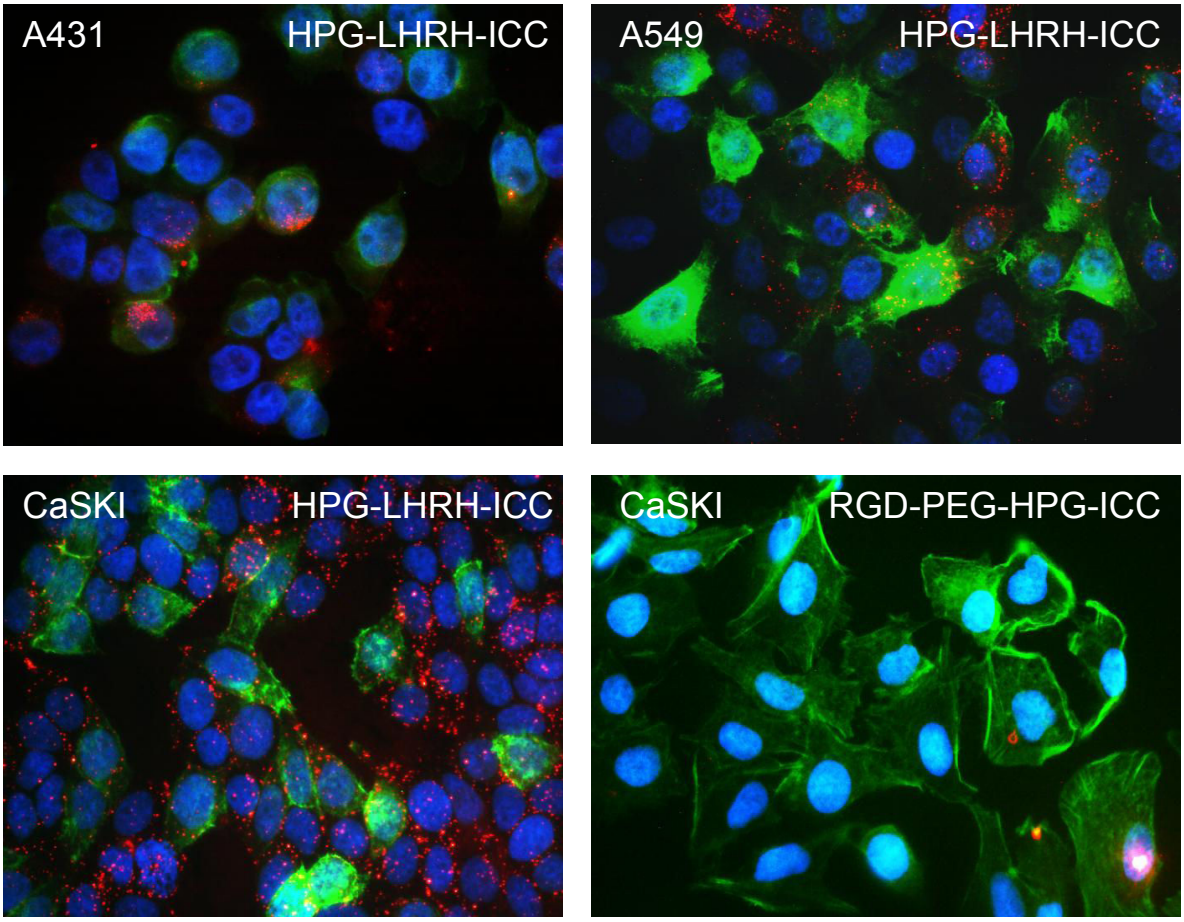


**Figure 37.** Different cell lines were cultured for 4 hours with PG-conjugates (red), stained with phalloidin (cytoskeleton, green) and DAPI (nucleus, blue): A431 cells show only minimal signals after incubation with HPG-LHRH-ICC, signals for A549 are slightly stronger. In the cervical carcinoma cell line CaSKI a strong specific signal is demonstrated. In contrast, CaSKI cells bind no RGD-PEG-HPG-ICC. (Experiments performed by Dr. Pia Welker at mivenion GmbH).

## 5.3. Discussion and Conclusion

As mentioned before, endocytosis, in particular receptor-mediated endocytosis, constitutes an important cellular mechanism to take nutrients and transducer extracellular signals essential for cell homeostasis, proliferation, and differentiation into cells.[190] Depending on the cell type, receptor concentration, type of ligand, ligand valency, and concentration, many receptors follow more than one intracellular pathway. Although the investigations of the mechanisms of endocytosis have increased over the last few years, many aspects are still not understood in detail. In general, active targeting involves cellular uptake of small drug molecules and macrocarriers or nanocarriers decorated with molecules enabling them to be selectively targeted to diseased cells.[191] Many properties of nanocarriers play an important role for biomedical applications, including composition, architecture, etc., and can be selected based on other considerations such as type of imaging or therapeutic agents, their aqueous solubility, electric charge, chemical structure, etc.

Gyongyossy-Issa and coworkers[117] reported the conjugation of RGD, a short peptide sequence of Arg-Gly-Asp, to hyperbranched polyglycerol, to improve the activities of RGD peptides. The results clearly demonstrated an increase in platelet inhibitory function of RGD by two to three orders of magnitude. They also studied the effect of different molecular weight HPGs and the number of RGD peptides attached to each HPG molecule. In summary, the experiments have shown that the use of the higher molecular weight carriers with moderate levels of conjugated peptides, are suitable for the development of an antithrombotic drug.

Minko and coworkers[192] used the luteinizing hormone-releasing hormone (LHRH) as a targeting moiety to LHRH receptors that are overexpressed in the plasma membrane of several types of cancer cells. They demonstrated that the drug delivery system, a conjugation of LHRH, Camptothecin as an anticancer drug and poly(ethylene glycol) as a carrier, substantially limits adverse side effects on healthy tissues and significantly enhances the antitumor efficacy of the anticancer drug.

Therefore, the main objective of this work was to study the active cellular uptake mechanism of low molecular weight HPGs with two different peptides for investigation of receptor-mediated endocytosis pathways. The previous studies of hyperbranched polyglycerols in biomedical applications have shown that HPGs have a broad range of potential applications in medicine and pharmacology.[97,98,99,100,101]

Towards this direction, a 10 kDa HPG was labeled with ICC to image cancer cells and coupled with E-[c(RGDfK)2]-mal and a LHRH derivative respectively to study the endocytosis pathway in three different cancer cell lines. The studies were carried out for *in vitro* uptake of HPG-peptides in comparison to "naked" HPGs in epithelial human lung cancer cell line A549, human epidermoid carcinoma cells A431, and cervical cancer cell line CaSki (Figure 36, Figure 37).

A549 cells specifically express the integrin receptor $\alpha_v\beta_3$. The *in vitro* studies showed that the HPG-RGD conjugate is enriched selectively in the human lung cancer cell line A549, which suggests that this cell entry could be attributed to a receptor-mediated endocytosis pathway. In contrast, there is no cellular uptake in epidermoid carcinoma cells A431 and cervical cancer cell line CaSki, as expected, because this kind of cells can not express the integrin receptor $\alpha_v\beta_3$. In comparison to the HPG-RGD conjugate, the HPG-LHRH conjugate was detectable in all used human cancer cell lines.

In conclusion, it was shown for the polymeric class of hyperbranched polyglycerols that active cellular uptake is target-dependent. The results demonstrated that HPGs with a low molecular weight are potential candidates for the development of new target carrier systems. Based on these findings, future research can be directed towards combining HPG as transport system, ICC as fluorescence dye, specific peptides as targeting molecules, and anticancer drugs for drug delivery systems to be investigated in *in vivo* studies.

This data for hyperbranched polyglycerols and the reported results in chapter 3 and 4, suggest that cellular uptake of macromolecules can be optimized for several applications. In particular, HPG-based scaffolds demonstrate optimal biocompatibility and make it a good candidate for multivalent interactions.

# 6. *In vivo* Studies of Dye-labelled Hyperbranched Polyglycerols

Near-infrared imaging holds promise for *in vivo* cancer detection because of flow tissue, autofluorescence, and high tissue penetration depth. Many fluorochromes, which are used for *in vitro* studies cannot be used for *in vivo* imaging, because they absorb light with wavelength in the range of visible light.[193] This results in a limited use of these dyes, because of the high absorption coefficient of light in the visible spectra of the tissue. Beside this, there is the disadvantage of the autofluorescence of tissue, which is also in the visible wavelength range.

The most common NIR fluorophores for *in vivo* imaging are polymethines.[194] These cyanine dyes have superior optical properties for tumor imaging which includes quantitative sensitivity, inherent biological safety, photostability, increases quantum yield, and decreases photobleaching, and relative ease of use.[195] Molecules with an absorption and emission spectrum in the near infrared range between 650-900 nm can be efficiently used to visualize and investigate *in vivo* molecular targets.[30] Depending on tissue type, penetration depth of 7 to 14 cm are possible.[194]

Because of the advantages of these dyes and the results of the size-dependant cellular uptake of HPG-ICC conjugates (see chapter 3), there have been investigations of *in vivo* studies with different sizes of hyperbranched polyglycerols coupled with indotricarbocyanine derivates and Cy5.5 derivates, respectively. The hope is to diagnose diseases earlier, if possible, in their preliminary stages. Of special interest is the simultaneous visualization of the effect of a therapy during the therapy.[20] The development of noninvasive, high resolution imaging technologies for *in vivo* diagnostic was a further significant step.[21,22,23]

## 6.1. Synthesis of HPG-ITCC and HPG-Cy5.5

With an aim towards determining the tumor uptake dependency of dendritic polyglycerols on molecular weight, a series of hyperbranched amino-bearing polyglycerols with MWs ranging from 10 to 870 kDa was prepared in a one-pot synthesis as previously reported (Scheme 11).[133,131] Fluorescence labelled derivatives were successfully obtained by a maleimid-mediated coupling between a maleimido indotricarbocyanine dye (ITCC-mal) and the thiol groups from the pre-activated polyglycerol scaffolds as already mentioned in

Chapter 3. Briefly, the labelling of the dendritic amino-bearing polyglycerols was performed by a one-pot process, including a pre-activation of the polyglycerols through the reaction with 2-iminothiolane followed by a selective Michael addition between the maleimide groups of the ITCC-mal dye and the sulfhydryl groups from the thiolated polyglycerol in PBS solution at pH 7.

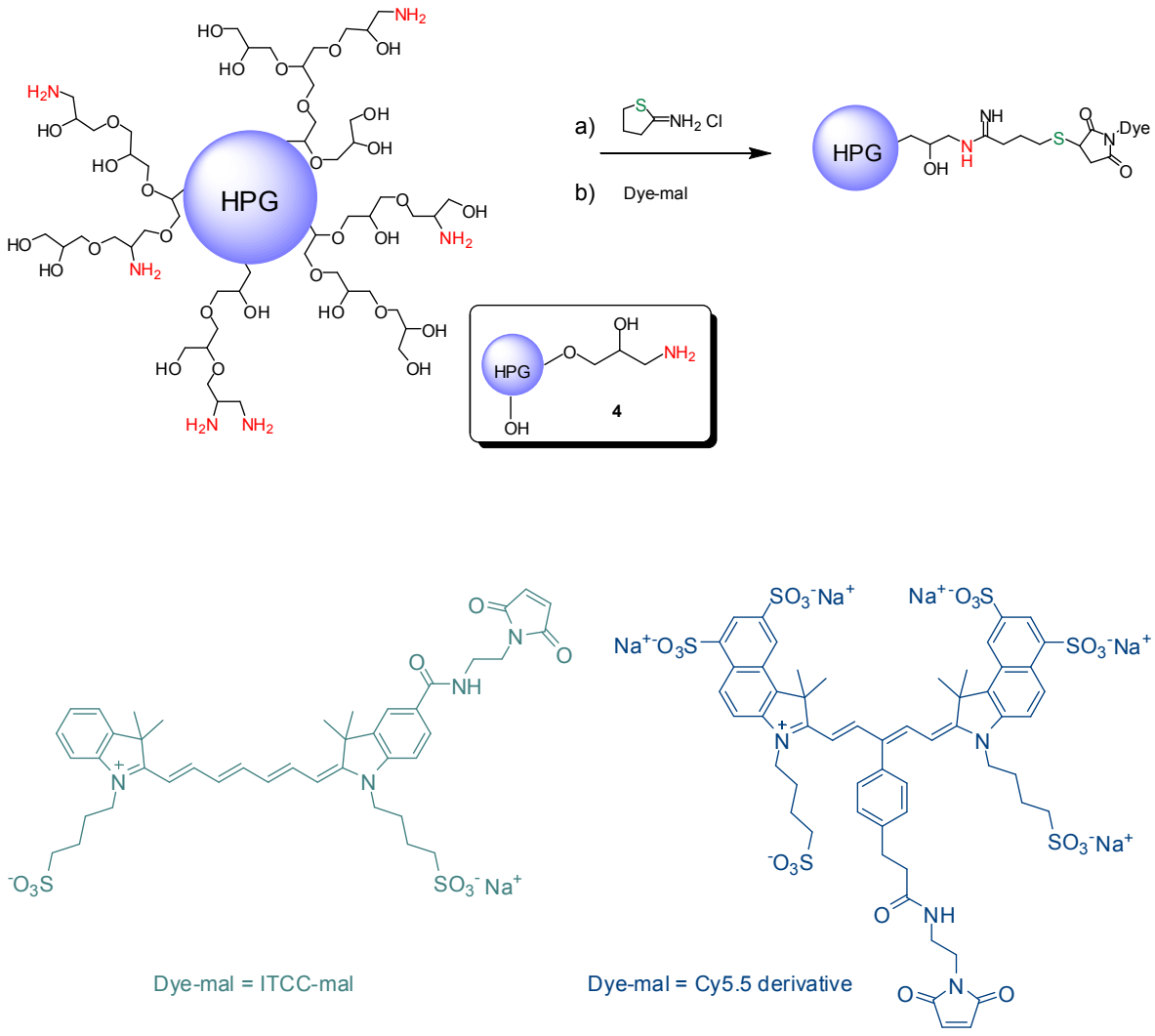


**Scheme 11.** Pathway for the synthesis of ITCC and Cy5.5 derivative labelled-polyglycerol conjugates. (a) phosphate/EDTA buffer, pH 7.0, r.t., 20 min and (b) phosphate/EDTA buffer, pH 7.0, r.t. 60 min. The depicted polymer structure represents only one possible isomer and a small part of the amino-bearing polyglycerol scaffold.

Analogous to the synthesis of HPG-ITCC, three different sized HPG-Cy5.5 conjugates (10, 120, and 475 kDa, Scheme 11) were prepared, and also a small molecular weight HPG (10 kDa) additionally with the active peptide RGD (Scheme 12).

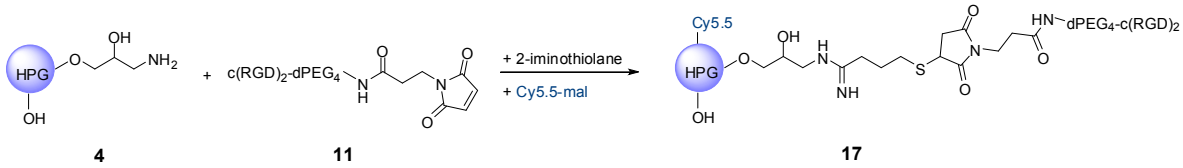


**Scheme 12.** Preparation of Cy5.5 labelled HPG-peptide.

## 6.2. Results

Analysis by dynamic light scattering (DLS) showed that the average diameters of these labelled polyglycerols increased with the MW of the hyperbranched polyglycerol, as expected, and were in the range of 0.8 to 21 nm. Zeta potential determinations demonstrated that the products have negative surface charge and that all values were in the similar range (-6 to -22 mV) as aimed for in the synthetic strategy. Table 6 summarizes the properties of the series of dendritic labelled-polyglycerol prepared.

**Table 6.** Differently sized HPGs under varying conditions and physical properties of the fluorescent polymers (their zeta potential and identification of the size *via* DLS).

| Nomenclature | Average MW of the core (kDa) | Surface charge | Mean diameter (nm)[a)] | Wt % of dye in the conjugate |
|---|---|---|---|---|
| $HPG_{10}$-ITCC | 10 | -7.34 | 0.8 ± 0.5 | 35.3 |
| $HPG_{20}$-ITCC | 20 | -8.33 | 6.5 ± 0.6 | 38.0 |
| $HPG_{20}$-PEG-ITCC[b)] | 36 | -13.1 | 15.6 ± 3.0 | 29.4 |
| $HPG_{120}$-ITCC | 120 | -6.35 | 11.7 ± 1.6 | 33.3 |
| $HPG_{208}$-ITCC | 208 | -15.8 | 10.1 ± 2.8 | 41.1 |
| $HPG_{475}$-ITCC | 475 | -13.41 | 16.2 ± 2.0 | 25.2 |
| $HPG_{870}$-ITCC | 870 | -22.0 | 21.0 ± 1.3 | 35.5 |
| $HPG_{10}$-Cy5.5 | 10 | c) | 1-3[c)] | 0.4 |
| $HPG_{120}$-Cy5.5 | 120 | c) | 9-11[c)] | 6.45 |
| $HPG_{475}$-Cy5.5 | 475 | c) | 15-17[c)] | 3.35 |
| $HPG_{10}$-RGD-Cy5.5 | 10 | c) | 3-4[c)] | 0.55 |

(a) Determined by dynamic light scattering. (b) HPG-20 with about 8 PEG molecules (2 kDa). (c) The fluorescence wavelength of the dye (λ = 676 nm) is too similar to the wavelength of the laser in the zeta potential analyzer (λ = 633 nm).

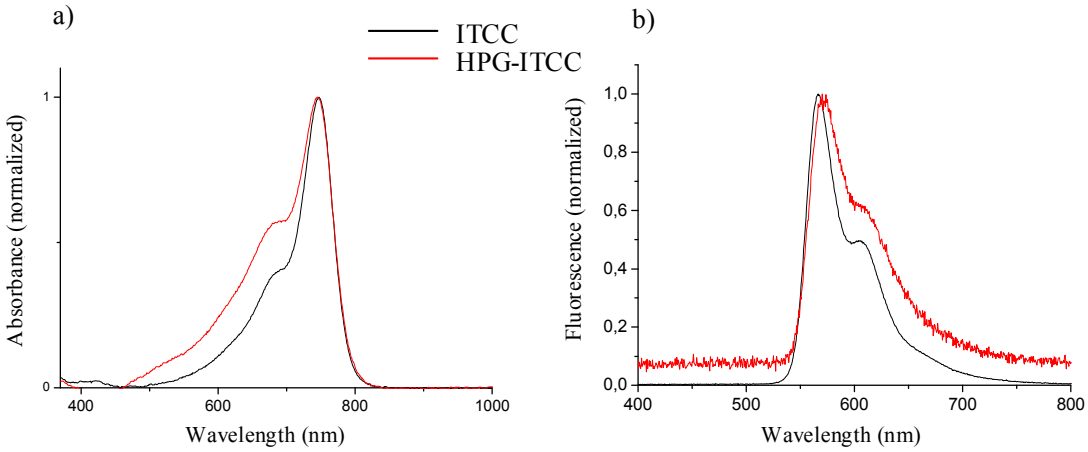


**Figure 38.** Absorbance (a) and fluorescence (b) spectra of free Indotricarbocyanine and HPG covalently coupled to Indotricarbocyanine (about 2%).

An increase of the shoulder is present relative to the maximum of the coupled dye. The absorption in this range has increased. Although there are no identifiable alterations in the maxima. There is a broadening of the absorption band, brought on by the coupling of cyanine dyes. The fluorescence maximum has also not shifted, and only a minor broadening is recognizable. An error of about ±1 % confirmed for the fluorescence quantum yield of the free dye the quantum yield for the coupled cyanine is equal to the free dye. Caused by the low loading Table 7 gives a summary of the absorption and fluorescence results.

**Table 7.** Absorbance and fluorescence data of free ITCC and HPG-ITCC.

| | ITCC | HPG-ITCC |
|---|---|---|
| Absorption maximum | 746 nm | 745 nm |
| Absorption (shoulder) | ~ 685 nm | ~ 685 nm |
| Fluorescence maximum | 774 nm | 774 nm |
| Fluorescence (shoulder) | - | - |
| Fluorescence quantum yield | $\phi$ = 8 % | $\phi$ = 9 % |

## 6.3. Animal study protocol

Hyperbranched polyglycerols are potentially viable choices as carriers because of their water solubility,[196,197] their biocompatibility properties both *in vitro*[131] and *in vivo*,[130] and the fact that polyether polyols can be synthesized in a controlled manner with

predetermined molecular weights and narrow molecular weight distributions.[120] In general the biocompatibility of polymers depends on their molecular weight. Brooks and coworkers reported *in vivo* studies of HPGs conducted on mice that revealed no sign of toxicity, weight disturbances, or undesirable effects after intravenous injection of a dose up to 1 g $kg^{-1}$ and after a period of 28 days.[120]

The preparation of dendritic multi shell architectures based on a PEG shell attached to HPG with a pH-labile linker was recently reported.[198] *In vivo* fluorescence imaging of tumor-bearing mice based on passive macromolecular targeting was demonstrated with the near-infrared indotricarbocyanine dye.[199] In addition, the effect of the size of the polymers is a critical issue for these systems. On the basis of physiological parameters such as hepatic filtration, tissue extravasation, tissue diffusion, and kidney excretion, it is clear that, along with surface composition, particle size is a key factor in the rapid clearance of circulating nanoparticles during systemic delivery and achieving of therapeutic efficacy.

Based on this easy visualization of the tumor accumulation of HPG-dye conjugates, a systematic study was performed to compare the size-dependant tumor uptake and extent of tumor uptake in four different tumor cell lines, i.e. for the HPG-ITCC conjugates, the human ovarian cancer cell line A2780 and the human colon carcinoma cell line HT29, and for the HPG-Cy5.5 conjugates, the breast cancer cell line 4T1-GFP and the colon carcinoma cell line C51.

**First study**

The mouse studies were conducted in accordance with the Physikalisch-Technische Bundesanstalt in Berlin, Germany, and were performed by Dr. habil. Bernd Ebert.

*In vivo* studies were performed on nude laboratory mice with genetic mutation inhibited immune system (absent thymus). The human ovarian cancer cell line A2780 was applicated subcutaneously and a resulted in tumor growth after two to three weeks. In the first studies groups of adult nude mice with three animals per group received slow i.v. injections of HPG-ITCC conjugates (10, 20, 120 kDa; each probe in 700 µl saline or PBS; application volume: 100 µl per 25 g body weight). Bioluminescence images were captured with an EMCCD-camera after 10 min, 1 h, 4 h, and 24 h. Representative images of mice after 24 h are shown in Figure 39. Glycerol-ITCC as negative control was not localized in the tumor. After 24 h, there were no significant signals observed in case of the small $HPG_{10}$-ITCC conjugate. Similarly, the low molecular weight $HPG_{20}$-ITCC conjugate was only detected in minimal amounts inside the tumor and a signal in the kidney could also be

noticed. On the other hand, the conjugate with the highest molecular weight (120 kDa) was found to be localized with a higher signal after 24 hours of incubation.

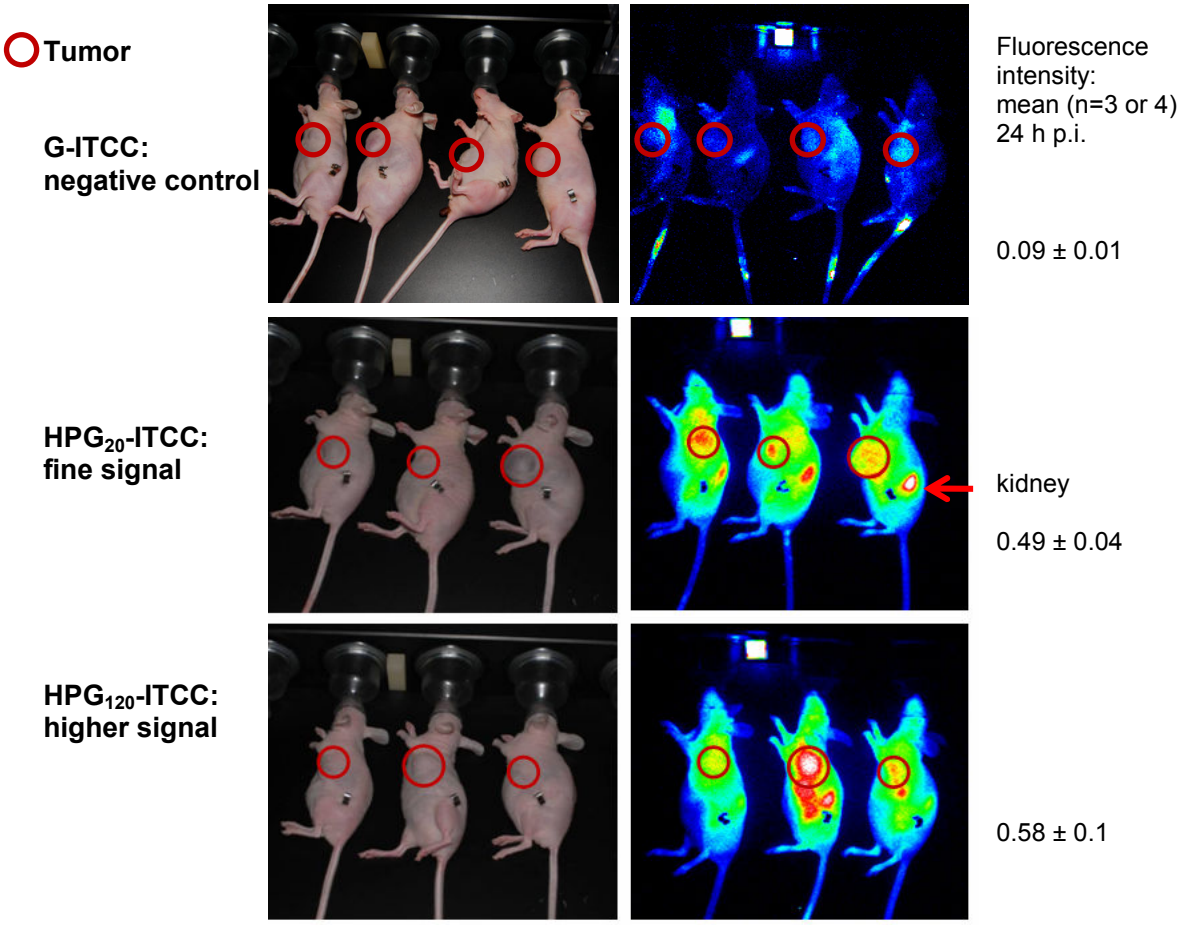


**Figure 39.** Representative sequences of bioluminescence images of mice after 24 h with G-ITCC a negative control. HPG-dye conjugate with higher molecular weight showed higher tumor internalization. (*In vivo* experiments were performed by Dr. habil. Bernd Ebert, Physikalisch-Technische Bundesanstalt in Berlin, Germany).

In addition, injection of fluorescent hyperbranched polyglycerols in non tumor bearing mice showed that the biodistribution of the polymer was almost the same as in the tumor bearing mice (Figure 40). HPG-dye conjugates were mainly eliminated by the renal system. Fluorescence was also observed in the liver and the intestine.

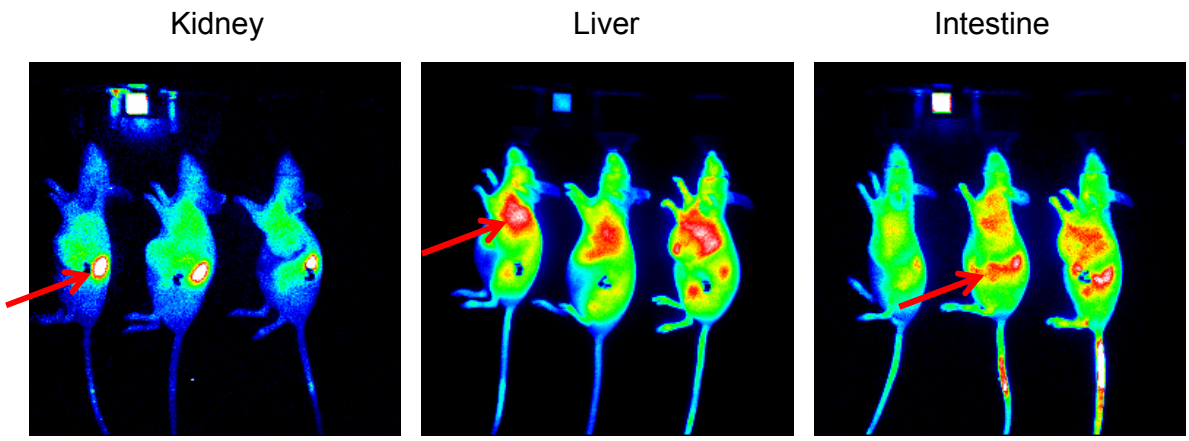


**Figure 40.** Histologic analysis of organs displaying fluorescence after polymer-dye injection. (*In vivo* experiments were performed by Dr. habil. Bernd Ebert, Physikalisch-Technische Bundesanstalt in Berlin, Germany).

The results of the first *in vivo* studies and also the in vitro results in Chapter 3 suggested a size-dependant tumor uptake, which generally points out appropriate polyglycerol diameters for cellular penetration in the range of 10-20 nm and molecular weights above 100 kDa. The analyses of organs in non tumor bearing mice suggest that the polymers were eliminated *via* the liver and the kidney. However, further research is necessary.

As a consequence, a second study was necessary to assure that the tumor uptake is size-dependant whereby the position of the tumor had to be changed so that the fluorescence of the organs did not disturb the fluorescence of the tumor.

**Second study**

The mouse studies were conducted in accordance with the Physikalisch-Technische Bundesanstalt in Berlin, Germany, and were performed by Dr. habil. Bernd Ebert.

Based on the results of the first *in vivo* studies a renewed investigation was performed. The human colon carcinoma cell line C51 was applicated subcutaneously on nude laboratory mice with genetic mutation inhibited immune system and tumor growth appeared two to three weeks later. Three groups of adult nude mice with three animals per group received slow i.v. injections of HPG-ITCC conjugates (20, 120, 870 kDa; each probe in 700 µl saline or PBS; application volume: 100 µl per 25 g body weight). Bioluminescence images were captured with an EMCCD-camera after 0 min, 10 min, 1 h, 3 h, 5 h, 24 h, and 48 h. After the fluorescence measurements the mice were killed, and the

organs of interest like kidney, liver, spleen, and the tumor obtained (Figure 41). In addition, the tumor was sliced. Subsequently a fluorescence image was recorded.

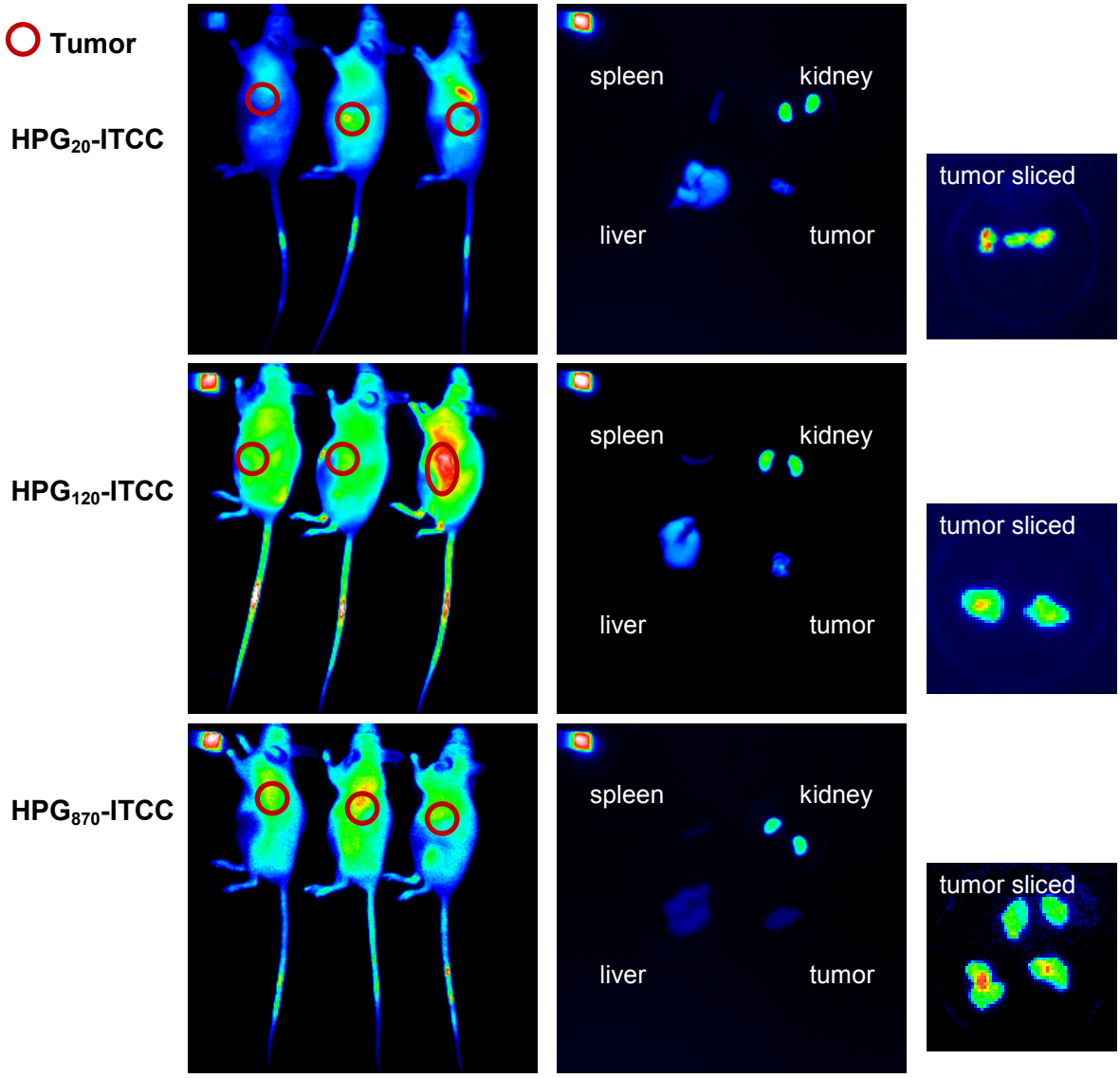


**Figure 41.** On the left: optical images of nude mice with 100 µl per 25 g body weight subcutaneous injection of HPG-ITCC conjugates (20, 120, 870 kDa). In the middle: removed organs and tumor. On the right: sliced tumor. (*In vivo* experiments were performed by Dr. habil. Bernd Ebert, Physikalisch-Technische Bundesanstalt in Berlin, Germany).

Figure 41 shows the most intensive optical images of nude mice after subcutaneous injection of HPG-ITCC conjugates (20, 120, 870 kDa). In the case of the $HPG_{20}$-ITCC, this meant already after the injection. After that, the intensity decreased within a couple of hours. On the whole, the intensity of the smallest polymer-dye conjugate was not very

distinctive, however, after subcutaneous injection of $HPG_{120}$-ITCC, the intensity increased continuously until approximately one hour and then began to fall (Figure 42).

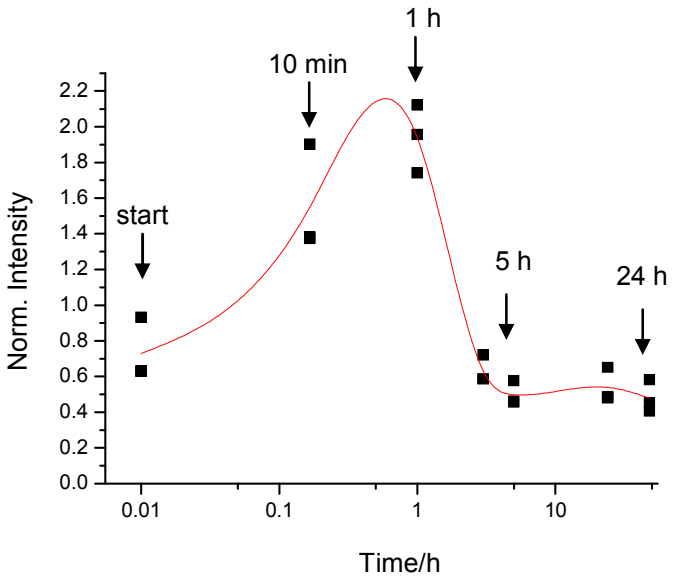


**Figure 42.** A plot of the signal efficiency of the fluorescence emission coming out from the animal vs. the time, after subcutaneous injection of $HPG_{120}$-ITCC.

In case of the highest molecular weight polymer-dye conjugate ($HPG_{870}$-ITCC) the most intensive optical image could be taken after 10 minutes after the injection of the compound. At this point, the fluorescence intensity decreased within 24 hours.

In all three cases, after the removal of the organs, an intensive signal enhancement localized in the regions corresponding to the kidneys was observed. Compared to the kidneys, the fluorescence intensity of the liver, a typical store organ, was slightly weaker, and it was even weaker in case of the spleens. This could mean that the excretion of the polymers meanly occurs *via* the kidneys. For a better interpretation of the excretion the urine has to be analyzed.

The results confirm the basic assumption of the size-dependant tumor uptake of hyperbranched polyglycerol labeled with a fluorescence dye. The optical imaging data of the $HPG_{120}$-ITCC conjugate indicate, at least in a first approximation, that this is the best compound for following *in vivo* studies, but additional assays are required to investigate the effective transfection *in vivo* of this synthesized systems.

For the next *in vivo* studies the following changes were taken into consideration: a better tumor implantation site than in the last studies (hip region), a new tumor model, a

polymer with a molecular weight between 120 and 870 kDa, and a low molecular weight hyperbranched polyglycerol coupled to a target molecule (RGD peptide).

**Third study**

The mouse studies were conducted in accordance with the Animal Imaging Center of UZH/ETH in Zürich, Switzerland. The experiments were performed by Dr. Divya Vats (Laboratory of Prof. Dr. Markus Rudin, Institute for Biomedical Technology, ETH Zürich).

For the third *in vivo* study new polymer-dye conjugates were synthesized. The dye used here was a Cy5.5 derivative, a reactive dye for the labeling of amino-groups in peptides, proteins, oligonucleotides, dendrimers, and hyperbranched polyglycerols. It is a fluorescent molecule that emits photons in the near infrared spectrum (emission maximum, $\lambda_{max}$ = 720 nm). Previous *in vivo* studies have shown that this dye and its derivatives can identify tumors with fewer than 2000 cancer cells making it 500 times more sensitive than MRI under operating conditions.[200]

This study reports the development of three different sized HPG-Cy5.5 conjugates (10, 120, and 475 kDa) and a small molecular weight compound (10 kDa) which is additionally coupled with a RGD peptide for active targeting, and the efficacy of this imaging agent in mouse models of the breast cancer cell line 4T1-GFP and the colon carcinoma cell line C51. The cancer cell lines are implanted directly in the hip region, one to the right (C51) and the other to the left (4T1-GFP). The images are of 8-10 week old nude mice (female) and were acquired when the tumors were approximately 4-8 mm in diameter. 2 mg of the compounds was injected per kg of the animal body weight. The animals were measured longitudinally after 0 min, 30 min, 1.5 h, 3 h, 6 h, 24 h, 36 h, and 48 h (Figure 43). For the last time point (i.e. 48 h after injection), the organs were harvested and imaged. The acquired images were subjected to spectral deconvolution to obtain true Cy5.5 spectra and then all the images compared over the longitudinal aquisition.

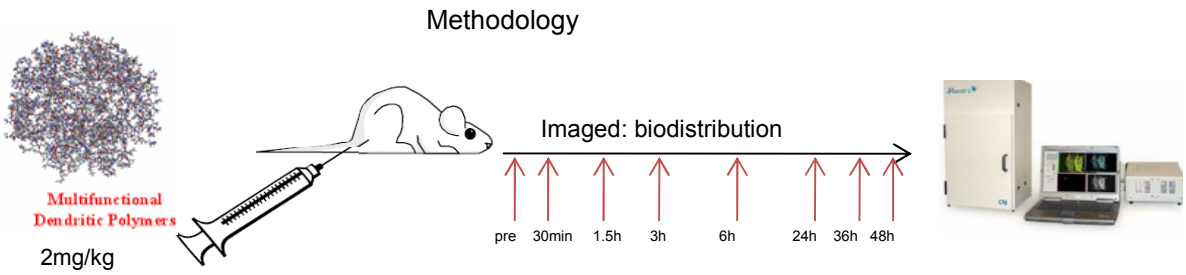


**Figure 43.** Schematic representation of the methodology of the measurements.

In Figure 44 the obtained images 0 min, 3 h, 6 h, 24 h, 36 h, and 48 h p.i. of an target specific conjugate (RGD-HPG-Cy5.5) are compared. Contrary to expectation, these images showed no significant accumulation occurs in the tumors. Only the kidneys and the backbone could be discerned. After 6 h the majority of activity has accumulated in the backbone. After 24 h the fluorescence intensity decreased and after 36 h only a very limited intensity was left in the backbone of the mouse.

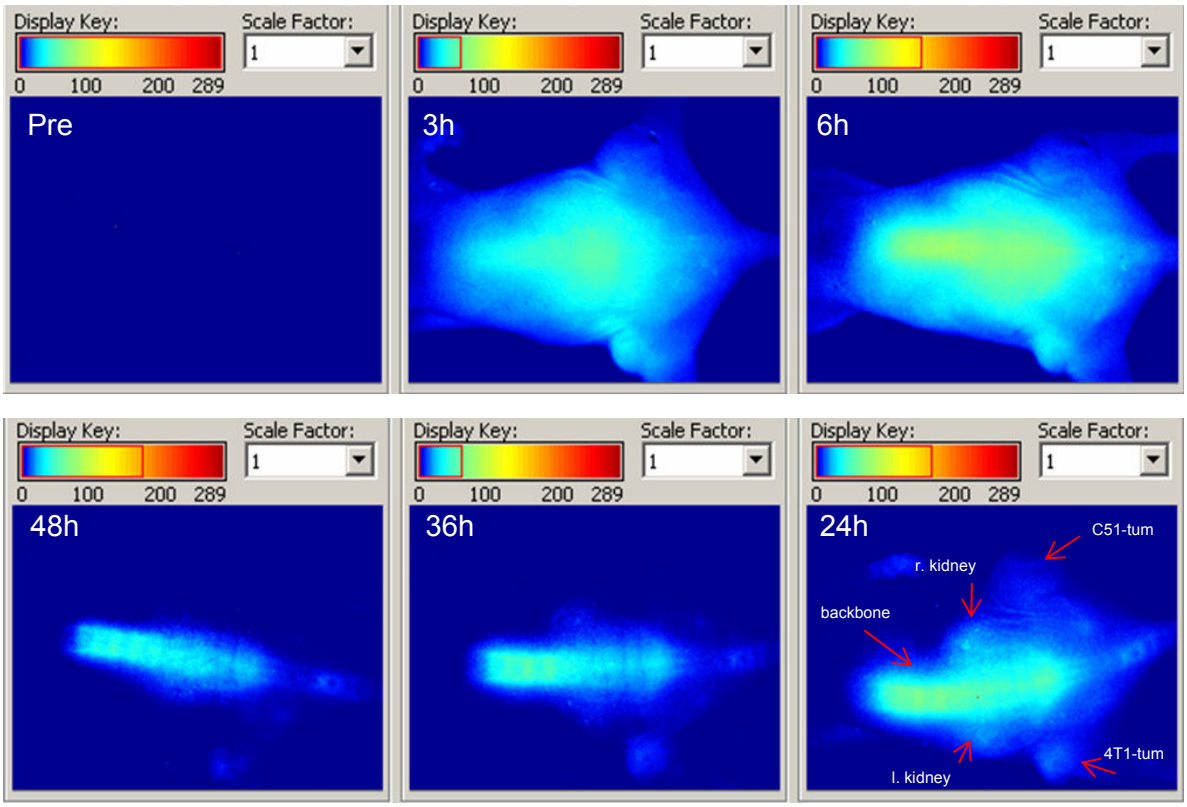


**Figure 44.** *In vivo* imaging of RGD-HPG-Cy5.5 (10 kDa of the starting polymer) at 0 min, 3 h, 6 h, 24 h, 36 h, and 48 h p.i. in a mouse. (Experiments performed by Dr. Divya Vats, Laboratory of Prof. Dr. Markus Rudin, Institute for Biomedical Technology, ETH Zürich).

The tumor uptake of $HPG_{10}$-Cy5.5 without an active target molecule was also investigated. As expected, in this case no tumor uptake was detected. In Figure 45 the obtained images 0 min, 30 min, 1 h, 3 h, 6 h, 24 h, 36 h, and 48 h p.i. of HPG-Cy5.5 are compared. The fluorescence intensity in the backbone region of the mouse first increased, and then after 6 h an intensity reduction was observed. The relatively even distribution of the polymer-dye conjugate can be explained with the EPR effect. Healthy endothelial cells are permeable for macro molecules with a molecular weight under 50 kDa and can be extracted by the lymph.

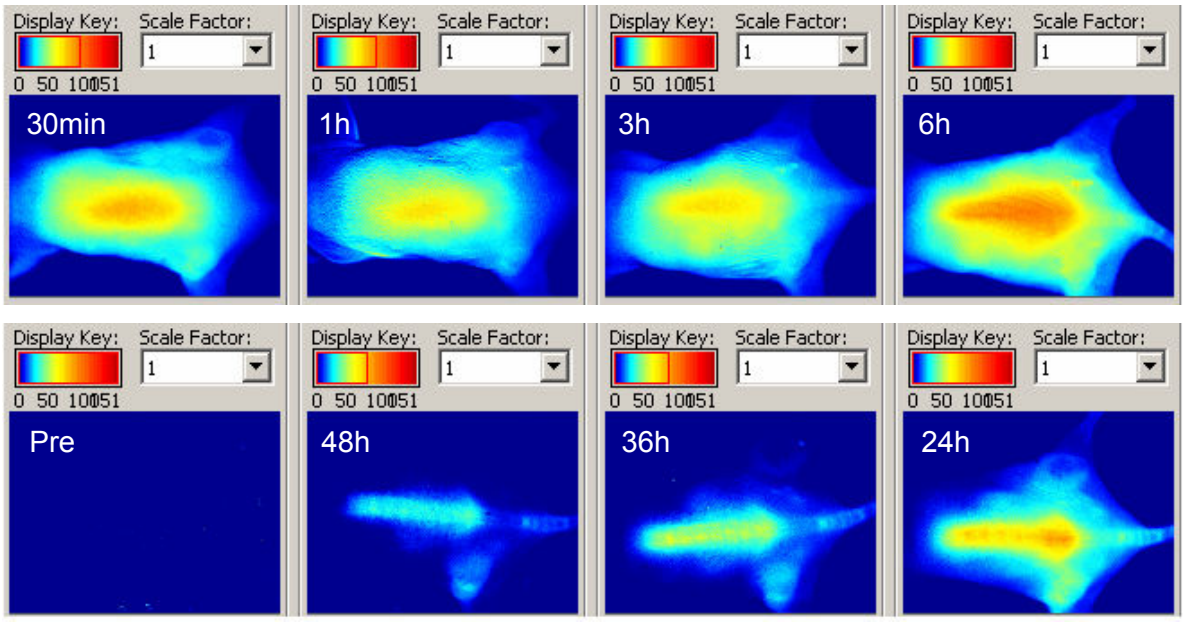


**Figure 45.** *In vivo* imaging of HPG-Cy5.5 (10 kDa of the starting polymer) at 0 min, 30 min, 1 h, 3 h, 6 h, 24 h, 36 h, and 48 h p.i. in a mouse. (Experiments performed by Dr. Divya Vats, Laboratory of Prof. Dr. Markus Rudin, Institute for Biomedical Technology, ETH Zürich).

The passive targeting is mainly dependent on the physicochemical properties of the carrier system, like the size of particles and the particle retaining characterizations of the tumor tissue (EPR-effect). To investigate this effect another experiment was done with a polymer-dye conjugate with a higher molecular weight. In Figure 46 the obtained images 0 min, 30 min, 1 h, 3 h, 6 h, 24 h, 36 h, and 48 h p.i. of HPG-Cy5.5 (120 kDa of the starting polymer) are compared. But even here, the fluorescence intensity was mainly observed in the backbone region of the mouse. The conjugate is extremely distributed and just a weak signal could be observed in both tumors. The intensity in the breast cancer was a little higher than in the colon carcinoma cell line. In addition, the accumulation at the backbone is also particularly pronounced. After 24 h the accumulation decreased.

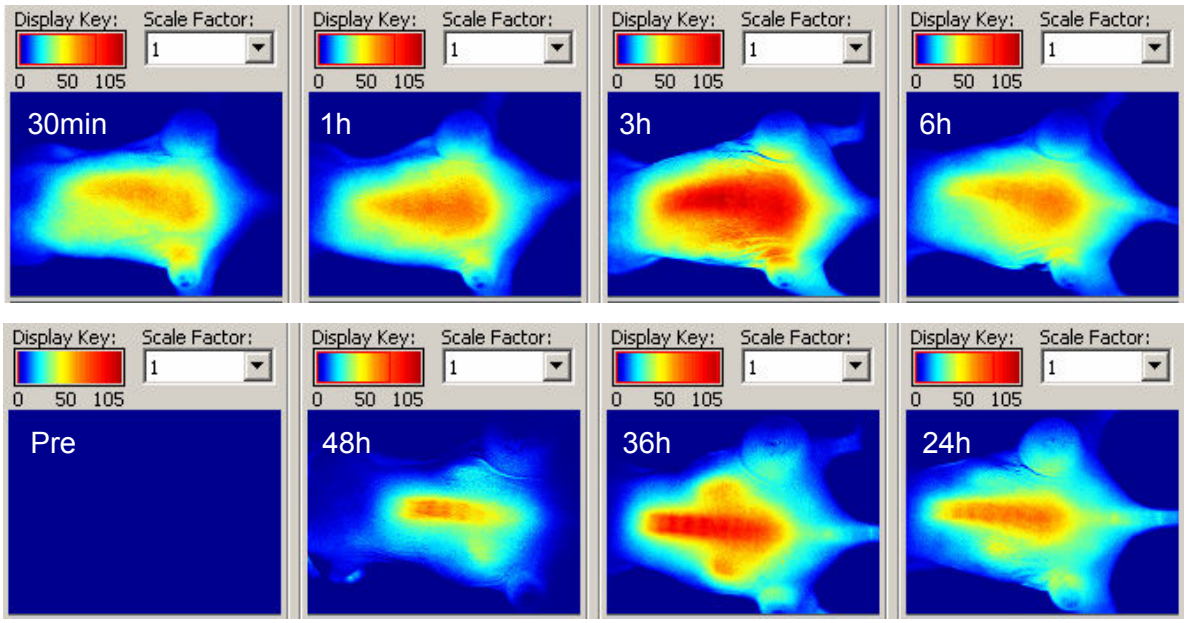


**Figure 46.** *In vivo* imaging of HPG-Cy5.5 (120 kDa of the starting polymer) at 0 min, 30 min, 1 h, 3 h, 6 h, 24 h, 36 h, and 48 h p.i. in a mouse. (Experiments performed by Dr. Divya Vats, Laboratory of Prof. Dr. Markus Rudin, Institute for Biomedical Technology, ETH Zürich).

The next study with a larger polymer-dye conjugate (475 kDa of the starting molecule) showed similar results. Again, a high distribution was observed. The fluorescence intensity increased in the first six hours and decreased after 24 h. Figure 47 showed an accumulation after 3 h in the breast cancer cell line 4T1-GFP and a slighter weaker accumulation in the colon carcinoma cell line C51. In addition, the accumulation at the backbone is again particularly pronounced.

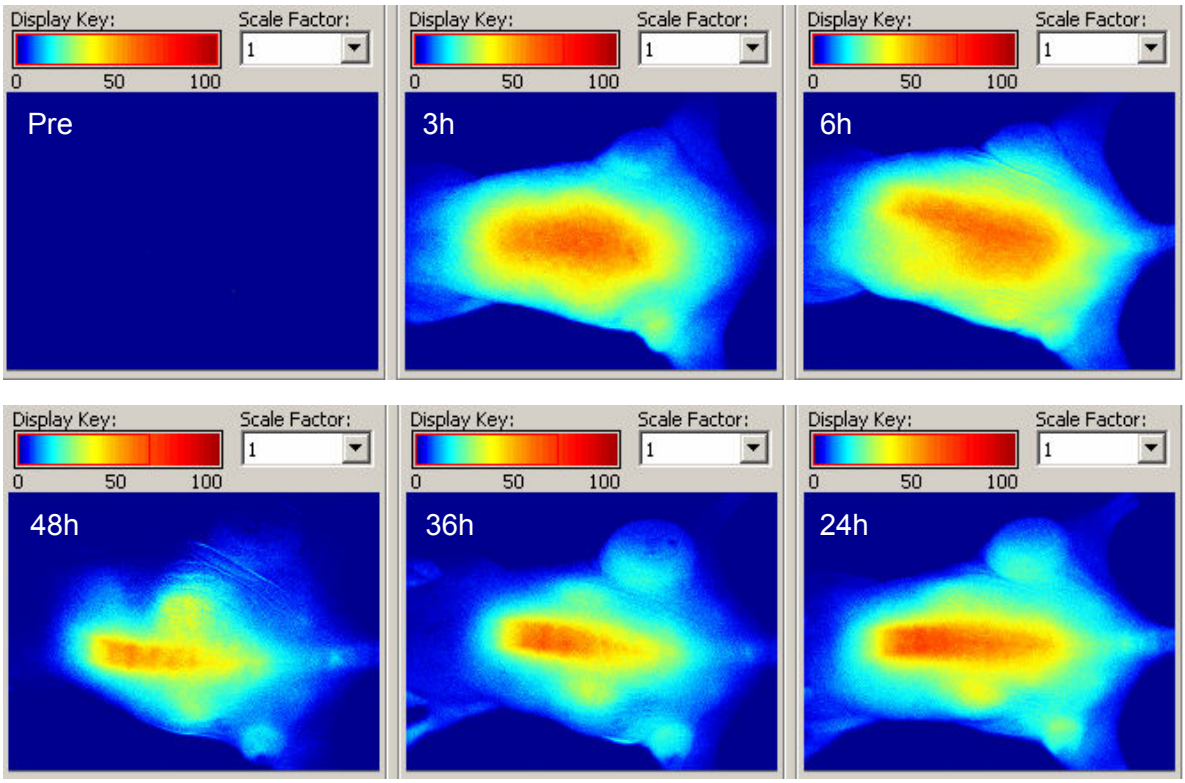


**Figure 47.** *In vivo* imaging of HPG-Cy5.5 (475 kDa of the starting polymer) at 0 min, 3 h, 6 h, 24 h, 36 h, and 48 h p.i. in a mouse. (Experiments performed by Dr. Divya Vats, Laboratory of Prof. Dr. Markus Rudin, Institute for Biomedical Technology, ETH Zürich).

For a good comparison of all four different sized polymer-dye conjugates, Figure 48 showed the last three *in vivo* images (after 24 h, 36 h and 48 h).

Here, as expected, the compound with the lowest molecular weight, $HPG_{10}$-Cy5.5 exhibited no significant accumulation in tumors. But contrary to all expectation, also the small compound with the RGD peptide as an active target molecule was not recognized in both tumors. The highest fluorescent intensity can be seen in the region of the backbone. In the case of the higher molecular weight compounds a weak accumulation can be detected in both tumors in the hip region, with a maximum at 120 kDa. It could be realized as well that the fluorescent intensity in the tumors decreased after 24 h and in return, an increase could be detected in the kidneys.

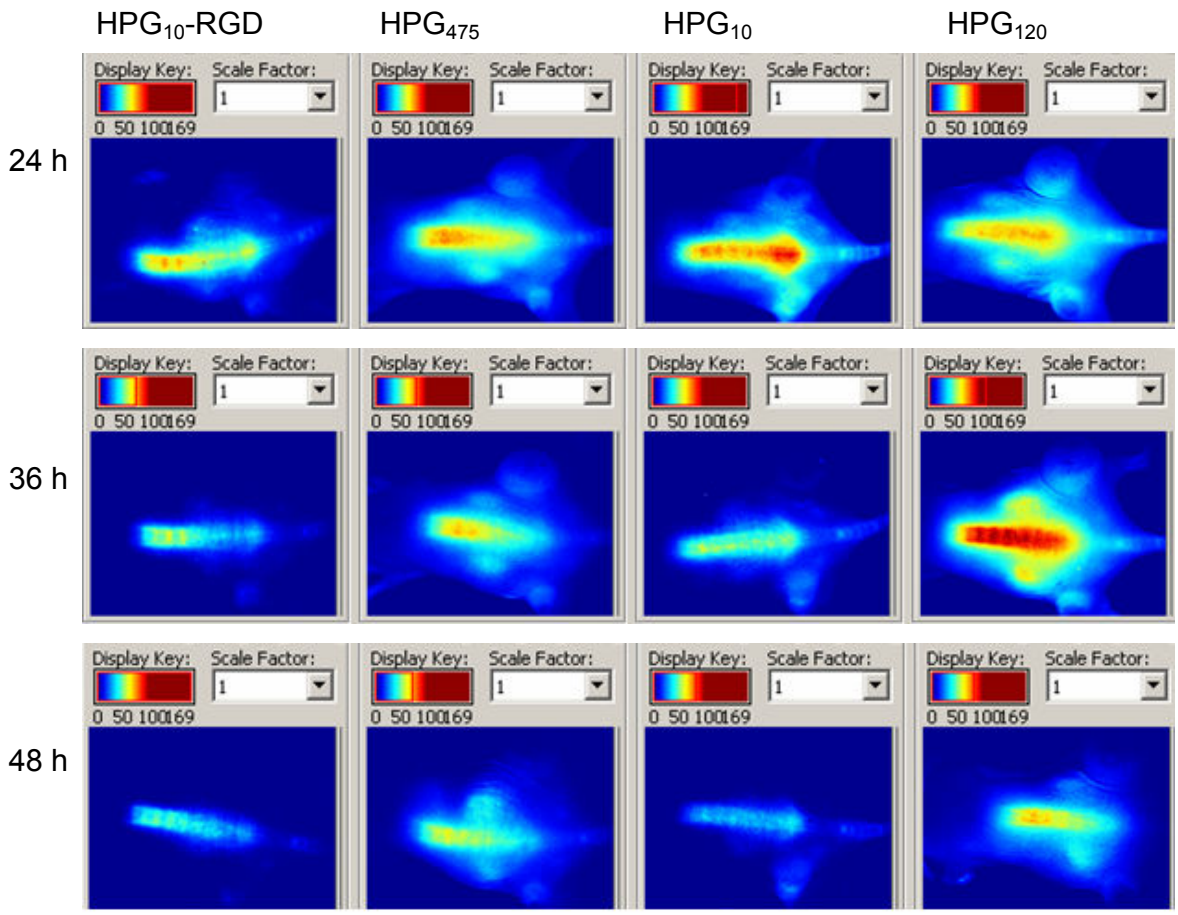


**Figure 48.** *In vivo* imaging of hyperbranched polyglycerols of different molecular weight and particle size plus a peptide coating polymer at 24 h, 36 h, and 48 h in a mouse with two different tumors. (Experiments performed by Dr. Divya Vats, Laboratory of Prof. Dr. Markus Rudin, Institute for Biomedical Technology, ETH Zürich).

In the last step (48 h after injection), the organs and tumors were harvested and imaged (Figure 49). The backbone, kidneys, and the liver had been removed to find out where the organs can be located after 48 h and if the polymer-dye conjugates egested over the kidneys or the liver. In case of the peptide-activated polymer after 48 h almost nothing can be seen. It can be assumed that the compound almost was excreted rapidly via the kidneys due to its relatively small size. Also the small compound without any active target molecules showed a wide distribution (see above) and after 48 h the highest fluorescence intensity could be recognized in the backbone region but not to a significant degree. Those mice with the injection of higher molecular weight polymer-dye conjugate showed a weak accumulation in both tumors and the liver and a high accumulation in the kidneys.

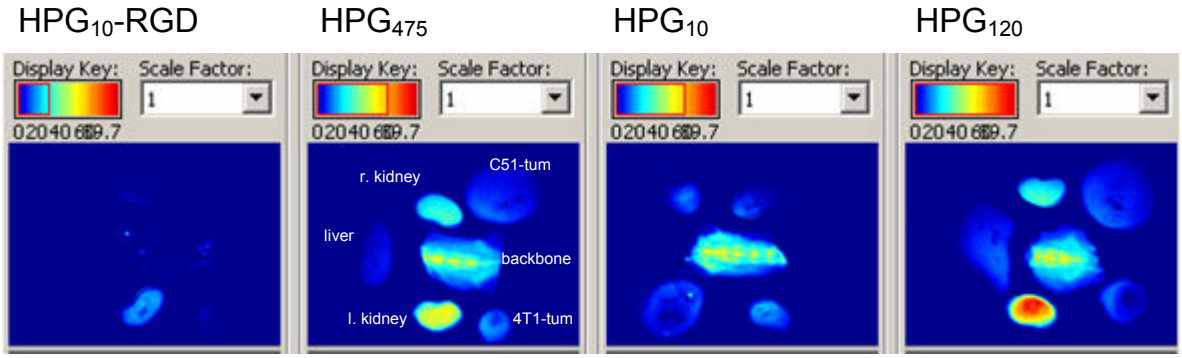


**Figure 49.** *In vivo* imaging of the sliced organs and tumors after 48 h. (Experiments performed by Dr. Divya Vats, Laboratory of Prof. Dr. Markus Rudin, Institute for Biomedical Technology, ETH Zürich).

## 6.4. Discussion and Conclusion

The observed dependence of the *in vivo* tumor uptake with regard to the molecular weight of hyperbranched polyglycerol confirmed the results described in literature with other polymers and also with polymer-drug conjugates: The pharmacokinetic of macromolecules is determined by the size of the molecules.[201,202,203] Macromolecules with a molecular weight of more than 30,000-40,000 Da are eliminated rapidly over the kidneys. Because of the mostly dense endothelial membrane of the blood vessels a distribution in healthy tissue is only possible to a limited degree.[204] In contrast, the capillary vessels of tumor tissue have an irregularly endothelial membrane which is permeable for macromolecules.[205,206] The intravenous administration of polymers with a higher molecular weight above approximately 30,000 Da leads to an extension of the plasma half-time as well as a targeted enrichment in the tumor tissue.[61,207,208,209]

Towards this direction, hyperbranched polyglycerols with different molecular weight were labelled with ITCC or respectively with a Cy5.5 derivative to image tumors *in vivo*. Three *in vivo* studies were carried out to verify which size of the polymer-dye conjugates is the best for tumor uptake. Already the first of these studies demonstrated a dependence of the size of the polymers. But in these studies errors were observed like the wrong position of the tumor where the fluorescence of the organs probably disturbed the detected fluorescence intensity of the tumors. It was interesting to note that the mean fluorescence signal inside the tumors was most significant after injection with 120 kDa with approximately 10 nm in size (Figure 39, Figure 41,Figure 46, and Figure 48).

With regard to the excretion of the polymer-dye conjugates an intensive enrichment could be localized in the kidneys in all cases. Compared to the kidneys, the fluorescence intensity of the liver, a typical store organ, was slightly weaker, and it was even weaker in the spleens. This could mean that the excretion of the polymers meanly occurs *via* the kidneys.

Even if the imaging results partially failed to meet the level of significance, tendencies were detectable. It can be concluded that this process is size dependent for the hyperbranched polyglycerols, i.e. higher the size, the more the tumor uptake. While the size is below 10 kDa, no uptake is expected. However, the fluorescence intensity in the cancer cells was lower after injection with dye labeled 475 or 870 kDa polyglycerol. It is therefore theoretically possible that these conjugates due to their size have a higher exocytosis rate and will therefore decline more rapidly than the 120 kDa polyglycerol.

It seemed noticeable that the HPG-RGD conjugate showed no detection in the tumors. It is possible that the target molecule is not specific for the chosen tumors or that the RGD loading was too low for a high tumor uptake. Just as with the other polymer-dye conjugates with higher molecular weight an improvement is necessary. It seemed that too many dye molecules at the HPG surface can influence the tissue selectivity. A lower level of dye or better shielding of the dyes, if possible, is necessary for better results. It is also necessary to quantify the polymer conjugates in the organs.

Based on these findings, future research should be conducted towards combining HPG-dye conjugates with a molecular weight around 120 and 400 kDa with a lower amount of dye and respectively active targeting molecules for *in vivo* studies to better understand the accumulation for this type of polymer.

.

# 7. Summary

In recent years, the interest in application of nanotechnology in medicine and pharmacy has considerably increased. This involves in particular the development of dendritic polymers as drug delivery systems. A few polymer protein conjugates such as the PEGylated form of the adenosine desaminase have already been approved as medication. Polyethylene glycol has many advantages such as the chemical stability under basic and neutral conditions, the good water solubility, non-toxicity, and functional groups for the coupling of drugs. A broad range of PEG applications and PEG carrier systems are protected by patents. That fact and a limited set of disadvantages of PEG, such as the prevention of the biodegradation what may lead to an accumulation in bodies in case of *in vivo* applications, have led to a search for alternative polymer transport systems. Hyperbranched polyglycerols (HPG) show the same positive characteristics and possibly of a higher functionality because of the multiple hydroxyl groups and a higher hydrophily.

In this work hyperbranched dendritic polyglycerols with different molecular weights were synthesized and functionalized (Figure 50). HPGs labeled with several fluorescent dyes were investigated with regard to size-dependant cellular uptake, intracellular behavior, receptor-mediated endocytosis, and their potential as transport carriers in *in vivo* studies.

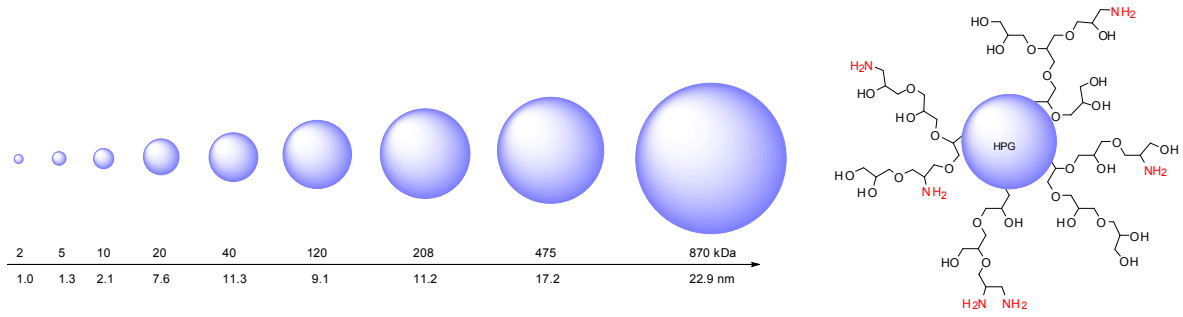


**Figure 50.** Functionalized HPGs with different molecular weights.

To study the mechanism of cellular internalization, hyperbranched polyether derivatives consisting of amino-bearing hyperbranched polyglycerols (HPGs) of varied molecular mass and size range were designed and synthesized (Chapter 3). HPGs were further fluorescently labelled by conjugating maleimido indocarbocyanine dye (ICC-mal). The conjugates were characterized by UV-Vis spectroscopy, fluorescence profile, zeta

potential, and dynamic light scattering. The uptake mechanism was studied by fluorescence activated cell sorting (FACS) analysis, fluorescence spectroscopy, and confocal microscopy with human lung cancer cells A549, human epidermoid carcinoma cells A431, and human umbilical vein endothelial cells (HUVEC) cells. For the first time, the results suggest that the higher-molecular-weight HPGs (40-870 kDa) predominantly accumulate in the cytoplasm much better than their low-molecular-weight counterparts (2-20 kDa). The HPG nanocarriers discussed here have many biomedical implications, particularly for delivering drugs to the targeted site.

In conclusion, it has been shown for the polymeric class of polyglycerols that cellular uptake is size-dependent (Figure 51). Cell entry dynamics is limited and mechanized for different polymeric architectures possessing varied molecular mass and size for endocytosis pathway. Notably, 120-870 kDa polyglycerols are internalized far than those with lower molecular weights, 2-20 kDa HPGs. The studies implicate development of nanocarriers with precise mass and size for drug delivery and other biomedical applications.

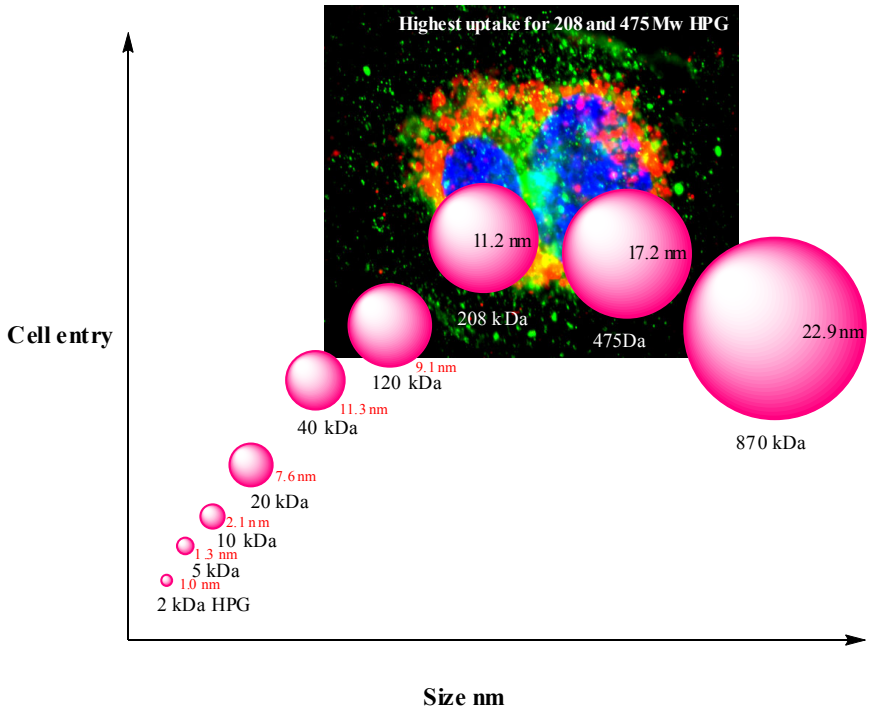


**Figure 51.** Size-dependant cellular uptake of hyperbranched polyglycerol.

The second section of the thesis (Chapter 4) described the specific cellular uptake and the transport mechanism in the different cell organelles with the help of selective fluorescent dyes for clathrin, early endosomes, Golgi apparatus, late endosomes, and

lysosomes (Figure 52). In addition, two inhibitors were used to investigate the endocytotic pathway. It could be demonstrated that cellular uptake of HPG-ICC (208 kDa) was found to occur primarily through clathrin-mediated endocytosis and probably dynamin-dependent endocytosis pathways, but the co-localization was quite weak. Particles with a molecular weight of 10 kDa were not taken up into the tumor cells. HPGs are quickly trafficked to the lysosomes, but show increased endosomal accumulation once the lysosomal compartments become saturated. It is demonstrated that HPG was not localized with the Golgi apparatus. Further works need to be done in using HPG-based drug delivery systems, which accumulate in the lysosomes and, as a result, are interesting because of the decreased pH value. That could allow delivery of a toxic drug into the cytosol of target cells.

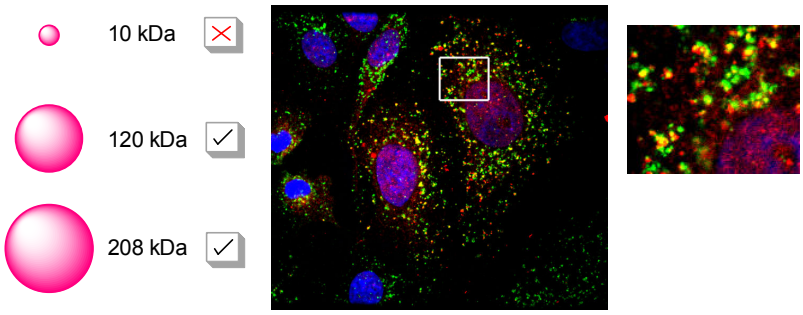


**Figure 52.** Co-localization of HPG-ICC (208 kDa) with LAMP1.

The third part of the thesis (Chapter 5) focused on the possible uptake of cells with low molecular weight HPG (10 kDa) using additional target functionalities. Towards this direction, HPG was labeled with ICC to image cancer cells and coupled with specific peptides (RGD, LHRH) to study the endocytosis pathway in three different cancer cell lines. In conclusion, it was shown that active cellular uptake is target-dependent for the polymeric class of hyperbranched polyglycerols (Figure 53). The results demonstrated that HPGs with a low molecular weight are potential candidates for the development of new target carrier systems.

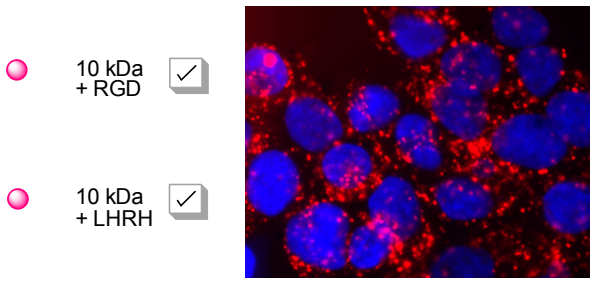


**Figure 53.** Fluorescence images of A549 lung epithelial cells RGD-PEG-HPG-ICC showed a high signal in A549 cells which is positive for the integrin receptor $\alpha_v\beta_3$.

In the fourth part of the thesis (Chapter 6), due to the results of the size-dependant cellular uptake of HPG-ICC conjugates (see chapter 3), *in vivo* studies with different sizes of hyperbranched polyglycerols coupled with Indotricarbocyanine maleimide (ITCC-mal) and a Cy5.5 derivates, respectively were performed within collaborations. After three test series it could be demonstrated that this process is also size dependent for HPGs. Conjugates with low molecular weight could not be detected with a specific accumulation in the tumor tissue. Surprisingly, the RGD functionalized conjugate also showed no signal in the tumors. It was interesting to note that the mean fluorescence signal inside the tumors was most significant after injection with 120 kDa with approximately 10 nm in size (Figure 54). In addition, it was observed that a high accumulation could be observed in the backbone.

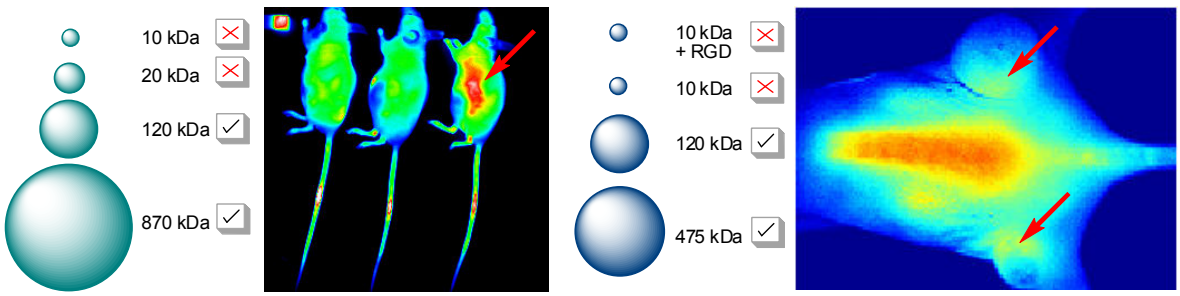


**Figure 54.** On the left: Optical images of nude mice with subcutaneous injection of HPG-ITCC (120 kDa). On the right: optical images of nude mice with subcutaneous injection of HPG-Cy5.5 (120 kDa).

However, further studies with a lower dye loading are necessary to confirm these initial observations.

In summary, the high molecular weight polyglycerols examined here presents themselves as an interesting platform for next generation biomaterials. The broad range of

positive characteristics, such like biocompatibility, non-toxicity, high water solubility, and the possibility of multiple functionalization of the surface, renders HPGs as an attractive molecular tool for *in vivo* transport systems.

# 8. Zusammenfassung und Ausblick

Die Anwendung von Nanotechnologie in der Medizin und Pharmazie hat in den letzten Jahren deutlich an Interesse gewonnen. Insbesondere die Entwicklung von dendritischen Polymeren als Wirkstoff-Transportsysteme hat den Weg in die Biomedizin gefunden. Einige Polymer-Protein-Konjugate, wie zum Beispiel die PEGylierte Form der Adenosin-Desaminase, sind bereits als Medikamente zugelassen. Polyethylenglykol weist viele Vorteile auf, wie zum Beispiel die chemische Stabilität unter basischen und neutralen Bedingungen, Wasserlöslichkeit, Ungiftigkeit und funktionelle Gruppen zur Kopplung von Wirkstoffen. Die Patentschützung einer Vielzahl von PEG-Anwendungen und -Transportsystemen und einige wenige Nachteile von PEG, wie zum Beispiel die Verhinderung des biologischen Abbaus, was bei *in vivo* Anwendungen zur Anreicherung im Körper führen kann, beschleunigen die Suche nach alternativen polymeren Transportsystemen. Hyperverzweigte Polyglycerine weisen dieselben positiven Eigenschaften von PEG auf, bieten jedoch noch zusätzlich die Möglichkeit einer höheren Funktionalisierung durch multiple Hydroxygruppen und eine höhere Hydrophilie.

Im Rahmen dieser Arbeit wurden hyperverzweigte dendritische Polyglycerine mit unterschiedlichem Molekulargewicht synthetisiert und funktionalisiert. Mit verschiedenen fluoreszierenden Farbstoffen versehen wurden sie auf ihre Größenabhängigkeit in Bezug auf deren passive beziehungsweise aktive Zellaufnahme, deren intrazellulären Verhaltens und auf ihre Effizienz als Transportmoleküle für *in vivo* Studien untersucht.

Im ersten Teil der vorliegenden Arbeit (Kapitel 3) wurden Amin-funktionalisierte hyperverzweigte Polyglycerine (HPG) mit unterschiedlichem Molekulargewicht synthetisiert. Um die zelluläre Aufnahme zu verfolgen wurden die Polymere mit dem fluoreszierenden Farbstoff Indocarbocyanin-maleimid (ICC-mal) verknüpft. Die Strukturen wurden mit verschiedenen Methoden, wie UV/Vis-Spektroskopie, Zeta Potential und Dynamischer Lichtstreuung, charakterisiert. Mittels FACS-Analyse (fluorescence-activated cell sorting), Fluoreszenz-Spektroskopie und Konfokal-Mikroskopie an menschlichen Lungenkrebszellen (A549), menschlichen Epidermoidcarcinomzellen (A431) und humanen umbilikalen venösen Endothelzellen (HUVEC), wurde der Aufnahmemechanismus untersucht. Die Ergebnisse zeigen, dass die HPGs mit höherem Molekulargewicht (40-870

kDa) vorwiegend im Cytoplasma akkumulieren. Im Gegensatz dazu findet man keine beziehungsweise nur eine geringe Aufnahme der Konjugate mit niedrigeren Molekulargewichten (2-20 kDa). Die funktionalisierten Polyglycerine wiesen keine Zelltoxizität auf und sind somit für *in vivo* Studien geeignet. Zusammenfassend präsentiert diese Klasse von Polymeren eine Größenabhängigkeit bei der Zellaufnahme (Figure 51). Polyglycerin bietet somit ein großes Potential als Wirkstoff-Transportsystem und in anderen biomedizinischen Anwendungen zu fungieren.

Im Rahmen des zweiten Teils der vorliegenden Arbeit (Kapitel 4) wurde die Zellaufnahme, sowie auch der weitere Transport in den unterschiedlichen Zellorganellen, mittels selektiver fluoreszierender Farbstoffe für Clathrin, frühe Endosomen, den Golgi Apparat, späte Endosomen und Lysosomen, untersucht. Zusätzlich wurden zwei Inhibitoren eingesetzt, um den Endozytoseweg zu verfolgen. Es konnte gezeigt werden, dass das HPG-ICC-Konjugat (208 kDa) überwiegend durch Clathrin-vermittelte Endozytose in die carcinomen Zellen gelangt, jedoch nicht ausschließlich. Partikel mit einem Molekulargewicht unter 40 kDa wurden nicht von der Zelle über Clathrin-vermittelte Endozytose aufgenommen  Die Polymerverbindungen landen sehr schnell in den Lysosomen, nachdem sie zuvor in frühen und späten Endosomen kurz angereichert wurden. Im Golgi Apparat konnte keine Anreicherung festgestellt werden. Weiterführende Arbeiten könnten sich daher damit beschäftigen, Wirkstoffe an HPGs zu koppeln, die dann in den Lysosomen angereichert werden und den sinkenden pH-Wert nutzen, um die „Fracht“ ins Zytosol der Zelle freizusetzen.

Der dritte Teil der vorliegenden Arbeit (Kapitel 5) befasste sich mit der Frage, ob die HPG-ICC-Konjugate mit einem niedrigeren Molekulargewicht (10 kDa) unter Verwendungen zusätzlicher *Targeting*-Funktionalitäten in die Zellen gelangen. Durch das Einführen von spezifischen Peptidstrukturen (RGD bzw. LHRH) konnte ein aktives Zell*targeting* nachgewiesen werden. Damit konnte demonstriert werden, dass auch HPGs mit einem geringen Molekulargewicht das Potential besitzen als Wirkstoff-Transportsysteme zu fungieren.

Beruhend auf den Ergebnissen der *in vitro* Studien wurden im vierten Teil der vorliegenden Arbeit *in vivo* Studien im Rahmen von Kooperationen durchgeführt. Nach der zusätzlichen Markierung von HPG, mit unterschiedlichen Molekulargewichten, mit Indotricarbocyanin-maleimid (ITCC-mal) bzw. einem Cy5.5-Derivat wurde die Verteilung im Maustumormodel untersucht. Nach drei durchgeführten Testreihen konnte wieder eine größenabhängige Aufnahme der Partikel nachgewiesen werden. Verbindungen mit

niedrigem Molekulargewicht zeigten keine spezifische Anreicherung im Tumorgewebe. Auch die RGD-funktionalisierten Konjugate wiesen kein aktives Tumor*targeting* nach. Für weitere Versuche sollten die Polymere mit anderen spezifischen *Target*molekülen getestet werden. Auch eine höhere Beladung mit der RGD-Sequenz auf der Polymeroberfläche könnte eine mögliche Lösung sein. Die besten Ergebnisse konnten mit dem fluoreszenzmarkierten HPG mit einem Molekulargewicht von 120 kDa erreicht werden. Zusätzlich konnte eine starke Ansammlung der Partikel am Rückgrat der Mäuse beobachtet werden. Es sind jedoch noch weitere Studien mit einer geringeren Farbstoffbeladung notwendig, um die ersten Beobachtungen zu bestätigen.

Zusammenfassend lässt sich feststellen, dass die in dieser Arbeit entwickelten Farbstoffkonjugate auf Basis der „großen“ hyperverzweigten Polyglycerine ein effektives und vielfältig einsetzbares Transportsystem für die spezifische und molekulare Bildgebung darstellen. Durch die vielen positiven Eigenschaften der HPGs, wie deren Biokompatibilität, deren Ungiftigkeit, die hohe Wasserlöslichkeit und insbesondere die Möglichkeit die Oberfläche multipel zu funktionalisieren, macht die Klasse dieser Polymere zu interessanten Kandidaten für *in vivo* Trägersysteme.

.

# 9. Outlook

The hyperbranched polyglycerols with a molecular weight up to 40 kDa presented in this thesis could be further investigated for their potential as therapeutic carrier systems.

The synthesis by emulsion polymerization (Scheme 1b) to obtain well-defined HPGs with molecular weights up to 1000 kDa and narrow polydispersities (PDI = 1.1-1.4) a wide range of possibility in designing polymers with specific sizes.[120] Due to their highly biocompatible nature, high loading capacity, good solubility, non toxicity, and low viscosity, these polymers are potential candidates of applications in medicine and pharmacology. The choice of ICC as fluorescent probe has already proven to be valuable in connection with HPG[144] due to its high labeling efficiency and good fluorescence quantum yield in the conjugated state. For subsequent *in vivo* imaging, the respective near-infrared homolog ICC can be applied.

In case of the peptide-coupled HPG in *in vitro* studies it suggests that cellular uptake also of low molecular weight macromolecules can be optimized for several applications. With regard to the *in vivo* studies there is room for improvement. Due to the fact that only the high molecular weight polymer-dye conjugates showed a positive result, further experiments with different active target molecules have to be investigated. Also a controlled loading of the target molecules and the fluorescence dyes is another option to obtain better results.

In conclusion, one of the most interesting features of these architectures is the possibility of the further functionalization of the polymer periphery. HPGs are emerging as a powerful, multifunctional nanotherapeutic platform for imaging and therapeutic applications. Looking into the future, there are a number of medical needs where multifunctional dendrimers and their derivatives might become important tools, in particular for early detection, diagnosis, and personalized treatment of diseases.

In summary, the high molecular weight polyglycerols examined here presents themselves as an interesting platform for next generation biomaterials. The broad range of positive characteristics renders HPGs as an attractive molecular tool to construct highly versatile drug delivery systems for the specific and molecular imaging.

# 10. Experimental Part

## 10.1. Materials

### 10.1.1. Chemicals

All solvents were purified by conventional methods prior to use. HPGs with various molecular weights ($M_n$ = 2, 5, 10, and 20 kDa) were prepared according to the previously published procedures. HPGs with higher molecular weight ($M_n$ = 120, 208, 475, and 870 kDa) were synthesized by myself according to the Brooks group published procedure or provided by the Brooks group. Indocarbocyanine, Indotricarbocyanine, and Cy5.5 derivatives dye were purchased from Mivenion GmbH (Berlin, Germany). $CH_3O$-PEG-$C_2H_4$-maleimide was purchased from Rapp Polymere GmbH (Tübingen, Germany). MAL-dPEG$^{TM}_4$-NHS ester was purchased from celares GmbH. The bis-cyclic peptide E-[c(RGDfK)2] was provided by the Research Group Macromolecular Prodrugs of Dr. Felix Kratz. All other chemicals, reagents, and solvents were of analytical grade and obtained from standard suppliers.

## 10.2. Analytical Methods

**NMR Spectroscopy**

$^1$H and $^{13}$C NMR spectra were recorded on a *Bruker* AC 250 (250 MHz; 125 MHz) or on an AMX 500 (500 MHz) instrument. As deuterated solvents, $(CD_3)_2CO$, $CDCl_3$, $D_2O$ and DMSO-$d_6$ were used. Chemical shifts δ are given in parts per million (ppm) according to the literature.[210]

**UV/Vis Spectroscopy**

The UV/VIS measurements were performed on a Scinco S-3150 spectrometer (range: 187 – 1193 nm; resolution: 1024 points) in millipore filtered water. All spectra were recorded at r.t. and were evaluated with the programs LabPro® Plus from Scinco Co., LTD., Microsoft® Excel 2000 from Microsoft Corporation, and Origin® 7.0 from OriginLab Corporation.

**Fluorescence Spectroscopy**

The fluorescence measurements were taken on a Jasco FP-6500 fluorescence spectrometer equipped with a thermostated cell holder, a DC-powered 150W Xenon lamp, a Hamamatsu R928 photomultiplier, and a variable slit system. Emission spectra were recorded in millipore filtered water.

**Dynamic Light Scattering (DLS) and Zeta Potential Measurement**

Dynamic light scattering and zeta potential measurements were carried out on a Zetasizer Nano ZS analyzer with integrated 4 mW He-Ne laser, $\lambda$ = 633 nm (Malvern Instruments Ltd, U.K.). Light scattering experiments were employed for determining the size of the HPG-dye complexes. Solutions of 1 mg/ml of polymer in 0.01 M phosphate buffer (pH 7.4) were freshly prepared and analyzed at 25 °C in a polystyrene cell. Before the experiment all samples were filtered through 0.22 and 0.45 μM Nylon filter, respectively. In all experiments the detector angle was fixed at 173°.

**Confocal Fluorescence Microscopy**

After mounting HeLa cells were imaged using a Zeiss Axiovert 200M-based PerkinElmer Life Sciences UltraView ERS dual spinning-disk system. 3D reconstruction was processed using Volocity software (Improvision).

**Gel Permeation Chromatography**

Molecular weights and polydispersities of polyglycerol samples were determined by gel permeation chromatography (GPC) on a Waters 2690 separation module fitted with a

DAWN EOS multiangle laser light scattering (MALLS) detector from Wyatt Technology Corp. with 18 detectors placed at different angles (laser wavelength = 690 nm) and a refractive index detector (Optilab DSP from Wyatt Technology Corp.).

**Dialysis**

Dialysis was performed with benzoylated cellulose membrane from the Sigma-Aldrich company, MWCO = 1000 or with regenerated cellulose membrane from the Roth company, MWCO = 4000-6000. Typical dialysis was carried out for 24-48 h with 1 liter of solvent that was exchanged after first 6 h of the process.

**Thin Layer Chromatography (TLC)**

Thin layer chromatography analysis was performed on Merck silica gel 60 and fluorescence indicator ($F_{254}$).

## 10.3. Synthesis of Hyperbranched Polyglycerols

### 10.3.1. Synthesis of HPGs with molecular weights $M_n$ = 2, 5, 10, and 20 kDa

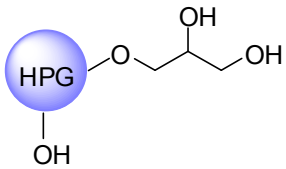


**1**

Polymerizations of HPG with molecular weights $M_n$ = 2, 5, 10, 20 kDa were prepared according to previously published procedures.[124,125]

### 10.3.2. Synthesis of HPGs with molecular weights $M_n$ = 90-870 kDa[120]

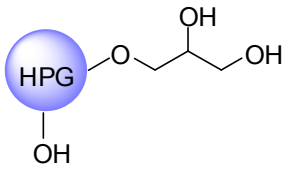


**1**

Synthesis of HPGs with higher molecular weights ($M_n$ = 90-870 kDa) were carried out in a three-neck round bottom flask equipped with a mechanical stirrer, a rubber septum through which reagents were added, and a dual manifold Schlenk line. The general procedure for the synthesis of HPGs was as follows. Initially trimethylolpropane (TMP) (0.124 g, 0.925 mmol) was added to the flask under argon atmosphere followed by 67 µl of potassium methylate solution in methanol (25 wt %). For higher molecular weights lower amounts of initiator were required. After 30 min stirring with a magnetic stirrer bar, until the bubbles of methanol were removed, the mixture was stirred for 2 more hours under vacuum. 12 ml of anhydrous 1,4-dioxane (0.141 mmol) was added. The flask was transferred in an oil bath and melted at 95 °C under argon atmosphere. With the help of a syringe pump 18 ml of glycidol (0.272 mmol) was added dropwise over a period of 20 h. The polymer and also the initiator are insoluble in either of the solvents which simply act as emulsifying agents to improve mixing. The mixture was quenched with methanol, and passed three times through cation-exchange resin (Amberlite IRC-150) for neutralization. The highly viscous polymer solution was slowly precipitated into acetone and stirred for 2 h. Acetone was decanted and the polymer was dissolved in a small amount of millipore water and was obtained by freeze-drying, as highly viscous, colourless polymer (Table 1, chapter 3.1).

$^1$H NMR (500 MHz, $(CD_3)_2CO$): δ (ppm) = 4.10-3.20 (m, HPG backbone), 1.30 (q, -$\underline{C}H_2$-$CH_3$, TMP core), 0.95 (t, -$CH_2$-$\underline{C}H_3$, TMP core). $^{13}$C NMR: (400 MHz, $(CD_3)_2CO$): δ (ppm) = 82.0-81.0 (HPG backbone, linear 1,3-unit), 80.5-79.5 (HPG backbone, dendritic unit), 74.5-73.5 (HPG backbone, linear 1,4-unit), 73.5-72.0 (HPG backbone, terminal/dendritic unit), 72.0-70.5 (HPG backbone, linear 1,3/1,4-unit), 65.0-64.0 (HPG backbone, terminal), 63.5-62.0 (HPG backbone, linear 1,3-unit).

## 10.4. Substitution Reactions on Hyperbranched Polyglycerols

### 10.4.1. General procedure for mesylation of HPG: *O*-Mesylpolyglycerol[127]

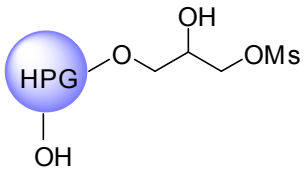


**2**

In a 100 ml flask HPG-OH was dissolved in pyridine and was cooled down to 0 °C with an ice bath. To this solution MsCl was added drop by drop that the temperature did not exceed 5 °C. The yellow mixture was stirred over night in the thawing bath. Then ice was added and the muddy mixture becomes clear. The solvent was evaporated and the remnant was dialyzed for 48 h in methanol to give a yellow honey like product.

$^{1}$H NMR (500 MHz, $(CD_3)_2CO$ or DMSO-$d_6$): δ (ppm) = 5.12-4.69 (functionalized sec. HPG groups), 4.75-4.25 (functionalized prim. HPG groups), 4.15-3.40 (HPG backbone), 3.30-3.10 (Ms-H), 1.50-1.25 (-$\underline{C}H_2$-$CH_3$, TMP core), 1.00-0.90 (-$CH_2$-$\underline{C}H_3$, TMP core). $^{13}$C NMR (400 MHz, $(CD_3)_2CO$ or DMSO-$d_6$): δ (ppm) = 84.2-69.0 (HPG backbone), 38.2-36.7 (Ms-C).

### 10.4.2. General procedure for azidation of *O*-Mesylpolyglycerol: Polyglycerolazide[127]

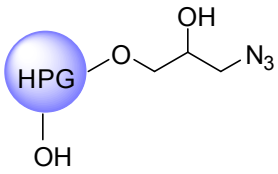


**3**

O-Mesylpolyglycerol was dissolved in DMF and $NaN_3$ was added. The mixture was stirred at 120 °C for 4 h. After cooling to room temperature the residual $NaN_3$ was removed *via* filtration. The yellow filtrate was concentrated in vacuo and the crude product was purified by dialysis in chloroform or methanol (24-48 h) to give yellow viscous oil.

$^{1}$H NMR (500 MHz, $CDCl_3$ or DMSO-$d_6$): δ (ppm) = 5.50-4.95 (functionalized sec. HPG groups), 4.95-4.35 (functionalized prim. HPG groups), 4.25-2.85 (HPG backbone), 1.65-1.30 (-$\underline{C}H_2$-$CH_3$, TMP core), 0.85-0.75 (-$CH_2$-$\underline{C}H_3$, TMP core). $^{13}$C NMR (400 MHz, $CDCl_3$ or DMSO-$d_6$): δ (ppm) = 82.5-50.1 (HPG backbone, functionalized HPG groups).

### 10.4.3. General procedure for amination of Polyglycerolazide: Polyglycerylamine[127]

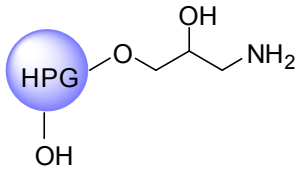


**4**

Polyglycerolazide was dissolved in p.a. THF in a one-necked flask. $H_2O$ und $PPh_3$ were added and $N_2$ formation was observed. While stirring over night, the amount of water in the reaction mixture was increased continuously drop by drop. Then the solvent was reduced and the concentrated solution was filtrated. The filtrate was extracted three times with chloroform. The aqueous phase was dialysed in water and then concentrated to dryness to deliver yellow viscous oil (Table 2, chapter 3.2).

$^{1}$H NMR (500 MHz, $(CD_3)_2CO$ or DMSO-$d_6$): δ (ppm) = 4.20-3.15 (HPG backbone), 3.35-2.39 (functionalized HPG groups). $^{13}$C NMR (400 MHz, $(CD_3)_2CO$ or DMSO-$d_6$): δ (ppm) = 84.5-64.1 (HPG backbone), 56.0-42.5 (functionalized HPG groups).

### 10.4.4. Succinate Functionalization of HPG [HPG-SA]

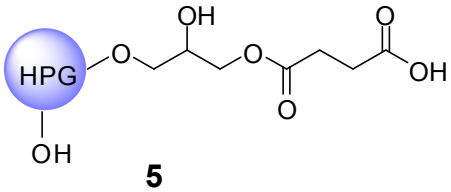


**5**

In a 100 ml flask HPG-OH (5 kDa, 0.5 g, 1.5 mmol) was dissolved in 40 ml DMF. Succinic anhydride (0.9 g, 9.0 mmol) and 0.123 ml TEA were added. The mixture was stirred at 50 °C for 5 h. After cooling to room temperature the oil was concentrated *in vacuo* and the

crude product was purified by dialysis in water (30 h) to give a colourless viscous oil (0.7 g, Conversion: ~ 25 %).

$^{1}$H-NMR (500 MHz, $CD_3OD$): δ (ppm) = 5.28-5.06 (broad m, CHOCO prim., 1H), 4.38-4.08 (broad m, $CH_2OCO$, 2H), 4.06-3.85 (broad m, CH-OH, $L_{14}$ and CH-OH, T), 3.85-3.42 (PG backbone), 2.64 (broad s, $OCOCH_2CH_2COOH$, 4H). $^{13}$C-NMR (500 MHz, $CD_3OD$): δ (ppm) = 176.2 (COOH), 174.5 (OCO).

### 10.4.5. PEGylation of HPG-SA [HPG-PEG]

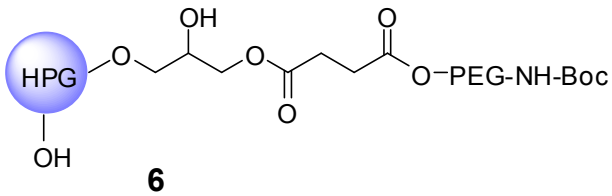


**6**

To a solution of HPG-SA (5.5 kDa, 0.05 g, 0.0454 mmol) and 10 ml DMF were added DCC (0.014 g, 0,0681 mmol), HOBt (0.012 g, 0,0908 mmol), OH-PEG-NH-Boc (5 kDa, 0.0227 g, 0,0454 mmol) and 20 µl DIPEA. The mixture was stirred over night at RT. After purification *via* dialysis in methanol (24 h) 0.07g of weak yellow viscous oil were obtained.

$^{1}$H-NMR (500 MHz, $CD_3OD$): δ (ppm) = 5.30-5.13 (broad m, CHOCO prim., 1H), 4.42-4.06 (broad m, $CH_2OCO$, 2H), 3.97-3.86 (broad m, CH-OH, $L_{14}$ and CH-OH, T), 3.77-3.46 (HPG and PEG backbone), 2.76-2.54 (m, $OCOCH_2CH_2COOH$, 4H), 1.44 (s, Boc, 9H).

### 10.4.6. General procedure for the coupling of hyperbranched polyglycerols with Indocarbocyanine-maleimide: HPG-ICC

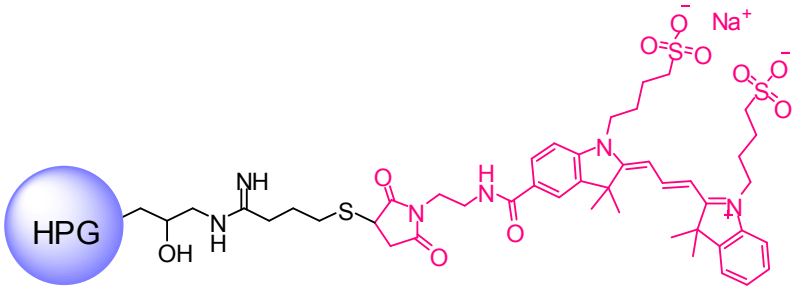


**9**

For the synthesis of HPG-ICC[211] a buffer solution with a pH 7.3 was freshly prepared (5 mM $H_2NaPO_4 \cdot H_2O$, 50 mM $HNa_2PO_4 \cdot 2H_2O$, 5 mM EDTA·$2H_2O$). ICC-mal was dissolved in 1 ml buffer solution, 2-Iminithiolane hydrochloride (2 eq.) was dissolved in 6 ml buffer solution and HPG was dissolved in 2 ml buffer solution. For one hour 2-Iminothiolane hydrochloride and ICC-mal were added alternately to the HPG/buffer solution. The mixture was stirred over night at room temperature. After separation with Sephadex G-25 Superfine the coupled product was purified *via* dialysis in water (24-48 h) and the solvent was almost completely evaporated to give an oily pink product. The products were kept in darkness.
The loading degree of dye is summarized in Table 8.

**Table 8.** Dye loading with ICC-mal.

| Molecular Weight (kDa) | Dye Loading (%) |
|---|---|
| 2 | 4 |
| 5 | 3 |
| 10 | 4 |
| 20 | 2 |
| 120 | 2 |
| 208 | 1.5 |
| 475 | 5 |
| 870 | 6 |

### 10.4.7. Procedure for the synthesis of HPG-PEG-ICC

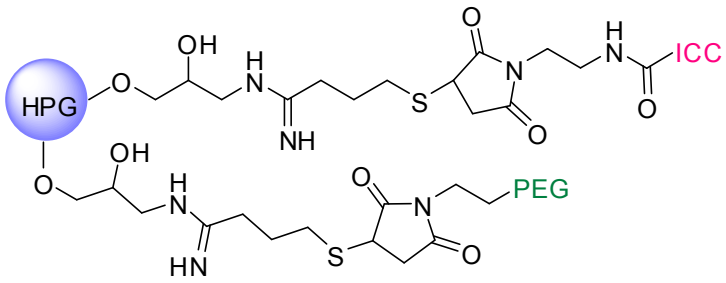


**10**

To achieve molecular weights between 20 and 120 kDa, 20 kDa HPG was coupled with a 2 kDa polyethylene glycol (PEG) at the same time with the dye. ICC-mal was dissolved in 2

ml buffer solution with a pH 7.3 (1.429 g of $H_2NaPO_4 \cdot H_2O$, 2.568 g of $HNa_2PO_4 \cdot 2H_2O$, 0.931 g EDTA, 0.5l $H_2O$), 2-Iminithiolane hydrochloride (2 eq.) was dissolved in 1 ml buffer, $CH_3O$-PEG-$C_2H_4$-maleimide was dissolved in 1 ml buffer, and HPG-20 was dissolved in 2 ml buffer. For one and a half hours 2-Iminothiolane hydrochloride, ICC-mal and PEG were added alternately to the HPG/buffer-solution. The mixture was stirred over night at room temperature. After separation with Sephadex G-25 Superfine the coupled product was purified *via* dialysis in water (48 h) and the solvent was evaporated.

### 10.4.8. Synthesis of c(RGD)$_2$-dPEG$_4$-mal

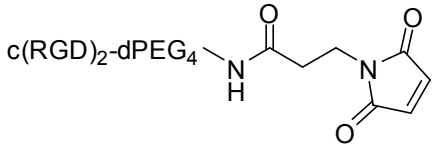


**11**

In a 25 ml flask Mal-dPEG$_4$-NHS ester (5 mg, 9.74 µmol) was dissolved in 3.5 ml DMF containing $H_2O$ (10%, v/v). The peptide c(RGD)$_2$NH$_2$ (13 mg, 9.86 µmol) was added. The mixture was kept two days at room temperature. The solvent was reduced in vacuum. The residue was extracted in chloroform (20 ml) and water (30 ml) and dried in vacuum. The compound was lyophilized at -75°C in Millipore water to obtain a white powder in 89% yield (15 mg, 8.74 µmol).
MS *m*/*z* = 1716.85 $[M+H]^+$, 1738.84 $[M+Na]^+$, 858.93 $[M]^{2+}$.

### 10.4.9. Synthesis of LHRH-mal

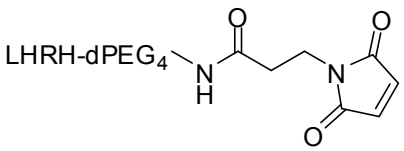


**12**

In a 25 ml flask Mal-dPEG$_4$-NHS ester (5.7 mg, 11.1 µmol) was dissolved in 3.5 ml DMF containing $H_2O$ (10%, v/v). The peptide LHRH (15 mg, 11.14 µmol) was added. The mixture was kept two days at room temperature. The solvent was reduced in vacuum. The

residue was extracted in chloroform (20 ml) and water (30 ml) and dried in vacuum. The compound was lyophilized at -75°C in Millipore water to obtain a white powder in 93% yield (18 mg, 10.32 µmol).

MS *m/z* = 1714.85 $[M+H]^+$, 1736.83 $[M+Na]^+$, 860.41 $[M]^{2+}$

### 10.4.10. Synthesis of c(RGD)2-dPEG4-HPG-ICC

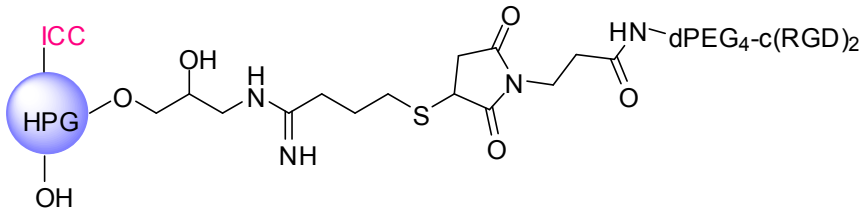


**13**

For the synthesis of c(RGD)$_2$-dPEG$_4$-HPG-ICC a buffer solution with a pH 7.3 was freshly prepared (5 mM $H_2NaPO_4 \cdot H_2O$, 50 mM $HNa_2PO_4 \cdot 2H_2O$, 5 mM EDTA·2$H_2O$). ICC-mal (4 mg, 5.0 µmol) was dissolved in 1 ml buffer solution, c(RGD)$_2$-dPEG$_4$-mal (5 mg, 3.0 µmol) was also dissolved in 1 ml buffer solution, 2-Iminithiolane hydrochloride (2.7 mg, 10.0 µmol) was dissolved in 1.5 ml buffer solution, and HPG (10 kDa, 25% $NH_2$ groups, 10 mg, 10 µmol) was dissolved in 1.5 ml buffer solution. For one hour 2-Iminothiolane hydrochloride, c(RGD)$_2$]-dPEG$_4$-mal and ICC-mal were added alternately to the HPG/buffer solution. The mixture was stirred over night at room temperature. After separation with Sephadex G-25 Superfine the coupled product was purified *via* dialysis in water (24-48 h) and the solvent was reduced in vacuo and the compound was lyophilized at -75°C in millipore water to give a pink powder. The products were kept in fridge.

### 10.4.11. Synthesis of c(RGD)$_2$-dPEG$_4$-HPG-Cy5.5

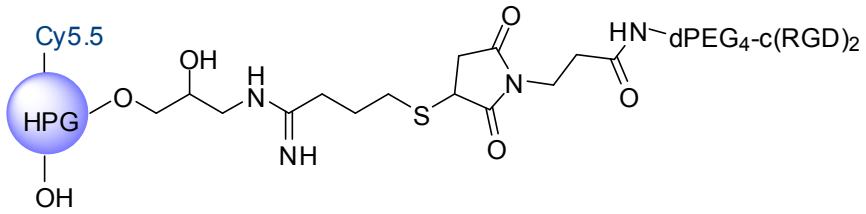


**14**

For the synthesis of c(RGD)$_2$-dPEG$_4$-HPG-Cy5.5 a buffer solution with a pH 7.3 was freshly prepared (5 mM $H_2NaPO_4 \cdot H_2O$, 50 mM $HNa_2PO_4 \cdot 2H_2O$, 5 mM EDTA·2H$_2$O). Cy5.5-mal (5 mg, 5.0 µmol) was dissolved in 1 ml buffer solution, c(RGD)$_2$-dPEG$_4$-mal (5 mg, 3.0 µmol) was also dissolved in 1 ml buffer solution, 2-Iminithiolane hydrochloride (2.7 mg, 10.0 µmol) was dissolved in 1.5 ml buffer solution, and HPG (10 kDa, 25% $NH_2$ groups, 10 mg, 10 µmol) was dissolved in 1.5 ml buffer solution. For one hour 2-Iminothiolane hydrochloride, c(RGD)$_2$]-dPEG$_4$-mal and Cy5.5-mal were added alternately to the HPG/buffer solution. The mixture was stirred over night at room temperature. After separation with Sephadex G-25 Superfine the coupled product was purified *via* dialysis in water (24-48 h) and the solvent was reduced in vacuo and the compound was lyophilized at -75°C in millipore water to give a pink powder. The products were kept in fridge.

### 10.4.12. Synthesis of LHRH-dPEG$_4$-HPG-ICC

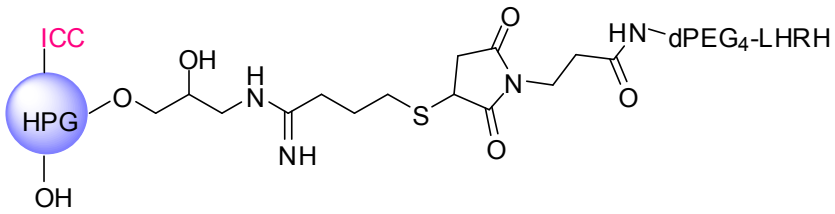


**15**

For the synthesis of LHRH-dPEG$_4$-HPG-ICC a buffer solution with a pH 7.3 was freshly prepared (5 mM $H_2NaPO_4 \cdot H_2O$, 50 mM $HNa_2PO_4 \cdot 2H_2O$, 5 mM EDTA·2H$_2$O). ICC-mal (4 mg, 5.0 µmol) was dissolved in 1 ml buffer solution, LHRH-dPEG$_4$-mal (5 mg, 3.0 µmol) was also dissolved in 1 ml buffer solution, 2-Iminithiolane hydrochloride (2.7 mg, 10.0 µmol) was dissolved in 1.5 ml buffer solution, and HPG (10 kDa, 25% $NH_2$ groups, 10 mg,

10 µmol) was dissolved in 1.5 ml buffer solution. For one hour 2-Iminothiolane hydrochloride, LHRH-dPEG$_4$-mal and ICC-mal were added alternately to the HPG/buffer solution. The mixture was stirred over night at room temperature. After separation with Sephadex G-25 Superfine the coupled product was purified *via* dialysis in water (24-48 h) and the solvent was reduced in vacuo and the compound was lyophilized at -75°C in millipore water to give a pink powder. The products were kept in fridge.

### 10.4.13. General procedure for the coupling of hyperbranched polyglycerols with Indotricarbocyanine-maleimide: HPG-ITCC

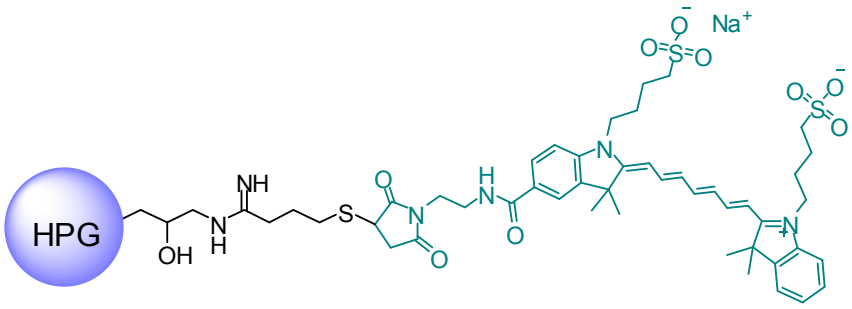


**15**

First a buffer solution with a pH 7.3 was prepared (1.429 g of $H_2NaPO_4 \cdot H_2O$, 2.568 g of $HNa_2PO_4 \cdot 2H_2O$, 0.931 g EDTA, 0.5l $H_2O$). ITCC-mal was dissolved in 1 ml buffer, 2-Iminithiolane hydrochloride was dissolved in 6 ml buffer, and HPG-$NH_2$ was dissolved in 2 ml buffer. During one hour 0.4 ml of 2-Iminithiolane hydrochloride and 0.33 ml of ITCC-mal were added alternately to the HPG-$NH_2$/buffer-solution. The mixture was stirred over night at room temperature. After separation with Sephadex G-25 Superfine the coupling product was purified *via* dialysis in water (24h), concentrated to dryness, followed by dissolved in a small amount of millipore water and freeze-drying, a dark blue green solid were obtained.

The loading degree of dye is summarized in Table 9.

**Table 9.** Dye loading with ITCC-mal.

| Molecular Weight (kDa) | Dye Loading (%) |
|---|---|
| 10 | 3 |
| 20 | 2 |
| 120 | 3 |
| 208 | 2 |
| 475 | 4 |
| 870 | 5 |

### 10.4.14. General procedure for the coupling of hyperbranched polyglycerols with Cy5.5 derivative: HPG-Cy5.5

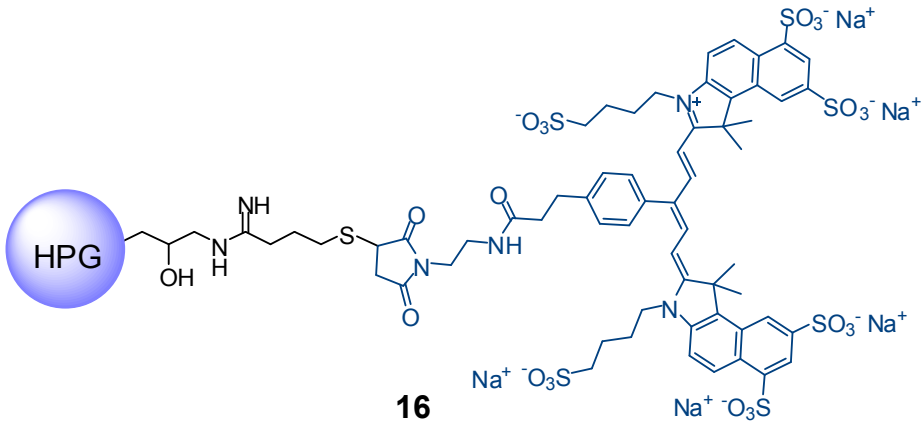


**16**

First a buffer solution with a pH 7.3 was prepared (1.429 g of $H_2NaPO_4 \cdot H_2O$, 2.568 g of $HNa_2PO_4 \cdot 2H_2O$, 0.931 g EDTA, 0.5l $H_2O$). Cy5.5-mal was dissolved in 1 ml buffer, 2-Iminithiolane hydrochloride was dissolved in 6 ml buffer, and HPG-$NH_2$ was dissolved in 2 ml buffer. During one hour 0.4 ml of 2-Iminithiolane hydrochloride and 0.33 ml of Cy5.5-mal were added alternately to the HPG-$NH_2$/buffer-solution. The mixture was stirred over night at room temperature. After separation with Sephadex G-25 Superfine the coupling product was purified *via* dialysis in water (24h), concentrated to dryness, followed by dissolved in a small amount of millipore water and freeze-drying, a dark blue solid were obtained.

The loading degree of dye is summarized in Table 10.

**Table 10.** Dye loading with Cy5.5 derivative.

| Molecular Weight (kDa) | Dye Loading (%) |
|---|---|
| 10 | 4 |
| 120 | 4 |
| 475 | 5 |

## 10.5. Experimental section of cell preparations

### 10.5.1. Cell preparations for HPG-ICC conjugates (for chapter 3.)

**Cell Culture**

The epithelial human lung cancer cell line A549 and human epidermoid carcinoma cells A431 were routinely propagated as follows: DEMEM medium, with 10 % fetal calf serum (FCS), 2 % glutamine, and penicillin/streptomycin (all from PAN Biotech) added. Cells were seeded into medium at 1 x $10^5$ cells/ml, cultured at 37 °C with 5 % $CO_2$, and split 1:5 two times a week. Human umbilical vein endothelial Cells (HUVEC) were cultured in endothelial cell growth medium with supplement–mix (Promocell). Cells were seeded into medium at 2 x $10^4$ cells/ml, cultured at 37 °C with 5 % $CO_2$ up to 80 % of confluence, and then split 1:4.

**Fluorescence activated cell sorting (FACS)**

For fluorescence activated cell sorting (FACS) 2 x $10^5$ cells/ml were cultured in 24-well plates with normal culture medium or medium containing $10^{-6}$ M test substance for 1 and 4 hours. Thereafter, cells were washed with PBS and detached with 200 µl/well accutase (PAA) and washed two times with PBS. Cells were fixed with 500µl 3% paraformaldehyde for 10 min at 4°C, stopped with 2 ml PBS and centrifuged with 250g, for 10 min at 4°C. Supernatants were removed and cells were suspended in 200 µl PBS with 0.5% bovine serum albumin (Roth). Fixed cells were kept at 4°C until analyzed in a FACS Calibur analysis instrument (Becton-Dickinson).

**Cytotoxicity Assays**

Viability of cells was analysed by FACS analysis. 2 x $10^5$ cells/ml were cultured in 24-well plates with normal culture medium or medium containing $10^{-6}$ M test substance for 1 and 4 hours**.** Size and granularity of cells were analysed and the percentage of viable cells calculated.

**Cytochemistry**

In the present studies, A549 or A431 cell were seeded at 5 x $10^4$ cells/ml in a 24-well culture plate on glass coverslips (Sigma) and cultured for 24 hours at 37°C. HUVEC cells were seeded at 1 x $10^4$ cells/ml and cultured for three days at 37 °C. Thereafter, cells were incubated with medium containing $10^{-6}$ M of dye-labelled test substances or $10^{-6}$M glycerol-ICC for different times at 37°C. Afterwards, cells were fixed with cold acetone, rinsed and covered with Alexa Fluor 488 Phalloidin (1:300, Molecular Probes). 4,6-diamidino-2-phenylindole (DAPI, Abcam) was used for nuclear counterstain. Endosomes were stained with mouse monoclonal anti-human-Mannose-6-phosphate-receptor antibody (late endosome marker, Abcam) and anti-mouse-Cy3 (Dianova) as fluorescence-labeled secondary antibody. Image acquisition was performed using a Leica DMRB microscope (Leica) or a confocal microscope (Carl Zeiss Jena). Images were taken with a digital camera (Spot 32, Diagnostic Instruments).

### 10.5.2. Cell preparations for HPG-ICC conjugates (for chapter 4.)

**Cell Culture**

A549 cells were cultured in Ham F12 K with 2mM L-Gln supplemented with fetal calf serum (FCS) and antibiotics in a humidified incubator at 37°C and 5 % $CO_2$.

**Nanoparticle Uptake**

A549 cells were seeded on poly-L-lysine coated glass coverslips and grown to a confluency of 60-70 %. After one washing step with PBS (pH 7.4) cells were incubated for 10, 30 or 60 minutes, respectively with nanoparticles (1 mg/ml) in Optimem supplemented with 5 µM HPG-$NH_2$ (1.05 mg/ml or 262.5 µg in 250 µl) in a humidified incubator at 37°C and 5 % $CO_2$. Then cells were placed on ice, washed three times for 5 min with ice-cold PBS buffer containing 10 mM $MgCl_2$ and fixed with 4 % paraformaldehyde, 4 % sucrose in PBS, pH

7.4, for 20 min. After fixation cells were washed two times with PBS and than blocked for 10 to 30 min in GSDB (Goat serum dilution buffer: 15 mM sodium phosphate buffer pH 7.4, 100 mM NaCl, 0,3% (v/v) Triton X-100 (20%), 30% (v/v) goat serum). Then cells were incubated with primary antibody in GSDB (Table 5) for 1h at room temperature with coverslips turned upside down on a droplet of antibody solution, washed three times for 5 min in GSDB w/o goat serum. After incubation with the secondary antibody in GSDB (1:100) for 1h at room temperature in humidity chamber, cells were washed two times for 5 min in GSDB w/o goat serum. Coverslips were dipped in distilled water to remove salt and then mounted onto glass slides using Immumount solution (Thermo Scientific) supplemented with 1 µg/ml DAPI.

**Inhibition**

A549 cells were seeded on glass coverslips in 24 well plates and allowed to attach for 24 h in 3 ml of DMEM medium (+10% FCS, 1% P/S, 1% Gln). After one washing step with PBS (pH 7.4) cells were pre-incubated for 20 min, in Optimem supplemented with 200 µM dynasore and 30 µM pitstop respectively (stocks are dissolved in DMSO) in a humidified incubator at 37°C and 5 % $CO_2$. After pre-incubation Optimem-inhibition solution were incubated or 10, 30 or 60 minutes with HPG-ICC (finally concentration: 1 mg/ml). Then cells were placed on ice, washed three times for 5 min with ice-cold PBS buffer containing 10 mM $MgCl_2$ and fixed with 4 % paraformaldehyde, 4 % sucrose in PBS, pH 7.4, for 20 min. After fixation cells were washed two times with PBS and than blocked for 10 to 30 min in GSDB (Goat serum dilution buffer: 15 mM sodium phosphate buffer pH 7.4, 100 mM NaCl, 0,3% (v/v) Triton X-100 (20%), 30% (v/v) goat serum). Then cells were incubated with primary antibody in GSDB (EEA1 1:100 mouse, CHC 1:50 mouse) for 1h at room temperature with coverslips turned upside down on a droplet of antibody solution, washed three times for 5 min in GSDB w/o goat serum. After incubation with the secondary antibody in GSDB (Gαm-Alexa488 1:100) for 1h at room temperature in humidity chamber, cells were washed two times for 5 min in GSDB w/o goat serum. Coverslips were dipped in distilled water to remove salt and then mounted onto glass slides using Immumount solution (Thermo Scientific) supplemented with 1 µg/ml DAPI.

### 10.5.3. Cell preparations for HPG-ICC-peptide conjugates (for chapter 5.)

**Cell Culture**

The epithelial human lung cancer cell line A549, the human epidermoid cell line A431, and the human cervical carcinoma CaSKI cells (cell line service) were routinely propagated as follows: DEMEM medium, with 10 % fetal calf serum (FCS), 2 % glutamine, and penicillin/streptomycin (PAN Biotech) added. Cells were seeded into medium at 1 x $10^5$ cells/ml, cultured at 37 °C with 5 % $CO_2$, and split 1:5 two times a week.

**Cytochemistry**

In the present study, A549, A431 or CaSKI cells were seeded at 5 x $10^4$ cells/ml in a 24-well culture plate on glass coverslips (Sigma), and cultured for 24 hours at 37°C. Thereafter, cells were incubated with medium containing $10^{-6}$or $10^{-7}$ M of test substances for 4 hours at 37°C. Afterwards, cells were fixed with cold acetone and rinsed. Actin cytoskeleton was stained by incubation with Alexa Fluor 488 Phalloidin (green) for 1 hour. 4,6-diamidino-2-phenylindole (DAPI, Abcam) was used for nuclear counterstain. Image acquisition was performed using a Leica DMRB microscope (Leica). Images were taken with a digital camera (Spot 32, Diagnostic Instruments).

### 10.5.4. Fluorescence imaging (for chapter 6.)

**First and second study**

These investigations were carried out by the Physikalisch-Technische Bundesanstalt (PTB) in Berlin.

Fluorescence images were taken with a Visiluxx II of the Fa. Visitron Systems GmbH. The system consists of a EMCCD camera (Roper Scientific, Nikon objective AiS 24/2). This device is limited exclusively specific for luminescence measurements. Two filter LP800 (Omega Optical AG-LP800/50) were used for fluorescence measurements in the near-infrared (NIR) spectral range. These filters were meant for the suppression of the excitation light (OD = optical density, takes approx. 10).

A LED-Array $\lambda$ = 740 nm (Roithner Lasertechnik) has been introduced in the investigation chamber for excitation of the fluorescence. A shortpass-filter $\lambda_{50\%}$ = 750 nm (Omega Optical 3rd Millenium 3RD750SP) was positioned directly behind the LED-Array to

suppress the long wavelength spectral components. The LED was run in the cw-modus (500 mA).

The sedation of the animals was realised with a Visiluxx system (EZAnesthesia). This system supplied with help of a three-way tap an incubation chamber and a distributor in the dark box the measuring system. Five animals can be connected simultaneously. Isofluran in mixture with oxygen was used as narcotic. The induction of anaesthesia was observed with 5 % (v/v) in the incubation chamber. The Isofluran was reduced to 2 % (v/v) for the subsequent permanent sedation. The animals were connected to the breathing masks. Additionally, for a better assignment of the position of the tumors, a conventional reflexion image of the animals was taken.

Bioluminescence images were captured with the EMCCD-camera after 0 min, 10 min, 1 h, 3 h, 5 h, 24 h, and 48 h (detector temperature: -70 °C, accumulation: 10, objective diaphragm: 2, exposure time: 0.1 s, EMGain: 3000, Pre-Gain: 1, rate: 5 MHz, resolution: 16 bit, binning 2 x 2). After the fluorescence measurements the animals were killed, kidney, liver, spleen and the tumor have been obtained from mice. Subsequently a fluorescence image was recorded.

**Third study**

The images are of 8-10 week old nude mice (female), bearing two types of subcutaneous tumors: left thigh flank has 4T1-GFP (breast carcinoma) and right thigh has C51 (colon carcinoma, metastatic to lungs). The images were acquired when the tumors were 4-8 mm in diameter (appx.). 2 mg of the compounds was injected per kg of the animal body weight (so assuming the body weight of each mouse to be an av. 25 mg; one can calculate the total amount injected in each mouse). The animals were measured longitudinally according to the plan given on the first slide of the presentation. For the last time point (i.e. 48 h after injection), the organs were harvested and imaged (what is missing here is the compound blood pool). The acquired images were subjected to spectral deconvolution to obtain true Cy5.5 spectra and then all the images compared over the longitudinal aquisition.

# 11. References


[1] K. Strebhardt, A. Ullrich, *Nature Reviews Cancer* **2008**, *8*, 473.

[2] G. Kohler, C. Milstein, *Nature* **1975**, *256*, 495.

[3] H. Ringsdorf, *J. Polym. Sci Polym Symp* **1975**, *51*, 135.

[4] R. Duncan, *Nat Rev Drug Discovery* **2003**, *2*, 347.

[5] R. Duncan in *Encyclopedia of Molecular Cell Biology and Molecular Medicine*, Vol. 14 (Hrsg.: R. A. Meyers), Wiley-VCH, Weinheim, **2005**, S. 163.

[6] A. Godwin, K. Bolina, M. Clochard, E. Dinand, S. Rankin, S. Simic, S. Brocchini, *J Pharm Pharmacol* **2001**, *53*, 1175.

[7] H. Staudinger*, Berichte der deutschen chemischen Gesellschaft*, **1920**, *53*, 1073.

[8] P.A. Vasey, S.B. Kaye, R. Morrison, C. Twelves, P. Wilson, R. Duncan, A.H. Thomson, L.S. Murray, T.E. Hilditch, T. Murray, S. Burtles, D. Fraier, E. Frigerio, J. Cassidy, *Clinical Cancer Research*, **1999**, *5*, 83.

[9] R. Haag, F. Kratz, *Angew Chem*, **2006**, *118*, 1218.

[10] Further information: http://www.starpharma.com.

[11] S. Reichert, M. Calderón, K. Licha, R. Haag, *"Multivalent Dendritic Architectures in Theranostics"* in "Multifunctional Nanoparticles for Medical Applications - Imaging, Targeting, and Drug Delivery" 2010, Springer book chapter, submitted.

[12] C. Brus, H. Petersen, A. Aigner, F. Czubayko, T. Kissel, *Bioconjugate Chem*, **2004**, *15*, 677.

[13] S. Mukherjee, L. Das, L. Kole, S. Karmakar, N. Datta, P. K. Das, *J Infectious Diseases*, **2004**, *189*, 1024.

[14] F. M. Veronese, O. Schiavon, G. Pasut, R. Mendichi, L. Andersson, A. Tsirk, F. Ford, G. Wu, S. Kneller, J. Davies, R. Duncan, *Bioconjug Chem*, **2005**, *16*, 775.

[15] I. Gilham, *Drug Discovery World Fall*, **2002**, *17*, 23.

[16] K. Riehemann, S. W. Schneider, T. A. Luger, B. Godin, M. Ferrari, H. Fuchs, *Angew Chem*, **2009**, *121*, 886.

[17] V. Wagner, D. Wechsler, Technologiefrüherkennung, Nanobiotechnologie II: Anwendungen in der Medizin und Pharmazie, **2004**, (Band 50).

[18] J. M. Oliveira, A. J. Salgado, N. Sousa, J. F. Mano, R. L. Reis, *Science*, **2010**, *35*, 1163.

[19] I. J. Majoros, A. Myc, T. Thomas, C. B. Mehta, J. R. Baker Jr., *Biomacromolecules*, **2006**, *7*, 572.

[20] R. Weissleder, U. Mahmood, *Radiology*, **2001**, *219*, 316.

[21] T. Yeh, W. Zhang, S. Ildstad, C. Ho, *Magn Reson Med*, **1995**, *33*, 200.

[22] M. J. Paulus, S. S. Gleason, S. J. Kennel, P. R. Hunsicker, D. K. Johnson, *Neoplasia*, **2000**, *2*, 62.

[23] A. Becker, C. Hessenius, K. Licha, B. Ebert, U. Sukowski, W. Semmler, B. Wiedenmann, C. Grötzinger, *Nat Biotechnol*, **2001**, *19*, 327.

[24] A. A. Bogdanov Jr., R. Weissleder, H. W. Frank, A. V. Bogdanova, N. Nossif, B. K. Schaffer, E. Tsai, M. I. Papisov, T. J. Brady, *Radiology*, **1993**, *197*, 701.

[25] A. A. Bogdanov Jr., C. Martin, A. V. Bogdanova, T. J. Brady, R. Weissleder, *Bioconjug Chem*, **1996**, *7*, 144.

[26] M. Lewin, N. Carlesso, C. H. Tung, X. W. Tang, D. Cory, D. T. Scadden, R. Weissleder, *Nat Biotechnol*, **2000**, *18*, 410.

[27] L. L. Muldoon, G. Nilaver, R. A. Kroll, M. A. Pagel, X. O. Breakefield, E. A. Chiocca, B. L. Davidson, R. Weissleder, E. A. Neuwelt, *Am J Pathol*, **1995**, *147*, 1840.

[28] R. Weissleder, C. H. Tung, U. Mahmood, A. Bogdanov Jr., *Nat Biotechnol*, **1999**, *17*, 375.

[29] C. Bremer, V. Ntziachristos, U. Mahmood, C. H. Tung. R. Weissleder, *Der Radiologe*, **2001**, *41*, 131.

[30] U. Mahmood, R. Weissleder, *Mol Cancer Ther*, **2003**, *2*, 489.

[31] Y. Lin, R. Weissleder, C. H. Tung, *Mol Imaging*, **2003**, *2*, 87.

[32] X. Intes, J. Ripoll, Y. Chen, S. Nioka, A. G. Yodh, B. Chance, *Medical Physics*, **2003**, *6*, 1039.

[33] T. Conrad, molecular imaging – medizinische Bildgebung der nächsten Generation. Hausarbeit zur Vorlesung "Medizinische Informatik" **2001/02** an der FU Berlin

[34] K. Licha, C. Olbrich, *Adv Drug Deliv Reviews*, **2005**, *57*, 1087.

[35] B. Ballou, L. A. Ernst, A. S. Waggoner, *Curr Med Chem*, **2005**, *12*, 795.

[36] B. Riefke, K. Licha, W. Semmler, *Radiology*, **1997**, *37*, 749.

[37] C. Bremer, V. Ntziachristos, R. Weissleder, *Eur Radiol*, **2003**, *13*, 231.

[38] K. Licha, B. Riefke, B. Ebert, C. Grotzinger, *Acad Radiol*, **2002**, *9*, 320.

[39] G. R. Cherrick, S. W. Stein, C. M. Leevy, C. S. Davidson, *J Clin Invest*, **1960**, *39*, 592.

[40] B. Pierce, R. Birge, *IEEE J Quantum Electron*, **1992** , *18*, 114.

[41] S. Oda, Y. Segawa, P. H. Kim, S. Namba, N. Kodama, *Jpn J Appl Phys*, **1989**, *2*, 1977.

[42] I. J. Fox, W. H. Wood, *Mayo Clin Proc*, **1996**, *35*, 732.

[43] W. Bäumler, C. Ables, S. Karrer, T. Wei, H. Messmann, M. Landthaler, R. M. Szeimies, *Br J Cancer*, **1999**, *80*, 360.

[44] S. Fickweiler, R. M. Szeimies, W. Bäumler, P. Steinbach, S. Karrer, A. E. Goetz, C. M. Abels, F. Hofstädter, M. Landthaler, *J Photochem Photobiol B: Biol*, **1997**, *38*, 178.

[45] D. B. Shealy, M. Lipowska, J. Lipowski, N. Narayanan, S. Sutter, L. Strekowski, G. Patonay, *Anal. Chem.*, **1995**, *67*, 247.

[46] S. Daehne, U. Resch-Genger, O. S. Wolfbeis, Near-infrared dyes for high technology applications, NATO ASI Series, **1998**, Kluwer Academic Publishers, London.

[47] A. R. Menjoge, R. M. Kannan, D. A. Tomalia, *Drug Discovery Today*, **2010**, *15*, 171.

[48] E. R. Gillies, J. M. J. Fréchet, *J Am Chem Soc*, **2002**, *124*, 14137.

[49] E. R. Gillies, J. M. J. Fréchet, F. C. Szoka, *Mol Pharmaceutics*, **2005**, *2*, 129.

[50] A. G. Schatzlein, B. H. Zinselmeyer, A. Elouzi, C. Dufes, Y. T. A. Chim, C. J. Roberts, M. C. Davies, A. Munro, A. I. Gray, I. F. Uchegbu, *J Controlled Release*, **2005**, *101*, 247.

[51] T. Minko, S. S. Dharap, R. I. Pakunlu, Y. Wang, *Curr Drug Targets*, **2004**, *5*, 389.

[52] Y. Luo, G. D. Prestwich, *Curr Cancer Drug Targets*, **2002**, *2*, 209.

[53] Y. Matsumura, H. Maeda, *Cancer Res*, **1986**, *46*, 6387.

[54] H. Maeda, J. Wu, T. Sawa, Y. Matsumura, K. Hori, *J Controlled Release*, **2000**, *65*, 271.

[55] R. K. Jain, *Cancer Metathesis Rev*, **1987**, *6*, 559.

[56] R. K. Jain, *Cancer Res*, **1987**, *47*, 3039.

[57] M. E. Fox, C. S. Francis, J. M. J. Fréchet, *Acc Chem Res*, **2009**, *42*, 1141.

[58] K. Knop, R. Hoogenboom, D. Fischer, U. S. Schubert, *Angew Chem*, **2010**, *122*, 2.

[59] K. Yazawa, M. Fujimori, J. Amano, Y. Kano, S. Taniguchi, *Cancer Gene Ther*, **2000**, *2*, 269.

[60] M. Stroh, J. P. Zimmer, D. G. Duda, T. S. Levchenko, K. S. Cohen, E. B. Brown, D. T. Scadden, V. P. Torchilin, M. G. Bawendi, D. Fukumura, R. K. Jain, *Nat Med*, **2005**, *6*, 678.

[61] Y. Noguchi, J. Wu, R. Duncan, J. Strohalm, K. Ulbrich, T. Akaike, H. Maeda, *Jpn J Cancer Res*, **1998**, *89*, 307.

[62] T. Minko, J. Khandare, S. Jayant, In: Matyjaszewski K, Gnanou Y, Leibler L (ed) Macromolecular Engineering: From Precise Macromolecular Synthesis to Macroscopic Material Properties and Application, **2007**, Wiley-VCH.

[63] S. Jayant, J. Khandare, Y. Wang, A. P. Singh, N. Vorsa, T. Minko, *Pharm Res*, **2007**, *24*, 2120.

[64] T. Okuda, S. Kawakami, N. Akimoto, T. Niidome, F. Yamashita, M. Hashida, *J Controlled Release*, **2006**, *116*, 330.

[65] K. M. Kitchens, R. B. Kolhatkar, P. W. Swaan, H. Ghandehari, *Mol Pharmaceutics*, **2007**, *5*, 364.

[66] M**.** Najlah, A. D'Emanuele**,** *Curr Opin Pharmacol*, **2006**, *6*, 522.

[67] S. D. Conner, S. L. Schmid, *Nature*, **2003**, *422*, 37.

[68] S. Mayor, R. E. Pagano, *Nat Rev Mol Cell Biol*, **2007**, *8*, 603.

[69] L. Lopes, L. M. F. Godoy, C. C. de Oliveira, J. Gabardo, R. J. G. Schadeck, D. de Freitas Buchi, *Micron*, **2006**, *37*, 277.

[70] E. M. Schmid, H. A. T. McMahon, *Nature*, **2007**, *448*, 883.

[71] A. Benmerah, C. Lamaze, *Traffic*, **2007**, *8*, 970.

[72] E. J. Ungewickell, L. Hinrichsen, *Curr Opin Cell Biol*, **2007**, *19*, 417.

[73] I. R. Nabi, U. L. Phuong, *J Cell Biol*, **2003**, *161*, 673.

[74] S. Gold, P. Monaghan, P. Mertens, T. Jackson, *PLoS*, **2010**, *5*, 1.

[75] R. Wiwattanapatapee, B. Carreno-Gomez, N. Malik, R. Duncan, Pharm Res, 2000, 17, 991.

[76] R. Jevprasesphant, J Penny, D. Attwood, A. D'Emanuele, *J Controlled Release*, **2004**, *97*, 259.

[77] P. Tallury, K. Payton, S. Santra, *Nanomedicine*, **2008**, *3*, 579.

[78] A. M. Smith, H. W. Duan, A. M. Mohs, S. M. Nie, *Adv Drug Delivery Rev*, **2008**, *60*, 1226.

[79] S. Chono, T. Tanino, T. Seki, K. Morimoto, *J Pharm Pharmacol*, **2007**, *59*, 75.

[80] F. Osaki, T. Kanamori, S. Sando, T. Sera, Y. Aoyama, *J Am Chem Soc*, **2004**, *126*, 6520.

[81] K. Y. Win, S. S. Feng, *Biomaterials*, **2005**, *26*, 2713.

[82] C. Cortez, E. Tomaskovic-Crook, A. P. R. Johnston, A. M. Scott, E. C. Nice, J. K. Heath, F. Caruso, *ACS Nano*, **2007**, *1*, 93.

[83] W. Jiang, B. Y. S. Kim, J. T. Rutka, W. C. W. Chan, *Nat Nanotechnol*, **2008**, *3*, 145.

[84] Y. H. Jin, S. Lohstreter, D. T. Pierce, J. Parisien, M. Wu, C. Hall, J. X. J. Zhao, *Chem Mater*, **2008**, *20*, 4411.

[85] I. B. Mosbah, R. Franco-Go, H. B. Abdennebi, R. Hernandez, G. Escolar, D. Saidane, J. Rosello-Catafau, C. Peralta, *Transplant Proc*, **2006**, *38*, 1229.

[86] R. K. Kainthan, M. Gnanamani, M. Ganguli, T. Ghosh, D. E. Brooks, S. Maiti, J. N. Kizhakkedathu, *Biomaterials*, **2006**, *27* 5377.

[87] E. G. R. Fernandes, A. A. A. De Queiroz, G. A. Abraham, J. San Roma, *J Mater Sci: Mater Med*, **2006**, *17*, 105.

[88] R.H. Kienle, A.G. Hovey, *J Am Chem Soc*, **1929**, 51, 509.

[89] G. Odian, *Principles of polymerization*, **1991**, Wiley VCH.

[90] P. J. Flory, *J Am Chem Soc*, **1941**, *63*, 3083.

[91] P. J. Flory, *J Am Chem Soc*, **1941**, *63*, 3091.

[92] P. J. Flory, *J Am Chem Soc*, **1941**, *63*, 3096.

[93] P. J. Flory, *J. Am. Chem. Soc.* **1952**, *74*, 2718.

[94] H. R. Kricheldorf, Q. Z. Zang, G. Schwarz, *Polymer*, **1982**, *23*, 1821.

[95] Y. H. Kim, O. W. Webster, *Polym Prepr*, **1988**, *29***,** 310.

[96] C. J. Hawker, R. Lee, J. M. J. Frechet, *J Am Chem Soc*, **1991**, *113*, 4583.

[97] C. Gao, D. Yan, *Prog Polym Sci*, **2004**, *29*, 183.

[98] A. Sunder, R. Mülhaupt, R. Haag, H. Frey, *Adv Mater*, **2000**, *12*, 235.

[99] A. Sunder, R. Hanselmann, H. Frey, R Mülhaupt, *Macromol*, **1999**, *32*, 4240.

[100] C. C. Lee, J. A. MacKay, J. M. J. Fréchet, F. C. Szoka, Nat Biotechnol, **2005**, 23, 1517.

[101] P. Kolhe, J. Khandare, O. Pillai, S. Kannan, M. Lieh-Lai, R. M. Kannan, *Biomaterials*, **2006**, *27*, 660.

[102] R. K. Kainthan, J. Janzen, E. Levin, D. V. Devine, D. E. Brooks, *Biomacromolecules*, **2006**, 7, 703.

[103] R. Haag, A. Sunder, J.-F. Stumbé, *J Am Chem Soc*, **2000**, *122*, 2954.

[104] R. Haag, *Chem Eur J*, **2001**, 7, 327.

[105] M. Calderón, M. A. Quadir, M. Strumia, R. Haag, *Biochimie*, **2010**, *92*,1242.

[106] K. Tyagarajan, E. Pretzer, J. E. Wiktorowicz, *Electrophoresis*, **2003**, *24*, 2348.

[107] A. Warnecke, I. Fichtner, G. Sass, F. Kratz, *Arch Pharm*, **2007**, *340*, 389.

[108] R. Haag, F. Kratz, M. Calderón, EP08006471.0, **2008**.

[109] R. Haag, F. Kratz, M. Calderón, EP09001693.2, **2009**.

[110] F. Kratz, *Expert Opin Investig Drugs*, **2007**, *16*, 855.

[111] H. Türk, R. Haag, S. Alban, *Bioconjug Chem*, **2004**, *15*, 162.

[112] J. Dernedde, A. Rausch, M. Weinhart, S. Enders, R. Tauber, K. Licha, M. Schirner, U. Zügel, A. von Bonin, R. Haag, *PNAS*, **2010**, *107*, 19679.

[113] S. Reichert, *Diploma Thesis*, Freie Universität Berlin, Germany, **2006**.

[114] S. Reichert, A. Wiehe, S. Gräfe, V. Albrecht, R. Haag, in *7th International Symposium on Polymer Therapeutics: From laboratory to clinical practice*, Valencia, Spain, **2008**, p. P9.

[115] W. Fischer, M. Calderón, A. Schulz, I. Andreou, M. Weber, R. Haag, *Bioconjugate Chem*, **2010**, *21*, 1744.

[116] M. D. Pierschbacher, E. Ruoslahti, *Nature*, **1984**, *309*, 30.

[117] J. G. Zhang, O. B. Krajden, R. K. Kainthan, J. N. Kizhakkedathu, I. Contantinescu, D. E. Brooks, M. I. C. Gyongyossy-Issa, *Bioconjug Chem*, **2008**, *19*, 1241.

[118] P. Kolhe, J. Khandare, O. Pillai, S. Kannan, M. Lich-Lai, R. Kannan, *Pharm Res* **2004**, *21*, 2185.

[119] D. Wilms, F. Wurm, J. Nieberle, P. Böhm, U. Kemmer-Jonas, H. Frey, *Macromolecules* **2009**, *42*, 3230.

[120] R. K. Kainthan, E. B. Muliawan, S. G. Hatzikiriakos, D. E. Brooks *Macromolecules*, **2006,** *39,* 7708.

[121] C. J. Bettinger, R. Langer, J. T. Borenstein, *Angew Chem Int Ed*, **2009**, *48*, 5406.

[122] W. Decheng, F. Qiang, H. Junlian, *J Appl Polym Sci*, **2006**, *101*, 509.

[123] A. Sunder, R. Mülhaupt, *Patent* DE 19947631 A1 (**1998**).

[124] S. Roller, H. Zhou, R. Haag, *Mol Divers* **2005**, *9*, 305.

[125] H. Türk, R. Haag, S. Alban, *Bioconjug Chem*, **2004**, *15*, 162-167.

[126] W. Burchard, *Adv Polym Sci*, **1999**, *143*, 125.

[127] S. Roller, Dissertation, **2005**, Dortmund.

[128] S. Roller, H. Zhou, R. Haag, *Mol*. *Diversity*, **2005**, *9*, 305.

[129] C. R. Noller, C. A. Luchetti, E. M. Acton, R. A. Bernhard, *J Am Chem Soc*, **1953**, *75*, 3851.

[130] R. K. Kainthan, D. E. Brooks, *Biomaterials*, **2007**, *28*, 4779.

[131] R. K. Kainthan, S. R. Hester, E. Levin, D. V. Devine, D. E. Brooks, *Biomaterials*, **2007**, *28*, 4581.

[132] L. A. Tziveleka, C. Kontoyianni, Z. Sideratou, D. Tsiourvas, C. M. Paleos, *Macromolecular Bioscience*, **2006**, *6*, 161.

[133] R. Haag, H. Frey, *Reviews in Molecular Biotechnology*, **2002**, *90*, 257.

[134] M. Calderón, R. Graeser, F. Kratz, R. Haag, *Bioorg Med Chem Lett*, **2009**, *19*, 3725.

[135] S. K. Rodal, G. Skretting, O. Garred, F. Vilhardt, B. van Deurs, K. Sandvig, *Mol Biol Cell*, **1999,** 10, 961.

[136] H. Kautz, A. Sunder, H. Frey, *Macromol Symp*, **2001**, *163*, 67.

[137] J. Z. Rappoport, S. M. Simon, *J. Cell Science*, **2002**, *116*, 847.

[138] S. J. Doxsey, F. M. Brodsky, G. S. Blank, A. Helenius, *Cell*, **1987**, *50*, 453.

[139] O. Shupliakov, *Neuroscience*, **2009**, *158*, 204.

[140] J. B. Hughes, C. Berger, M. S. Rodland, M. Hasmann, E. Stang, I. H. Madshus, *Mol Cancer Ther*, **2009**, *8*, 1885.

[141] G. Sahay, V. Gautam, R. Luxenhofer, A. V. Kabanov, *Biomaterials*, **2010**, *31*, 1757.

[142] M. Saad, O. B. Garbuzenko, E. Ber, P. Chandna, J. J. Khandare, V. P. Pozharov T. Minko, *J Control Rel*, **2008**, *130*, 107.

[143] V. P. Torchilin, *Nature Reviews, Drug Discovery*, **2005**, *4*, 145.

[144] J. Khandare, A. Mohr, M. Calderón, P. Welker, K. Licha, R. Haag, *Biomaterials*, **2010**, *31*, 4268.

[145] I. Goldstein, S. Hoffstein, J. Gallin G. Weissmann, *PNAS*, **1973**, *70*, 2916.

[146] S. M. Moghimi, A. C. Hunter, J. C. Muray, *Pharmacol. Rev.*, **2001**, *53*, 283.

[147] M. S. Robinson, *Curr Opin Cell Biol*, **1994**, *6*, 538.

[148] E. Ungewickell, D. Branton, *Nature*, **1981**, *289*, 420.

[149] C. Rodemer, V. Haucke, *Handb Exp Pharmacol*, **2008**, 105.

[150] E. Macia, M. Ehrlich, R. Massol, E. Boucrot, C. Brunner, T. Kirchhausen, *Dev Cell*, **2006**, *10*, 839.

[151] M. E. Abazeed, J. M. Blanchette, R. S. Fuller, *J Biol Chem*, **2005**, *280*, 4442.

[152] E. Macia, M. Ehrlich, R. Massol, E. Boucrot, C. Brunner, T. Kirchhausen, Dev Cell, 2006, 10, 839.

[153] F.-T. Mu, J. M. Callaghan, O. Steele-Mortimer, H. Stenmark, R. G. Parton, P. L. Campbell, J. McCluskey, J.-P. Yeo, E. P.C. Tock, B.-H. Toh, *J. Biol. Chem.*, **1995**, *270*, 13503.

[154] M. A. Stamnes, J. E. Rothman, *Cell*, **1993**, *73*, 999.

[155] J. P. Luzio, B. M. Mullock, P. R. Pryor, M. R. Lindsay, D. E. James, R. C. Piper, *Biochem Soc Trans*, **2001**, *29*, 476.

[156] B. Storrie, M. Desjardins, *Bioessays*, **1996**, *18*, 895.

[157] G. M. Griffiths, *Trends Cell Biol*, **1996**, *6*, 329.

[158] P. Saftig, J. Schröder, J. Blanz, M. Schwake, *Molekulare Medizin*, **2008**, *14*, 344.

[159] R. Matteoni, T. E. Kreis, *J Cell Biol*, **1987**, *105*, 1253.

[160] K. Funato, W. Beron, C. Z. Yang, A. Mukhopadhyay, P. D. Stahl, *J Biol Chem*, **1997**, *272*, 16147.

[161] B. P. Lawrence, W. J. Brown, *J Cell Sci*, **1992**, *102*, 515.

[162] H. K. Niewenhuis, J. J. G. van Oosterhout, E. Rozemuller, F. van Iwaarden, J. J. Sixma, *Blood*, **1987**, *70*, 838.

[163] B. C. S. Atkinson, B. F. D. Ernst, A. H. Ghrist, W. H. Clark, *Hybridoma*, **1985**, *4*, 243.

[164] H. Hotta, A. H. Ross, K. Huebner, M. Isobe, S. Wendeborn, M. V. Chao, R. P. Ricciardi, Y. Tsujimoto, C. M. Croce, H. Koprowski, *Cancer Res*, **1988**, *48*, 2955.

[165] J. Tatzel, M. Zerial, *BIOspektrum*, **2007**, *13*, 34.

[166] F. Aksu, *Zeitschrift für Neurologie des Kindes- und Jugendalters und ihre Grenzgebiete*, **2007**, *2*, 49.

[167] K. M. Kitchens, R. B. Kolhatkar, P. W. Swaan, H. Ghandehari, *Mol Pharmaceutics*, **2008**, *5*, 364.

[168] K. M. Kitchens, A. Foraker, R. Kolhatkar, P. Swaan, H. Ghandehari, *Pharm Res*, **2007**, *24*, 2138.

[169] D. S. Goldberg, H. Ghandehari, P. W. Swaan, *Pharm Res*, **2010**, *27*, 1547.

[170] Y. Kurtoglu, S. Kannan S, *Int J Pharm*, **2010**, *384*, 189.

[171] C. Treiber, M.A. Quadir, P. Voigt, M. Radowski, S. Xu, L. M. Munter, T.A. Bayer, M. Schaefer, R. Haag, G. Multhaup, *Biochemistry*, **2009,** *48*, 4273-4284.

[172] E. Fischer, *Chem Ber*, **1894**, *27*, 2985.

[173] G. Karp, *Molekulare Zellbiologie*, 1. Ausgabe, Springer, Berlin, **2005**.

[174] E. Rouslahti, M. D. Pierschbacher, *Science*, **1987**, *238*, 491.

[175] R. Haubner, D. Finsinger, H. Kessler, *Angew Chem*, **1997**, *109*, 1440.

[176] R. O. Hynes, *Cell*, **2002**, *110*, 673.

[177] S. E. D'Souza, M. H. Ginsberg, E. F. Flow, *Trends Biochem. Sci.* **1991**, *16*, 246.

[178] D. Cox, T. Akoi, J. Seki, Y. Motoyama, K. Yoshida, *Med Res Rev*, **1994**, *14*, 195.

[179] M. Janssen, W. J. Oyen, L. F. Massuger, C. Frielink, I. Dijkgraaf, D. S. Edwards, M. Radjopadhye, F. H. Corstens, O. C. Boerman, *Cancer Biother Radiopharm*, **2002**, *17*, 641.

[180] D. Polyak, C. Ryppa, A. Eldar-Boock, P. Ofek, A. Many, K. Licha, F. Kratz, R. Satchi-Fainaro, *Polym Adv Technol*, **2011**, *22*, 103.

[181] A. V. Schally, A. Arimura, A. J. Kastin, *Science*, **1971**, *173,* 1036.

[182] H. Matsuo, Y. Baba, R. M. Nair, A. Arimura, A. V. Schally, *Biochem Biophys Res Commun*, **1971**,*43*,133.

[183] G. Emons, A. V. Schally, *Hum Reprod*, **1994**, *9*, 1364.

[184] A. V. Schally, *Peptide*, **1999**, *10*, 1247.

[185] J. Engel, A. V. Schally, "*Agonists and antagonists of LHRH in the treatment of cancer*", in: Kastin AJ (ed) Handbook of biologically active peptides. Academic Press, New York, **2006**.

[186] T. Minko, M. L. Patil, M. Zhang, J. J. Khandare, M. Saad, P. Chandna, O. Taratula, "*LHRH-Targeted Nanoparticles for Cancer Therapeutics*" in: *Methods Mol Biol*, **2010**, *624*, 281.

[187] A. V. Schally, A. Nagy, *Life Sci*, **2003**, *72*, 2305.

[188] C. Ryppa, H. Mann-Steinberg, I. Fichtner, H. Weber, R. Satchi-Fainaro, M. L. Biniossek, F. Kratz, *Bioconjugate Chem*, **2008,** *19,* 1414.

[189] R. Haubner, W. A. Weber, A. J. Beer, E. Vabuliene, D. Reim, M. Sarbia, K.-F. Becker, M. Goebel, R. Hein, H.-J. Wester, H. Kessler, M. Schwaiger, *PLoS Medicine*, **2005**, *2*, 70.

[190] S. D. Conner, S. L. Schmid, *Nature*, **2003**, *422*, 37.

[191] M. Smola, T. Vandamme, A. Sokolowski, *Int J Nanomedicine*, **2008**, *3*, 1.

[192] S. S. Dharap, Y. Wang, P. Chandna, J. J. Khandare, B. Qiu, S. Gunaseelan, P. J. Sinko, S. Stein, A. Farmanfarmaian, T. Minko, *PNAS*, **2005**, *36*, 12962.

[193] M. Rudin, *Imaging in drug discovery and early clinical trials*, **2005**, Birkhäuser Verlag Basel.

[194] J. Rao, A. Dragulescu-Andrasi, H. Yao, *Curr Opin Biotechnol*, **2007**, *18*, 17.

[195] P. P. Ghoroghchian, M. J. Therien, D. A. Hammer, *Nanomedicine and Nanobiotechnology*, **2009**, *1*, 156.

[196] A. Sunder, R. Mülhaupt, H. Frey, *Macromolecules*, **2000**, *33*, 309.

[197] A. Sunder, J. Heinemann, H. Frey, *J Chem Eur*, **2000**, *6*, 2499.

[198] S. Xu, Y. Luo, R. Graeser, A. Warnecke, F. Kratz, P. Hauff, K. Licha, R. Haag, *Bioorg Med Chem Lett*, **2009**, *19*, 1030.

[199] M. A. Quadir, M. R. Radowski, F. Kratz, K. Licha, P. Hauff, R. Haag, *J Controlled Release*, **2008**, *132*, 289.

[200] M. Veiseh, P. Gabikian, S.-B. Bahrami, O. Veiseh, M. Zhang, R. C. Hackman, A. C. Ravanpay, M. R. Stroud, Y. Kusuma, S. J. Hansen, D. Kwok, N. M. Munoz, R. W. Sze, W. M. Grady, N. M. Greenberg, R. G. Ellenbogen, J. M. Olson, *Cancer Res*, **2007**, *67*, 6882.

[201] M. Hashida, Y. Takakura, *J Controlled Release* **1994**, *31*, 163.

[202] Y. Takakura, M. Hashida, *Pharm Res* **1996**, *13*, 820.

[203] M. Nishikawa, Y. Takakura, M. Hashida, *Adv Drug Delivery Rev* **1996**, *21*, 125.

[204] Y. Takakura, R. I. Mahato, M. Hashida, *Adv Drug Delivery Rev* **1998**, *34*, 93.

[205] R. K. Jain, *Cancer Res* **1990**, *50*, 814.

[206] R. K. Jain, *J Controlled Release* **1998**, *53*, 49.

[207] L. W. Seymour, Y. Miyamoto, H. Maeda, B. Brereton, J. Strohalm, K. Ulbrich, R. Duncan, *Europ J Cancer* **1995**, *31A*, 766.

[208] H. Maeda, L. W. Seymour, Y. Miyamoto, *Bioconj Chem* **1992**, *3(5)*, 351.

[209] F. Kratz, U. Beyer, *Drug Delivery* **1998**, *5*, 281.

[210] M. Hesse, H. Meier, B. Zeeh, in *Spektroskopische Methoden in der organischen Chemie*, **2005**, Thieme Georg Verlag, Germany.

[211] K. Licha, C. Hessenius, A. Becker, P. Henklein, M. Bauer, S. Wisniewski, B. Wiedenmann, W. Semmler, *Bioconjugate Chem*, **2001,** *12,* 44.

# Curriculum Vitae

For reasons of data protection,
the curriculum vitae is not included in the online version

**Talks:**

- *"Fluorescent Dyes for Molecular Imaging"* (2008)

- *"Cellular Entry"* (2009)

- *"Size-dependant Cellular Uptake of Dendritic Polyglycerol"* (2010)

**Poster presentations:**

- *"Synthesis of dendritic tetrapyrroles for the PDT",* S. Reichert, A. Wiehe, S Gräfe, V. Albrecht, R. Haag; 7th ISPT: From Laboratory to Clinical Practice; Valencia, 2008.

- *"Size-dependant Cellular Uptake of Dendritic Polyglycerol",* S. Reichert, M. Calderón, J. Khandare, P. Welker, D. Mangoldt, K. Licha, R. K. Kainthan, D. E. Brooks, R. Haag; 8th ISPT:
From Laboratory to Clinical Practice; Valencia, 2010.

- *"Stimuli-responsive Nanostructures for Drug and Gene Delivery"*, M. Calderón, W. Fischer, S. Reichert, M. A. Quadir, R. Haag; Day of Chemistry; Berlin, 2010.

**Publications:**

- *"Size-dependant Cellular Uptake of Dendritic Polyglycerol"*, S. Reichert, M. Calderón, J. Khandare, P. Welker, D. Mangoldt, K. Licha, R. K. Kainthan, D. E. Brooks, R. Haag, *Small*, 2011, 7, 820-829.

- *"Multivalent Dendritic Architectures in Theranostics"*,
S. Reichert, M. Calderón, K. Licha, R. Haag, book chapter in *Multifunctional Nanoparticles for Medical Applications - Imaging, Targeting, and Drug Delivery* **2011**, in press, Springer series: *Nanostructure Science and Technology*, eds. Robt. Prud'homme & Sonke Svenson.

- *"Fluorescence imaging with multifunctional polyglycerol sulfates: novel polymeric near-IR probes targeting inflammation"*, K. Licha, P. Welker, M. Weinhart, N. Wegner, S. Kern, S. Reichert, I. Gemeinhardt, C. Weissbach, B. Ebert, R. Haag, M. Schirner, *Bioconjugate Chemistry*, 2011, submitted.

- *"Active Cellular Uptake of Hyperbranched Polyglycerol"*, S. Reichert, P. Welker, M. Calderón, K. Licha, F. Kratz, R. Haag, *ChemBioChem*, 2011, in preparation.